C.P. No. 734

C.P. No. 734

MINISTRY OF AVIATION

AERONAUTICAL RESEARCH COUNCIL

CURRENT PAPERS

8ft x 8ft Tunnel Tests on a Model of the De Havilland 'Blue Streak'

by

G. F. Moss, B.Sc. and D. Isaacs, B.Sc.

LONDON: HER MAJESTY'S STATIONERY OFFICE

1964

PRICE 10s 6d NET

U.D.C. No. 533.665 : 533.6.013.15 : 533.6.013.412 : 533.6.048.2 : 533.6.011.35/5 [G7] Blue Streak (42)

C.P. No. 734

July, 1961

8 FT × 8 FT TUNNEL TESTS ON A MODEL OF THE DE HAVILLAND 'BLUE STREAK'

by

G. F. Moss, B.Sc.
and
D. Isaacs, B.Sc.

SUMMARY

Six component balance tests have been made on a 1/30th scale model at Mach numbers from 0.95 to 2.80. Some measurements of static pressure over the engine pods were made, and an investigation of the dynamic stability in pitch carried out.

The results show that there are significant effects due to head shape and fins on the size of the de-stabilizing pitching moments in a typical trajectory. The effect of body vortices on the measured static pressure is shown and the derived negative aerodynamic damping coefficients given. The reason for the latter is shown to be the presence of a step in the body profile, but the total damping is likely to be adequate for the rigid mode on the full scale missile.

Replaces R.A.E. Tech. Note No. Aero 2770 - A.R.C. 23 743.

LIST OF CONTENTS

		Page
1	INTRODUCTION	6
2	MODEL DETAILS	6
3	DETAILS OF TESTS	7
	3.1 Test range	7
	3.2 Axes and definitions	7
	3.3 Subsonic wall corrections	7
	3.4 Accuracy	7
	3.5 Presentation of results	8
4	RESULTS AND DISCUSSION	8
	4.1 Normal force and pitching moment	8
	4.1.1 The effect of the rear step	9
	4.1.2 The effect of the fins	9
	4.1.3 Effect of incidence	9
	4.1.4 Lift curve slope and stability at $\theta = 0^{\circ}$	9
	4.1.5 Pitching moment	10
	4.1.6 Comparison with results from other tunnels	10
	4.2 Rolling moments	10
	4.3 Axial force	11
	4.4 Pressure measurements	11
	4.5 Dynamic instability in pitch	11
	4.5.1 Oscillatory characteristics	11
	4.5.2 Aerodynamic factors	12
	4.5.3 Model geometry and roll position	12
	4.5.4 Implications full scale	12
	4.5.5 Discussion	12
5	CONCLUSIONS	13
LIST OF REFERENCES		14
APPENDIX 1		15
ILLUSTRATIONS - Figs.1-85		-
DETACHABLE ABSTRACT CARDS		-

LIST OF ILLUSTRATIONS

	Fig.
General arrangement of model	1
Axes system	2
Assumed C.G. position of missile	3
Model photographs	4&5
Schlieren photographs : $\theta = 10^{\circ}$	6

LIST OF ILLUSTRATIONS (Contd)

	Fig.
$-C_z$ v θ : With head 'B' at M = 0.95	7
C_m v θ : " " " " "	8
$-C_z$ v θ : " " " " M = 1.13	9
C_m v θ : " " " " "	10
$-C_z$ v θ : " " " " M = 1.19	11
C_m v θ : " " " " "	12
$-C_z$ v θ : " " " " M = 1.40	13
C_m v θ : " " " " "	14
$-C_z$ v θ : " " " " M = 1.4	15
C_m v θ : " " " " "	16
$-C_z$ v θ : " " " " M = 1.60	17
C_m v θ : " " " " "	18
$-C_z$ v θ : " " " " M = 2.00	19
C_m v θ : " " " " "	20
$-C_z$ v θ : " " " " M = 2.40	21
C_m v θ : " " " " "	22
$-C_z$ v θ : " head 'D' " M = 1.40	23
C_m v θ : " " " " "	24
$-C_z$ v θ : " " " " M = 1.60	25
C_m v θ : " " " " "	26
$-C_z$ v θ : " " " " M = 2.00	27
C_m v θ : " " " " "	28
$-C_z$ v θ : " " " " M = 2.40	29
C_m v θ : " " " " "	30

LIST OF ILLUSTRATIONS (Contd)

	Fig.
$-C_z$ v θ : With head 'D' at M = 2.80	31
C_m v θ : " " " " "	32
$-C_z$ v θ : " head 'E' " M = 0.95	33
C_m v θ : " " " " "	34
$-C_z$ v θ : " " " " M = 1.19	35
C_m v θ : " " " " "	36
$-C_z$ v θ : " " " " M = 1.40	37
C_m v θ : " " " " "	38
$-C_z$ v θ : " " " " M = 1.60	39
C_m v θ : " " " " "	40
$-C_z$ v θ : " " " " M = 2.00	41
C_m v θ : " " " " "	42
$-C_z$ v θ : " " " " M = 2.40	43
C_m v θ : " " " " "	44
$-C_z$ v θ : " " " " M = 2.80	45
C_m v θ : " " " " "	46
Effect of head shape on C_z at $\phi = 0^o$: Rear step filled	47
" " " " " C_m " " " " "	48
Effect of the rear step on C_z	49
" " " " " " C_m	50
Effect of θ on lift slope and C.P. position	51-58
Effect of head shape on lift slope and C.P. position at M = 1.6	59-60
" " " " " " " at $\theta = 0^o$	61
" " " " " C.P. position at $\theta = 0^o$	62

LIST OF ILLUSTRATIONS (Contd)

	Fig.
Effect of Mach number and ϕ on lift slope at $\theta = 0^{\circ}$	63-66
" " " " " " " C.P. position at $\theta = 0^{\circ}$	67-70
Aerodynamic de-stabilizing moment at $\theta = 6^{\circ}$, $\phi = 0^{\circ}$	71-72
Comparison of results from 8' x 8', 8' x 6' and 3' x 3' tunnels	73-76
Rolling moments : head 'E', no fins	77
" " : effect of fins	78
Axial force coefficients at $\theta = 0^{\circ}$	79
Base drag corrections	80
Body static pressure distribution	81
Effect of stagnation pressure and M on θ for vibration onset	82
Structural damping for pitching vibrations	83
Approximate aerodynamic damping coefficient	84
Schlieren photographs : head 'B', M = 2.0	85

1 INTRODUCTION

Blue Streak is an inertia-guided ballistic missile approximately 70 ft long and 10 ft in diameter. The missile is to be powered by two rocket motors at the rear and since aerodynamic stability is negative, stable flight is to be achieved by servo control of the rocket nozzles swivelling in gymbals. The maximum value of the dynamic pressure for the proposed trajectory is 750 lb/ft^2 and occurs at an altitude of 40,000 ft when the Mach number is 1.6, but high values occur from high subsonic speeds up to a Mach number of about 3. Under these conditions the angular movement required of the nozzles is likely to be near the maximum available, so that there are two main problems from an aerodynamic point of view, firstly, the non-linearities and associated peak values at transonic speeds, and secondly the static stability at supersonic speeds up to about M = 3.0 (with particular reference to speeds near M = 1.6). The transonic problems have been investigated in Refs.1 and 2 in some detail using the present model in the 8 ft × 6 ft and 3 ft × 3 ft tunnels at R.A.E. The present tests were principally intended to check the stability at supersonic speeds up to M = 2.8, but a short investigation of the dynamic stability in pitch was also made.

2 MODEL DETAILS

The model, which was of 1/30th scale, represented the proposed flight layout in some detail, as may be seen in Fig.1. The basic shape is a cylinder 4.88 calibres long, the last 0.63 calibres being reduced to 0.9 calibres diameter to form a 'step' in the body profile. Heads of various shapes were fixed to the forward end of this cylindrical body, and for some tests four small stub fins were fitted immediately ahead of the rear step.

The complicated nature of the model is likely to cause some confusion, particularly when previous tunnel work is referred to. The state of the model for the present tests, unless stated otherwise, was as follows:-

Basic model configuration

(a) Engine pods included, but squared off at the base.

(b) Fuel pipes and the small body fairing included.

(c) Splines on both nose and body exposed.

(d) Rear step in body profile present.

(e) Fins and 'nose blister' (Refs.1 and 2) not included.

The four head shapes 'A', 'B', 'D' and 'E' used are shown in Fig.1, and it should be noted that in the configuration with head 'E', an extra nose fairing and two rear fairings (aft of the step) were included. The squaring off of the engine pods and the fin design were both new developments for these tests. A few extra tests were made with the nose splines faired (by filling the grooves between them), with the rear body step filled by means of an annular sleeve, and with the engine pods extended as in Refs.1 and 2. The stub fins were fitted for some of the tests with heads 'B' and 'D', but for the later tests with head 'E' these were not used since the inclusion of fins full scale had been abandoned.

The model was sting mounted and two internal strain gauge balances were used : a six component balance for the tests with heads 'A', 'B' and 'D', and a five component balance (no axial force) for the tests with head 'E'. Both balances had moment reference points just aft of the 'shoulder'. Base pressure was measured inside the hollow model and the effects of secondary flows were avoided by means of a baffle attached to the sting (Fig.4).

Transition was not fixed by means of wires or roughness bands, since the exposed splines would have been adequate in this respect. In the few cases tested with the splines faired there was a rapid change of profile at the same position which would have been equally effective.

3 DETAILS OF TESTS

The tests were made in the 8 ft × 8 ft supersonic tunnel at R.A.E. Bedford in three short series during September 1957, September 1958 and October 1959. The main part of the data was obtained from the last two series, but a few results from the first series, during which the rear step was faired throughout, have been included.

3.1 Test range

The Reynolds number for the tests was 0.75×10^6, based on calibre, except for the few results shown in Figs.47 to 50 from the first test series, where the Reynolds number was 1.21×10^6. The Mach number range was from $M = 1.13$ to $M = 2.80$, and in addition, some subsonic tests at $M = 0.95$ were made with head shapes 'B' and 'E'. At $M = 1.13$ there was some slight interference from the reflected bow shock at some incidences, but at and above $M = 1.19$ this shock was clear of the model base.

Both pitch and roll angles could be varied during the tests, and most of the data was obtained by pitching the model from $\theta = -4^\circ$ to $+12^\circ$ at roll settings of $\phi = 0$, 45 and 90°, but as a check on symmetry, a complete range of roll angles (i.e. $\pm 180^\circ$) was tested at $M = 0.95$, 1.19 and 1.20 with head 'B' and at $M = 1.40$ with head 'E'.

3.2 Axes and definitions

The axes system used is given in Fig.2. The roll setting angle is considered positive for a clockwise rotation from the zero position with the "small body fairing" uppermost, (Fig.1), and the pitch angle is defined as that between the missile axis and the free stream direction. The forces and moments presented here are quoted relative to an axis system moving with the missile in pitch but not in roll. The pitching moments are given about the expected full scale C.G. position, the variation of this with Mach number being shown in Fig.3.

The force coefficients have been based on the area $\frac{\pi d^2}{4}$ and the moment coefficients on $\frac{\pi d^3}{4}$, where 'd' is the missile calibre. The area for base drag correction was taken as $(0.9)^2 \frac{\pi d^2}{4}$, i.e. the area with the rear step allowed for, but without the base area of the pods.

3.3 Subsonic wall corrections

For the tests at $M = 0.95$ the correct speed was assumed to be the empty tunnel value increased by 0.43 of the peak rise measured at the tunnel walls. This correction was in fact only 0.005 in Mach number since the model was unusually small for the 8 ft × 8 ft tunnel (0.14% cross-sectional area ratio). No constraint corrections have been applied to lift curve slope or drag.

3.4 Accuracy

As a rough guide based on experimental scatter the following can be taken:-

θ and ϕ	$\pm 0.05^{\circ}$
$-C_z$, C_m and $-C_x$	± 0.01
C_ℓ	± 0.002
C_p	± 0.005

(See also reference in 3.5 to weight correction errors.)

3.5 Presentation of results

The main part of the data given here is presented as graphs of $-C_z$ and C_m against θ and ϕ in carpet form (Figs.7-46). In these carpets the nominal values of ϕ have been quoted since the variation due to aerodynamic load was very small, and in the resolution of the balance forces and moments for calculation of $-C_z$ and C_m the nominal values of ϕ have also been used. The pitch angles quoted, however, have been obtained by taking the mean of the plotted values at all the roll settings available. The actual values of θ, however, were usually within $\pm 0.05^{\circ}$ of the mean values quoted. Where tests with fins were made, these results have been included as dotted lines against θ only. The appropriate moment reference point in calibres aft of the shoulder ("C.A.S.") is given on each plot of C_m.

There was a small variation in $-C_z$, C_m and C_ℓ with roll angle when the model axis was along wind ($\theta = 0^{\circ}$), and since this was mainly due to slight errors in the application of model weight corrections rather than to tunnel flow deflections, it was considered best to make this line on each carpet straight, adjusting the whole of each constant $-\phi$ curve so that the slopes with respect to θ would not be affected. For the most part these corrections were within ± 0.02 for $-C_z$ and C_m and within ± 0.002 for C_ℓ.

The lift slopes and C.P. positions shown in Figs.51-70 and 73-76 were derived graphically. In one or two cases the slopes were also obtained by the method of least squares as a check on accuracy.

Base drag has been subtracted from the measured axial force in the usual way. This is shown in Fig.80.

4 RESULTS AND DISCUSSION

4.1 Normal force and pitching moment

The basic data is shown in Figs.7-46 for the model with heads 'B', 'D' and 'E'. In general the curves are surprisingly free from irregularities considering the model was far from aerodynamically clean. In this respect the symmetry of the results with roll angle is also notable, particularly at $M = 0.95$ (Figs.7 and 8), but this was not checked at higher speeds or with the blunter head 'D'. A few results from the first series of tests have been included in Figs.47 and 48 to show that the lift and stability results with head 'A' lie, as might be expected, between those with heads 'B' and 'D'. No other tests with head 'A' were made.

4.1.1 The effect of the rear step

Since the first series of tests were made with the rear step faired, and although there were other slight model differences, the selected comparisons with results from the later series shown in Figs.49 and 50 may be used to indicate the effect of the rear step on lift and stability. The lift curve slope is little changed, but the presence of the step appears to cause a small forward shift in the centre of pressure position particularly with the stub fins present (about 0.1 calibres). The induced flow separations at the step might well be expected to decrease the efficiency of the fins, but the flow structure near the step, pods and fins is complex, as may be judged from the oil flow photograph in Fig.5.

4.1.2 The effect of the fins

In Figs.7-46, the curves of normal force without the fins present are non-linear with incidence (due to the cross-flow body lift) and the pitching moment curves are almost straight, but with the fins added the normal force curves become steeper and the pitching moment curves very non-linear. The effect of the fins on pitching moment is particularly evident at M = 0.95 and the lower supersonic speeds (e.g. Figs.8 and 10) and at roll angles near 90° (i.e. when the engine pods are across the flow). The fins lie ahead of the pods with respect to the local flow and have the same disposition at both $\phi = 0^\circ$ and 90° (Fig.1). It is thus probable that the fins cause an adverse interference effect on the lift from the pods at $\phi = 90^\circ$ and that this adverse effect is reduced rapidly with increase of incidence. This is made clear by the lift slopes and C.P. positions given in Figs.51 and 52 which have been obtained from Figs.7 and 8 for the model with head 'B' at M = 0.95. The curves for $\phi = 0^\circ$ show the large effect of the fins on C.P. position which decreases steeply with incidence. Comparing the curves at $\phi = 90^\circ$ with those at $\phi = 0^\circ$, the rearward C.P. shift due to the pods is reduced at zero incidence by the presence of the fins from 2.7 calibres to 0.9 calibres, but at an incidence of 10° this reduction is only from 1.0 to 0.65 calibres. This adverse effect of the fins on the lift from the pods is much smaller at higher speeds.

4.1.3 Effects of incidence

The typical effect of incidence on the lift slope and centre of pressure position is shown in Figs.53-58 for the configuration with head 'E' and in Figs.59-60 with heads 'B', 'D' and 'E'. The orientation of the engine pods causes large changes in the rate at which the C.P. moves aft with incidence, particularly at speeds near M = 1. At M = 1.6, the C.P. position moves 1.1 calibres aft at $\phi = 0^\circ$ for a 10^c increase in θ, and at $\phi = 90^\circ$ this movement is 0.8 calibres. However, at M = 0.95 the C.P. movement is almost 2 calibres at $\phi = 0^\circ$ and only 0.5 calibres at $\phi = 90^\circ$. The inference is that the extra lift from the pods is larger at speeds near M = 1 than at higher speeds, but it decreases much more rapidly with incidence. The effect of removing the pods at $\phi = 0^\circ$ is shown in Ref.1 to be small (less than 0.15 calibres) and so the $\phi = 0^\circ$ case in the present tests can be taken as being equivalent to a 'pods off' condition.

4.1.4 Lift curve slope and stability at $\theta = 0^c$

As regards the lift slopes and C.P. position at zero incidence, there is a significant effect of head shape, as may be seen from Figs.61 and 62. The lift slope with the blunt shape 'D' is smaller than that with the conical head shape 'B' particularly at high speeds (20% lower at M = 2.4) but the position of the aerodynamic centre is hardly affected. On the other hand the comparatively small geometrical

differences between the heads 'B' and 'E' cause as much as a 0.5 calibre change in C.P. position at high speeds with little change in lift slope. This applies at all roll angle settings, but the rearward shift in C.P. position at $\phi = 90^{\circ}$, due to the pods, appears to be almost independent of head shape and decreases with increase of Mach number so that the C.P. position is almost stationary over the test range $0.95 \leq M \leq 2.8$.

The effect of fins and roll angle at $\theta = 0^{\circ}$ is summarised in Figs.63-70. The symmetry of lift slope and C.P. position with ϕ is worth noting, and the small influence of head shape on the effect of the fins and pods.

4.1.5 Pitching moment

From the preceding sections it is obvious that the forward position of the centre of pressure at $\phi = 0^{\circ}$ is the worst case from a control point of view, but the variation of lift slope missile C.G. position and dynamic pressure in flight will affect the maximum value of the de-stabilizing moment. In Figs.71 and 72 values of $C_{m_{C.G.}}$ at $\theta = 6^{\circ}$ are given, and using the expected variation of dynamic pressure full scale, the total static pitching moment about the C.G. has been calculated. The maximum pitching moment occurs with head 'E', and this is 9% higher than that with head 'B' although the differences in head shape are comparatively small. The configuration with the blunter head shape ('D') has much smaller moments at high speeds.

4.1.6 Comparison with results from other tunnels

This is shown in Figs.73-76. Tests have been made with the present model and balance in the R.A.E. 8 ft × 6 ft and 3 ft × 3 ft tunnels (Refs.1 and 2), but at an earlier date when the geometry of the model was less certain. It is thus difficult to find identical configurations and the examples shown here represent the nearest comparisons possible. The test results given from the 8 ft × 6 ft and 3 ft × 3 ft tunnels (at Reynolds numbers of 0.65×10^6 and 0.85×10^6 respectively) were made with a nose fairing similar to that used with head 'E' in the present tests. For $0.8 < M < 1.2$ the results of Ref.1 show that removing this fairing reduces $\frac{\partial C_z}{\partial \theta}$ by 0.0015 approximately and moves the C.P. position forward by 0.1 calibres. Allowance for these adjustments will reduce the discrepancy between the results from the three tunnels. If the pod extensions used in some of the tests can be assumed to have caused only slight effects, the overall impression from these comparisons is one of fair agreement.

4.2 Rolling moments

These are shown in Figs.77 and 78, and, as might be expected for this configuration, the general level is small and not likely to raise any problems full scale. There are several items of interest, however. Firstly, although the rolling moment at zero pitch angle is negligible with head 'B', this is by no means so with heads 'D' and 'E'. This 'basic' rolling moment varies with Mach number and may be due to wake interference between the nose fairing and the pods in the case of the model with head 'E', but the reason for this with the blunt head 'D' is obscure. Secondly, although the rolling moment varies smoothly with incidence, the variation with roll angle is far from symmetrical, presumably due to the asymmetry of the pipes. Finally, the effect of the fins is larger with the blunter head 'D' than with the conical head 'B', particularly at $\phi = 0^{\circ}$ when, apart from the pipes, the model is symmetrically disposed to the stream. The maximum value of the rolling moment coefficient occurs near $\phi = 60^{\circ}$, determined by the mutual interaction between the pipes, pods and fins.

4.3 Axial force

Fig.79 gives the values of $-C_x$ at $\theta = 0^\circ$ plotted against Mach number. The axial force coefficient with head 'B' reaches a maximum value at a Mach number of 1.2, but with the blunt head shape 'D' the axial force continues to rise rapidly with Mach number up to about M = 1.60, and remains roughly constant above M = 2.0 at a level more than twice that with head 'B'. The increase in axial force due to the fins is much larger with the blunter head shape 'D' than with head 'B', but the reason for this is not known.

A comparison is made with some results from the 8 ft × 6 ft tunnel tests[1] for the model with head 'B'. The values appear to agree at subsonic speeds but to differ by about 20% at supersonic speeds. This is much more than might be expected from the small model differences in the two cases, and can only be ascribed to interference effects from the reflected bow shock at low supersonic speeds.

4.4 Pressure measurements

Measurements of body static pressure are presented in Fig.81. These were obtained from a single static hole 0.69 calibres ahead of the rear step and at a clockwise roll angle of 34°. This static hole was positioned between two of the longitudinal splines but the effect of the local secondary flows on the measured pressures must have been quite small and can be ignored in this context.

Two points are worth noting. Firstly there is an asymmetry in the measured pressures on the two sides, presumably due to the presence of the fuel pipes, etc. Secondly, at the higher incidences there is an inflexion in the circumferential distribution of pressure due to the presence of a pair of body vortices. The effect of these is apparent at a pitch angle of 6° at speeds near M = 1, but at progressively higher angles at the higher speeds. There are also indications that the pressure field of the vortices is most intense near M = 1.40, when the general level of body static pressure is at a minimum.

4.5 Dynamic instability in pitch

During the routine tests of static stability it was noticed that there was a marked tendency for the model to become unsteady at high Mach numbers and high incidences. Similar experience was encountered during the 3 ft × 3 ft tunnel tests reported in Ref.2. This 'unsteadiness' made the measurement of static forces and moments difficult, and it was decided to make a special investigation of the phenomenon to try and determine its cause. Measurements of model amplitude and frequency were made under various conditions and some oil flow studies carried out. The results of these tests are given below.

4.5.1 Oscillatory characteristics

Film records of the model amplitude showed that the model 'unsteadiness' was in the form of a divergent pitching oscillation, approximately sinusoidal and with a frequency of 28 c.p.s. (equivalent to a reduced frequency based on diameter of 0.035 at M = 2). The frequency of oscillation was sensibly constant under all tunnel conditions since the aerodynamic stiffness was small compared with the structural stiffness. The oscillations, once started, appeared to diverge until the mechanical stops were reached, or, in the cases where no stops were fitted, until the aerodynamic excitation was balanced by the amplitude-sensitive structural damping (see Fig.83). Amplitudes as high as ±2°

were recorded on occasions, equivalent to a balance pitching moment signal stress of ±30,000 lb per sq in.

The axis of oscillation was at approximately one calibre aft of the 'shoulder', as may be seen from the Schlieren photographs in Fig.85. Both frequency and axis position were almost independent of the roll angle setting of the model.

4.5.2 Aerodynamic factors

As pitch angle was increased, a critical value was reached for the divergent oscillation to start, and this critical angle was independent both on Mach number and stagnation pressure, as may be seen in Fig.82. The effect of Mach number was not fully investigated, but at constant Reynolds number, instability worsened as the Mach number was increased to M = 2, thereafter recovering a little. No oscillations were encountered at subsonic speeds, but pitch angles greater than 10° were not investigated. The effect of stagnation pressure increase at constant Mach number was to lower the critical pitch angle and to worsen the hysteresis between increasing and decreasing values of θ. On one occasion at a high stagnation pressure, the oscillations, once started at a pitch angle of 8°, did not stop even when the angle was reduced to zero. At constant Reynolds number, the appreciable decrease in air density with increase in Mach number could have been expected to be favourable. The inference is that the adverse effect of Mach number increase must have been strong to override the effect of reduced density, at any rate up to M = 2.

4.5.3 Model geometry and roll position

The configuration with the pointed head 'B' appeared to be much more prone to vibration than that with the blunter head 'D'. On the other hand, the addition of the fins or rolling the model until the pods were across the pitching direction (i.e. $\phi \simeq 90°$) each stabilized the model, presumably by increasing the aerodynamic damping. However, the most significant effect of model geometry was that of fairing the rear step since this removed all tendency for vibrations to develop under all conditions even though the pitch angle was increased to 15°.

4.5.4 Implications full scale

At M = 2 the natural frequency of the full scale missile, considered as a rigid body oscillating about the C.G., is expected to be in the region of 1 c.p.s., and this fortuitously gives a reduced frequency very near that of the present model. However, the axis of natural oscillation full scale is expected to be a little over a calibre aft of that on the tunnel model, and if we assume that the instability is due to some rearward excitation, this means that the tunnel results can be taken as a little pessimistic on this account.

4.5.5 Discussion

The flow field over the step, investigated with surface oil, showed remarkable insensitivity to pitch angle, so it is difficult to ascribe the loss of stability to a change in the flow regime over the rear step (subject, say, to Mach number and Reynolds number). Again, there seems to be little chance of a wake resonance effect being responsible, since measurements with a transducer (which can be seen in the lower photograph of Fig.85) demonstrated that there was no disproportionate spectrum of model vibration frequency in the wake. The presence of non-linearities in the static stability curves was carefully looked for, using continuous line recorders, but no signs of these were observed.

In view of these observations and that there seems to be little doubt that the presence of the rear step was the prime cause of the instability, the most probable explanation would appear to be that the model has negative aerodynamic damping due to time lags in the separated flow at the rear step which, as pitch angle is increased, also increases, depending on Mach number and perhaps Reynolds number, until the positive structural damping of the rig is overcome and divergence ensues. At first this solution seemed unlikely since the frequency parameter was so low (stream wave-length is about 30 times the body length), but the damping coefficient of the basic body is probably very small, and could easily be made negative by very small lags in flow formation at the step.

In order to obtain some approximate values of the negative aerodynamic damping coefficient, the level of structural damping was measured by a decaying oscillation experiment and is shown in Fig.83. There is a large variation with model amplitude and a value at a semi-amplitude of $\pm 0.25^\circ$ has been arbitrarily selected to represent the level exceeded by the negative aerodynamic damping at divergence. The possible effects of Reynolds number were ignored, and at each recorded value of pitch angle for divergence, $-(m_\dot{\varphi} + m_w)$ was calculated using body calibre and the free stream values of U and ρ. The results are plotted in Fig.84, and, as in Fig.82, it is presumed that the scatter between successive tests was due to variations in structural damping. For the full scale missile, the amount of artificial positive damping included to correct the main servo loop lag is very much larger numerically than the values quoted in Fig.84. Thus no dynamic instability is likely full scale, provided there are no large adverse effects of Reynolds number and Mach number. It must, however, be noted that it is not within the scope of this investigation to say whether any of the bending modes of the full scale missile are likely to be affected.

5 CONCLUSIONS

(i) Static stability

In general the results are free from irregularities, but the orientation of the engine pods caused large changes in the movement of the C.P. with incidence, particularly at high subsonic and low supersonic speeds. These effects were very much accentuated with the stub fins present owing to fin-pod interference. The comparatively small geometrical differences between the head shapes 'B' and 'E' caused significant changes in C.P. position particularly at the high end of the speed range, but the large difference between shapes 'D' and 'B' caused less effect. The missile with the blunt head 'D', however, had a considerably lower lift-curve slope than with the conical heads (as much as 25% less at $M = 2.8$). The largest de-stabilizing pitching moments occur at a roll orientation of zero, and for a typical flight trajectory, the maximum moment at an incidence of 6° is likely to be 9% higher, with the 'E' head shape than with the 'B' and 'D' shapes.

(ii) Rolling moments

Although all the rolling moments measured were small, the increase due to the addition of the fins was more marked with the blunt head shape 'D'. The maximum rolling moment occurred at a roll setting of $\phi = 60^\circ$.

(iii) Axial force

The axial force coefficient with head 'B' was approximately 45% of that with head 'D' at speeds above $M = 1.6$, and the increase due to the fins was also much smaller.

(iv) Pressure measurements

These showed the presence of a body vortex field above incidences of 6° at the lower Mach numbers tested, this angle being progressively larger at higher speeds.

(v) Dynamic instability

Investigations of a divergent oscillation which occurred on the model under certain conditions have suggested that the missile full-scale is likely to have negative aerodynamic damping due to the presence of the rear step. The size of the coefficients measured in the tunnel, however, is very much smaller numerically than that already proposed for the main servo loop, and thus no instability of the rigid mode should occur in flight.

LIST OF REFERENCES

No.	Author(s)	Title, etc
1	Courtney, A.L.	8 ft × 6 ft tunnel tests on a model of the De Havilland Blue Streak at Mach numbers of 0.80 to 1.25. A.R.C.21756. April 1959.
2	Huntley, E.	Wind tunnel measurements of normal force and pitching moment at a Mach number of M = 2.00 on a 1:30 scale model of Blue Streak. A.R.C. C.P.732. May 1959.

APPENDIX 1

TESTS ON THE 1/30TH SCALE MODEL OF BLUE STREAK IN OTHER WIND TUNNELS

The tests reported in Ref.1 were made in the 8 ft x 6 ft transonic tunnel at R.A.E. Farnborough between February and April, 1957, and were principally concerned with the overall static stability at transonic speeds. The effects of fins (different to those of the present Note), alternative head shapes (A, B and C) and various other missile components such as external stringers, fuel pipes, rear pods, etc. were measured. The tests were made at a Reynolds number based on calibre of $0{\cdot}65 \times 10^6$, compared with a value of $0{\cdot}75 \times 10^6$ for the majority of the 8 ft x 8 ft tunnel tests. The results showed that, about the flight C.G. position, a roughly linear variation of C_m with θ existed, with no serious irregularities within the range of Mach numbers (0·80 to 1·25), roll angles (0° to 90°) and incidences (-3° to +15°) investigated, except with the fins present where there was some non-linearity, particularly at subsonic speeds. At zero incidence the values of $dC_m/d\theta$ were greater than was expected from earlier tests on simple cone-cylinders, however, this discrepancy was shown to be entirely attributable to the various model components (stringers, pipes, pods, rear steps etc.).

In order to obtain some preliminary results at supersonic speeds before the 8 ft x 8 ft wind tunnel became operative, the model was tested in the 3 ft x 3 ft tunnel at R.A.E. Bedford between April and July, 1957 [2]. Because of the large size of the model relative to the 3 ft x 3 ft working section, tests were possible at supersonic speeds at M = 2·0 only, due to shock wave reflection. Two head shapes were tested (A and B), and the effect of fins (identical to those tested in the 8 ft x 6 ft tunnel) pods, splines, pipes and rear step fairing determined. In addition the effect of the rear step fairing was measured at subsonic speeds, at M = 0·70 and 0·90, in order to check the discrepancy in $dC_m/d\theta$ which had been found in the transonic tests in the 8 ft x 6 ft tunnel. All tests were made at a Reynolds number based on calibre of $1{\cdot}24 \times 10^6$ except for the two configurations with head B (tested at M = 2·0 only), which were tested at a Reynolds number of only $0{\cdot}43 \times 10^6$, the restriction being due to model oscillations of the type described in the present Note, which were encountered at higher Reynolds numbers.

A comparison of the results obtained in all three tunnels shows fair to good agreement for the few comparable configurations, viz:-

(a) The variation of $dC_z/d\theta$, $dC_m/d\theta$ and x c.p. with Mach number for heads A and B at zero roll angle (present Note and Ref.1).

(b) The variation of C_z and C_m with θ at M = 0·8, 0·9 and 1·2 for head A at zero roll angle[1].

(c) The increments in $dC_z/d\theta$ and $dC_m/d\theta$ due to the presence of the rear step[1].

Printed in England for Her Majesty's Stationery Office by the Royal Aircraft Establishment, Farnborough. W.T.59.K.4

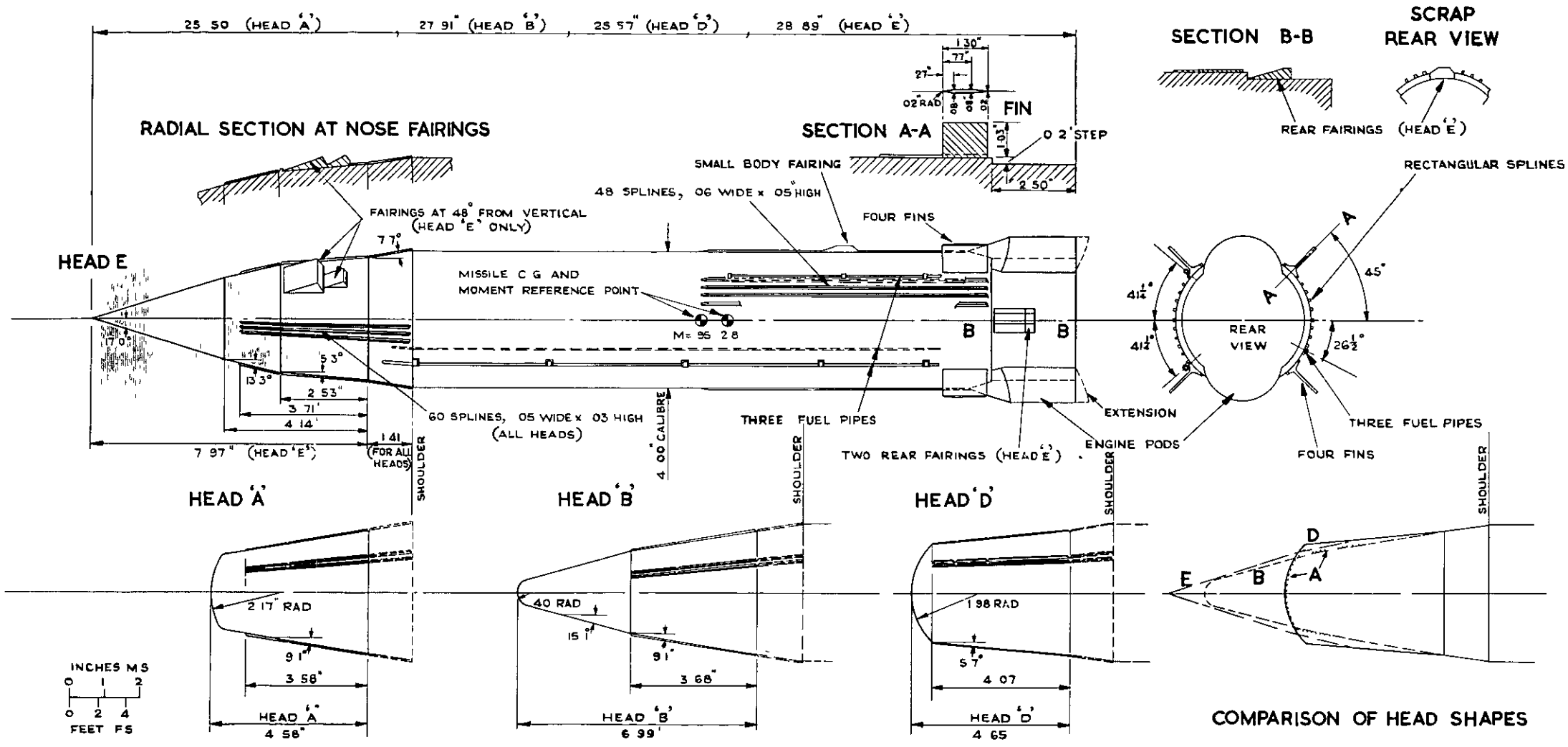

FIG.1. GENERAL ARRANGEMENT OF MODEL

AXES MOVE WITH MODEL IN PITCH
BUT NOT IN ROLL.

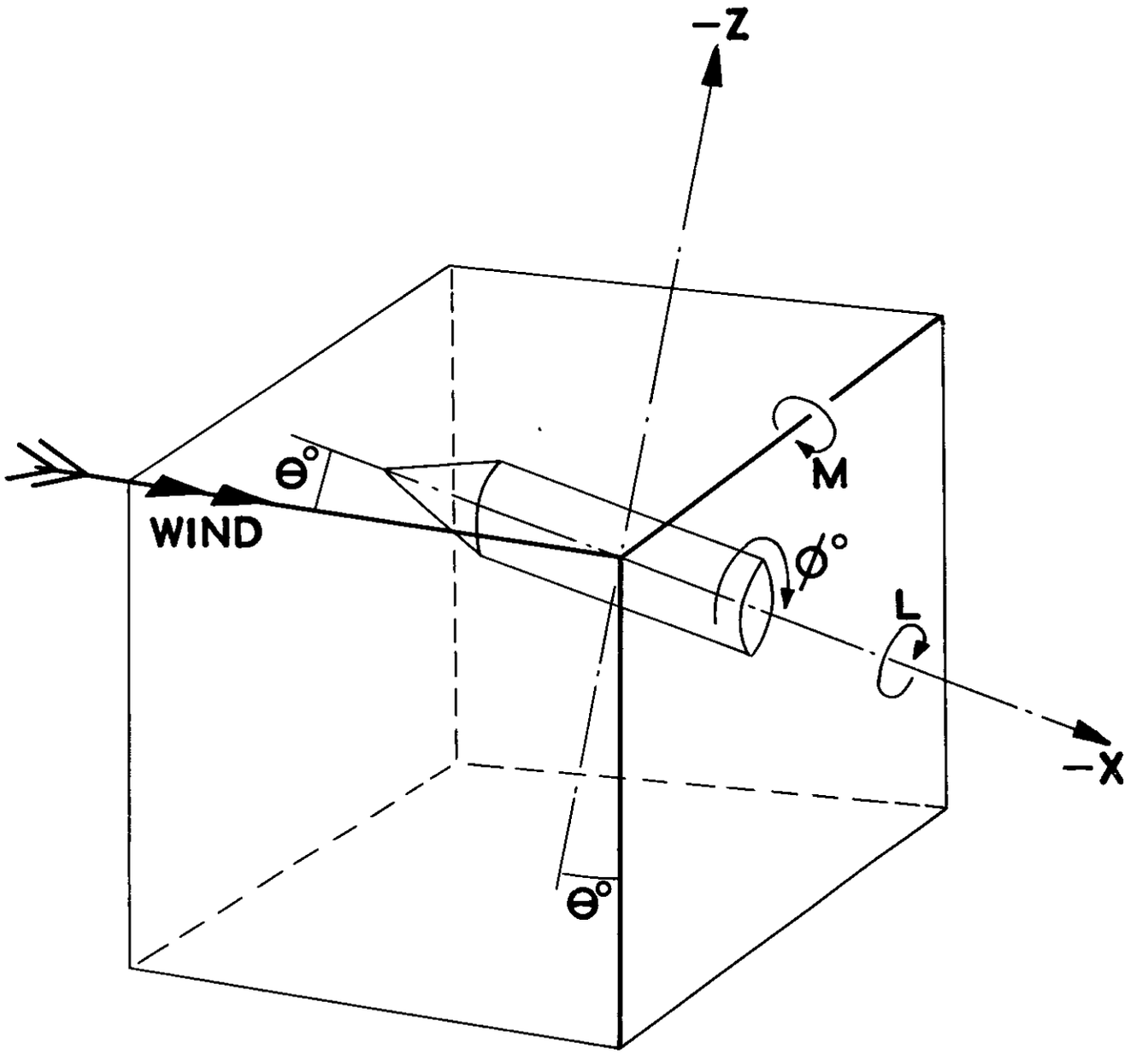

FIG. 2. AXES SYSTEM

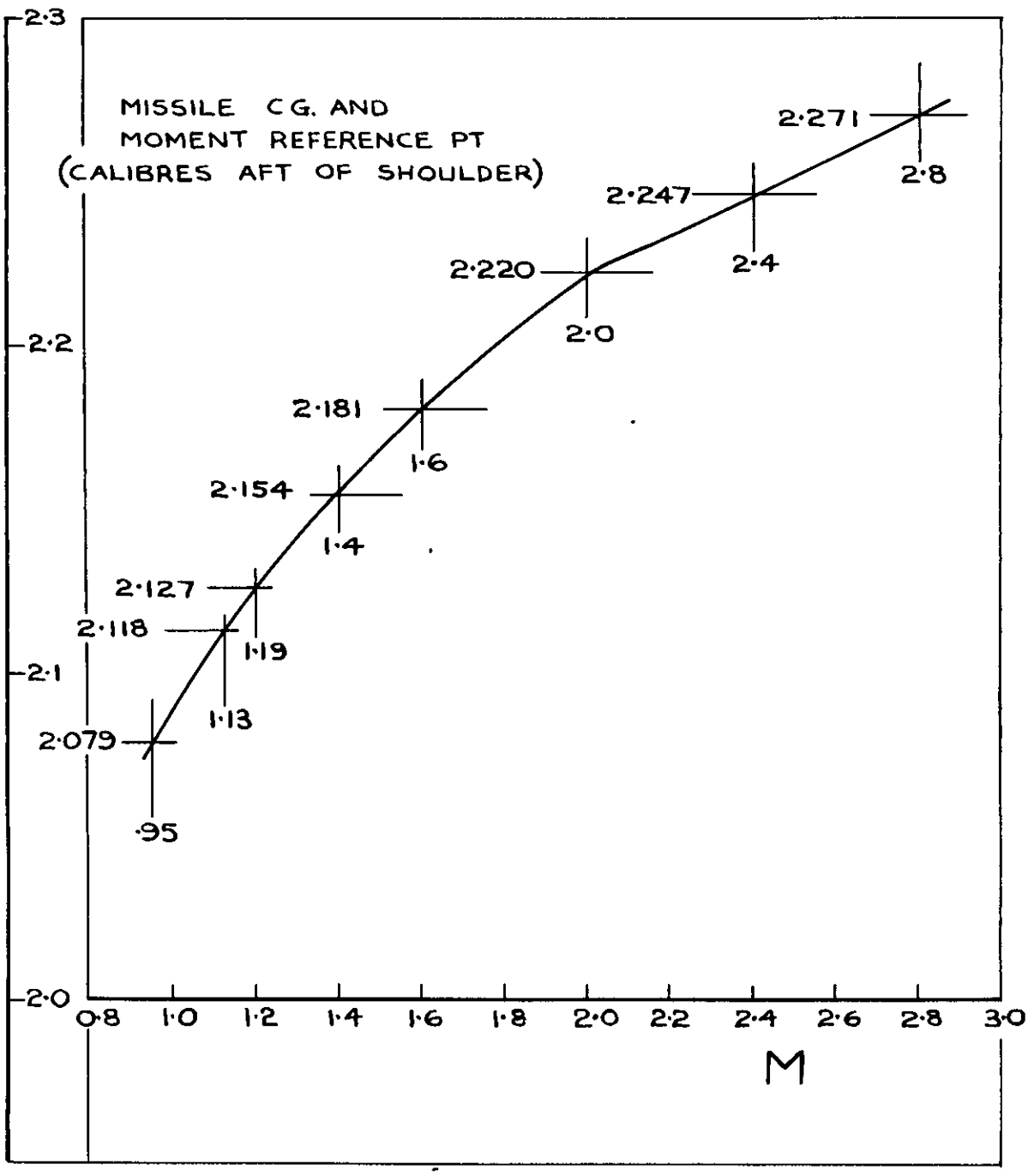

FIG. 3. ASSUMED C.G. POSITION OF MISSILE

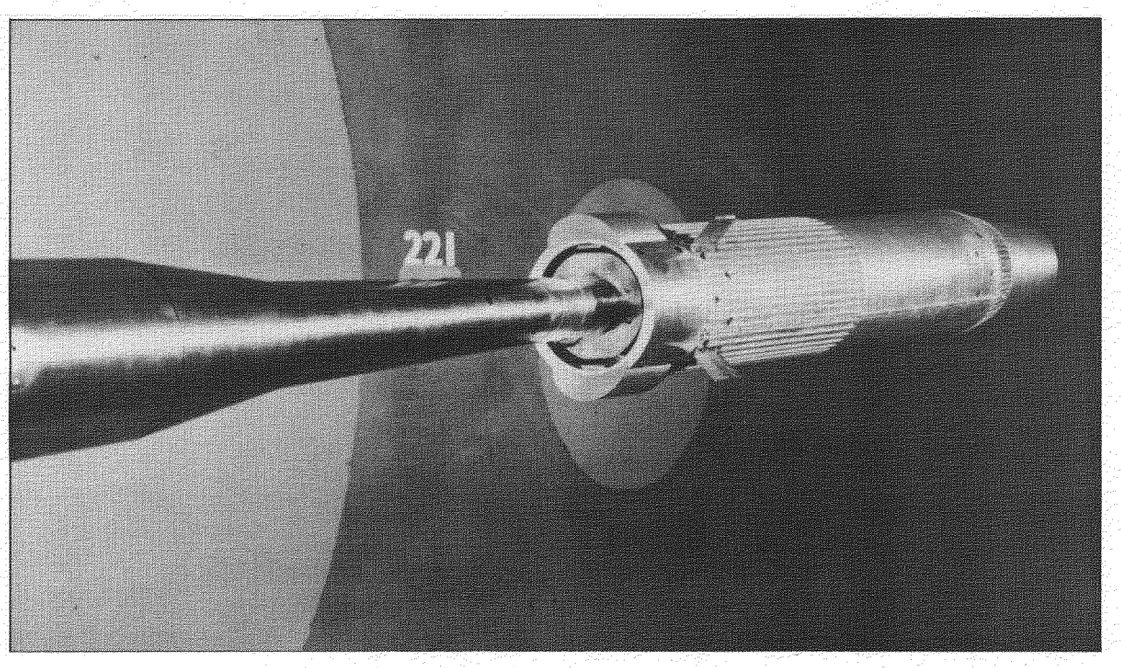

FIG.4. THE MODEL IN THE 8ft x 8ft WIND TUNNEL: HEAD 'D' WITH FINS: REAR STEP FILLED: NOSE SPLINES FAIRED: PODS EXTENDED

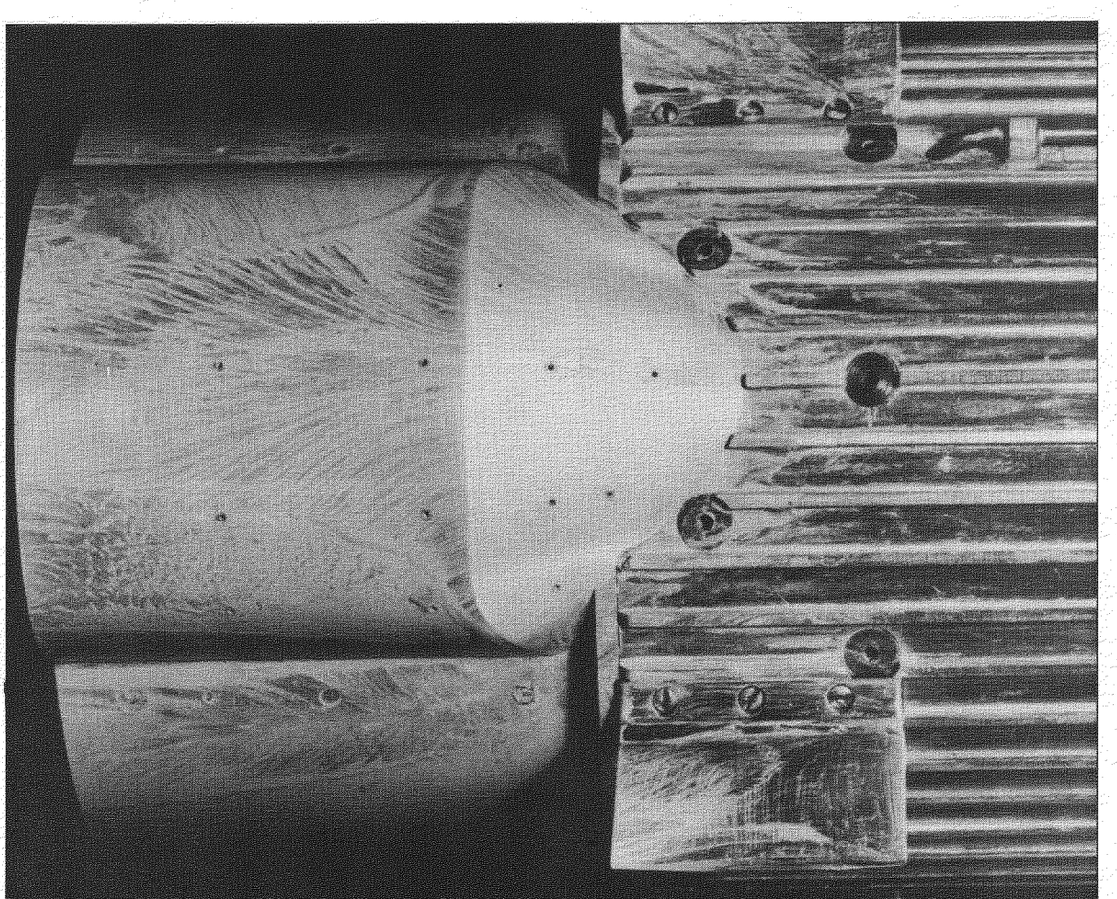

FIG.5. OIL FLOW STUDY OF THE TOP ENGINE POD: HEAD 'B' WITH FINS: M=2·00: $\phi = 0°$: $\theta = 12°$: STAG. PRESS. = 15 INS. MER.: WITH REAR STEP

FIG.4 & 5. MODEL PHOTOGRAPHS

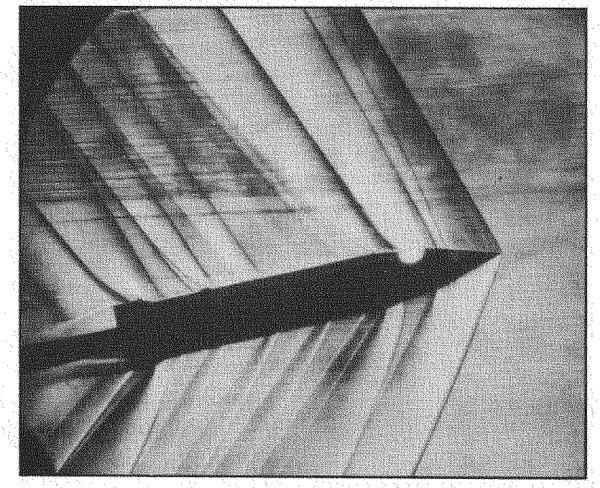

HEAD 'E'; $\phi = 0$; M = 1.20

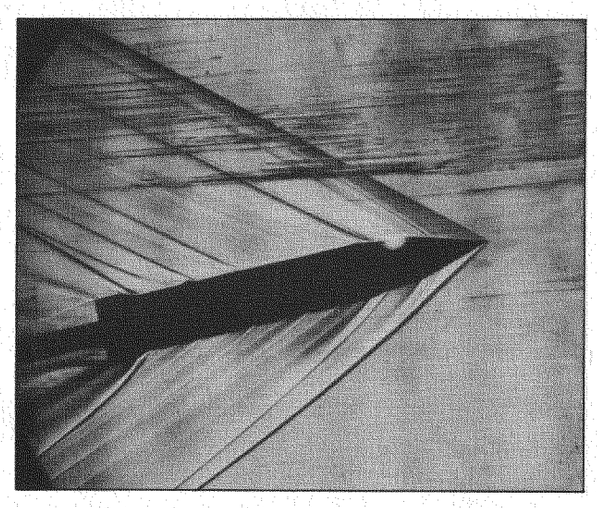

HEAD 'E'; $\phi = 0$: M = 2.00

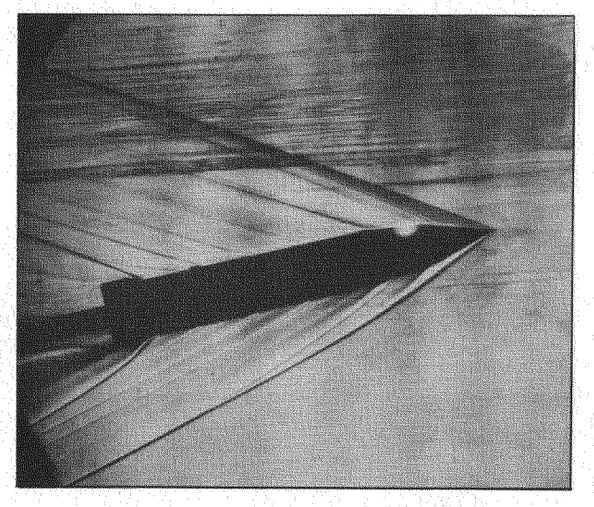

HEAD 'E': $\phi = 0$: M = 2.80

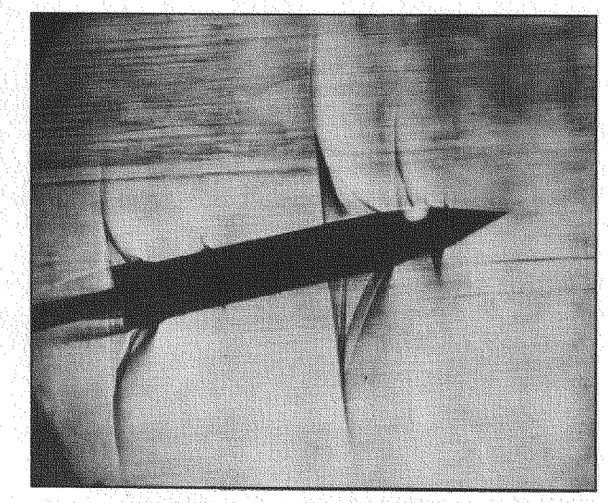

HEAD 'E': $\phi = 0$: M = 0.95

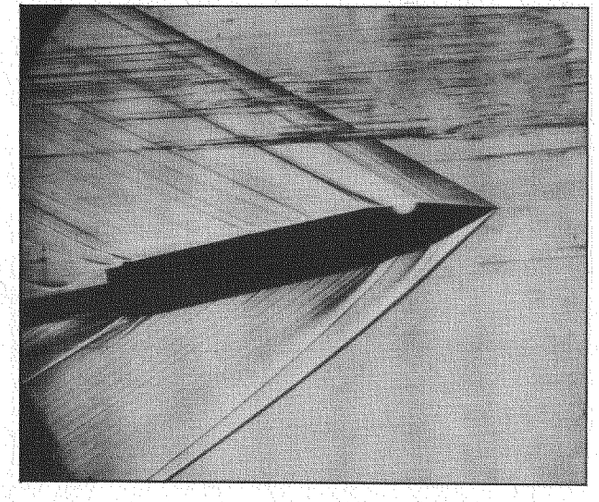

HEAD 'E': $\phi = 90^0$: M = 2.00

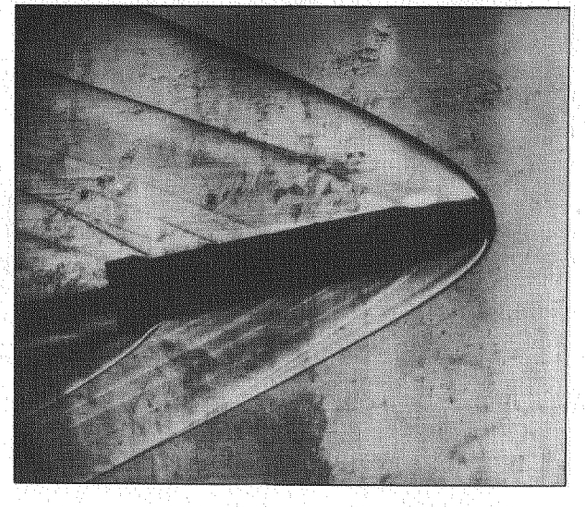

HEAD 'D': $\phi = 0$: M = 2.80

FIG.6. SCHLIEREN PHOTOGRAPHS: $\theta = 10°$

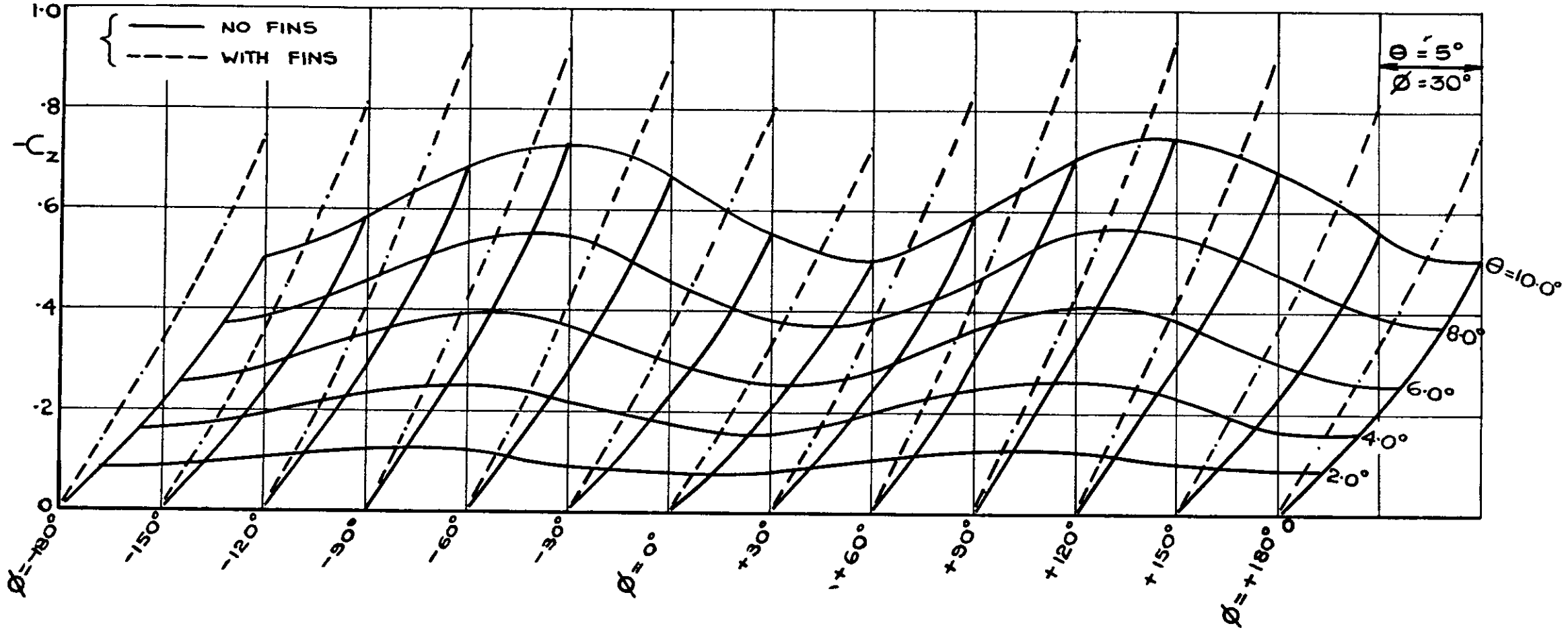

FIG. 7. : $-C_z$ v Θ : WITH HEAD 'B' AT M = 0·95.

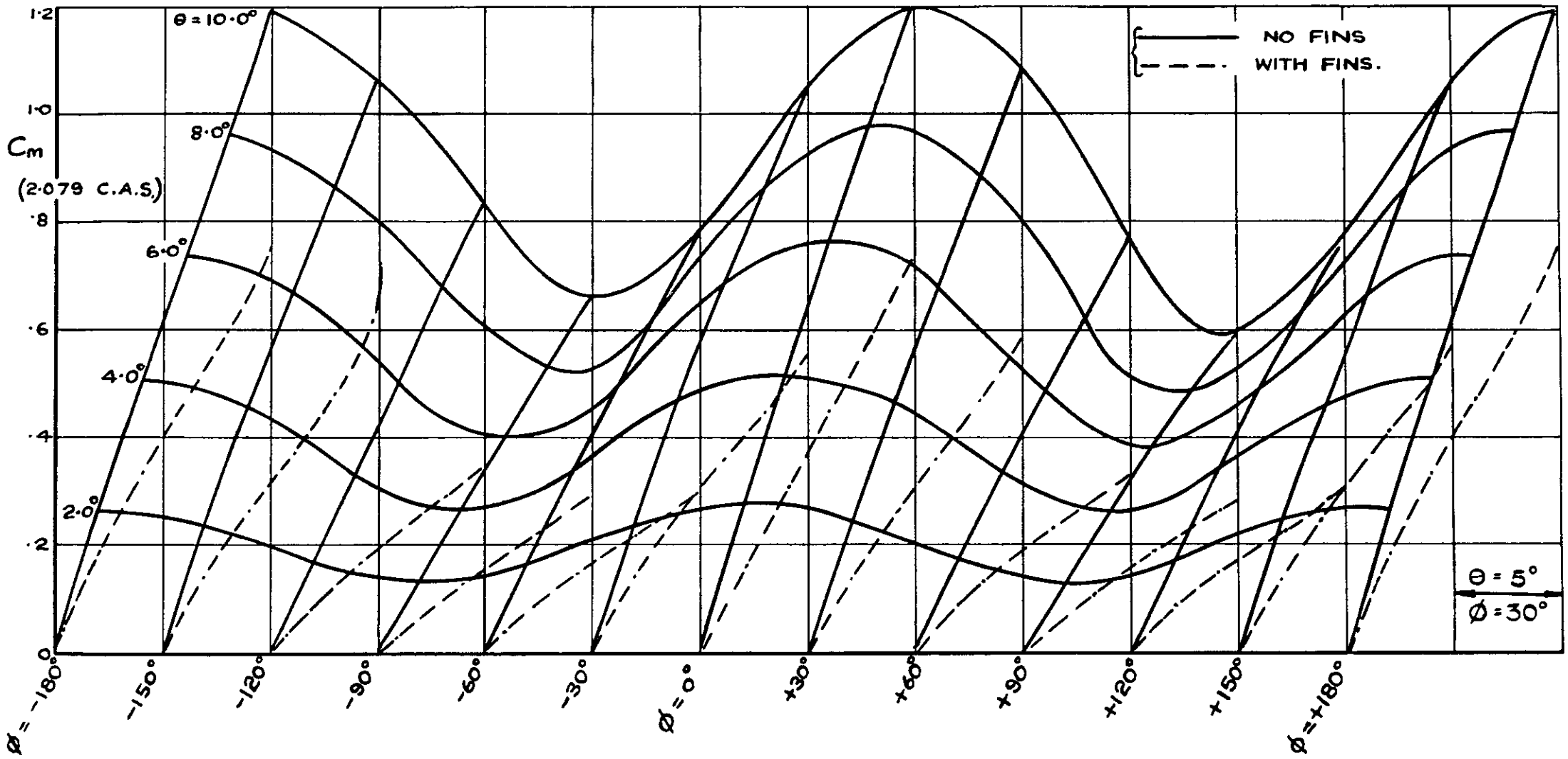

FIG 8: Cm v θ : WITH HEAD 'B' AT M = 0·95

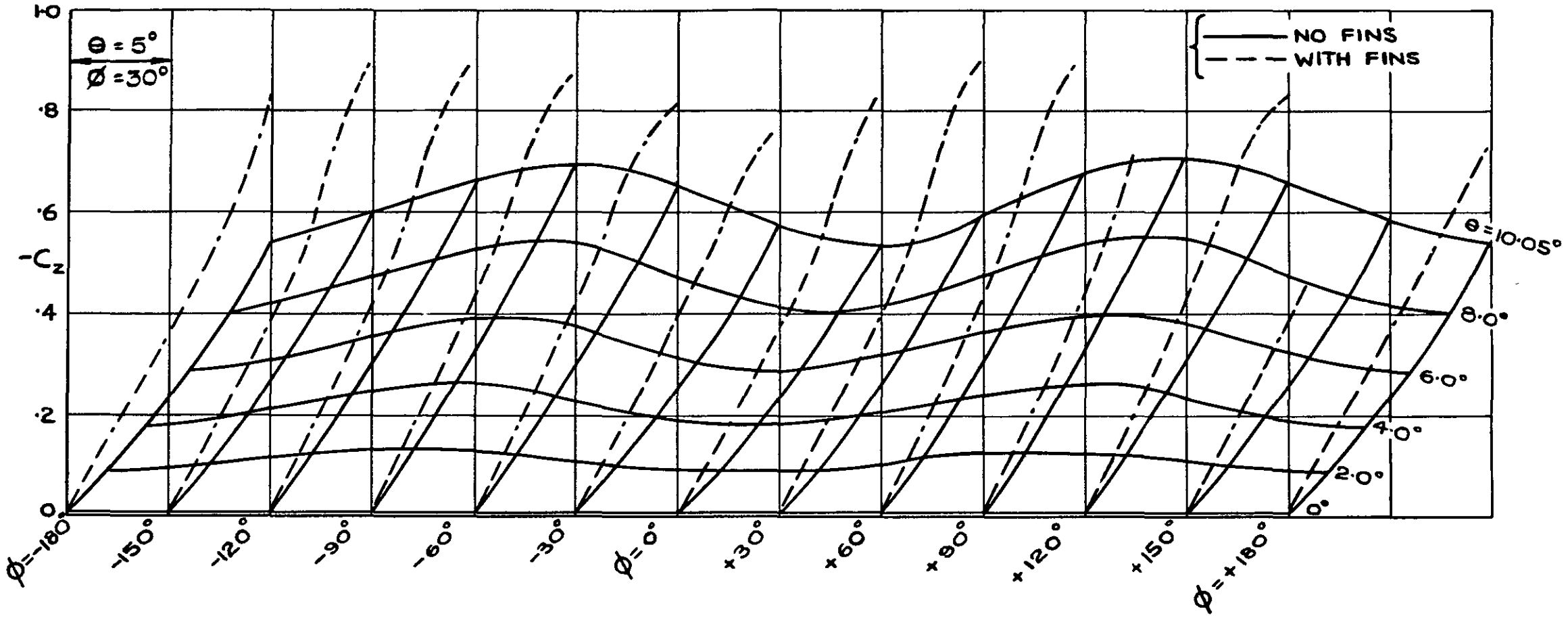

FIG. 9: $-C_z$ v Θ : WITH HEAD 'B' AT M = 1·13

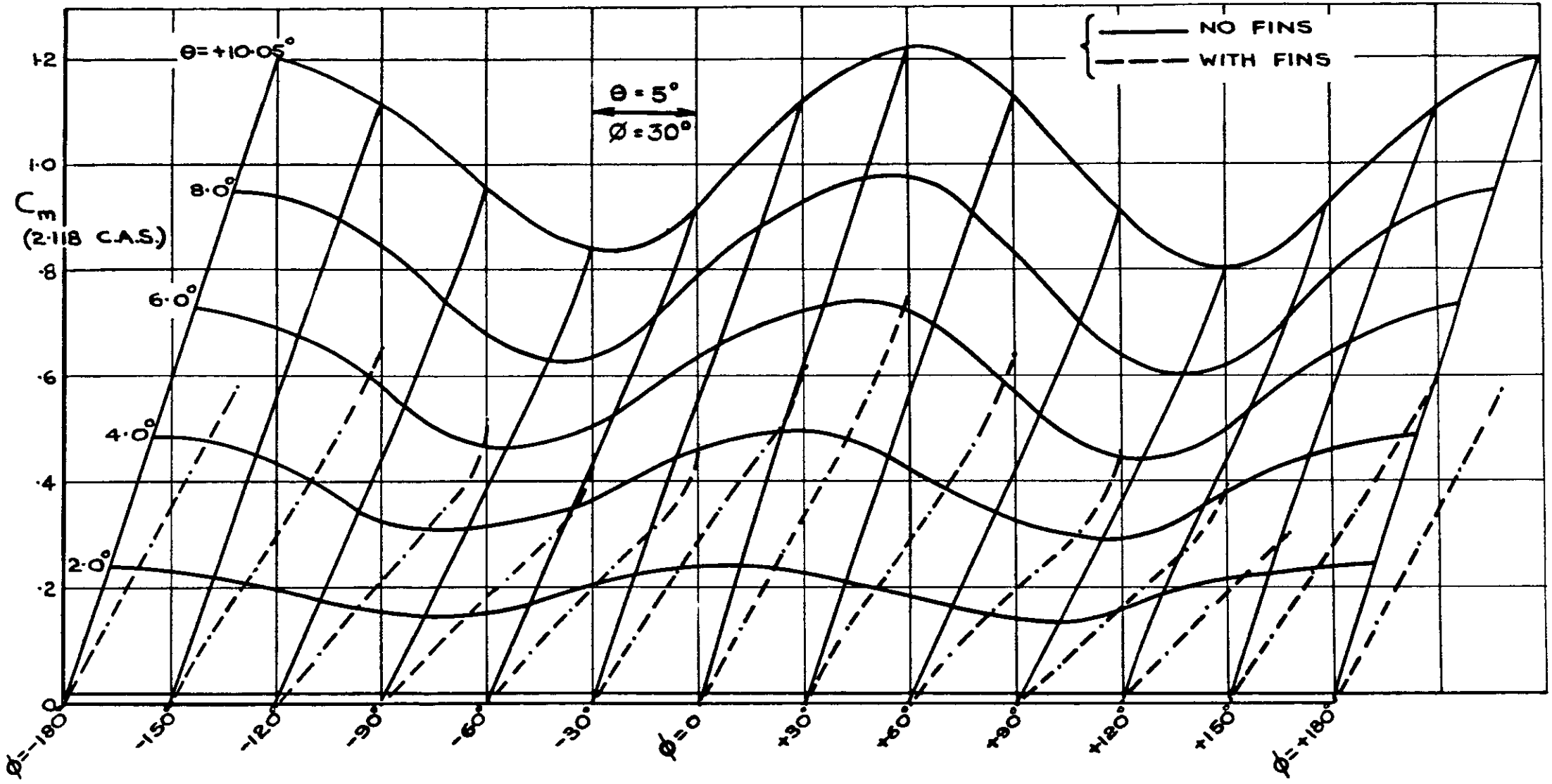

FIG. 10: C_m v Θ : WITH HEAD 'B' AT M=1·13

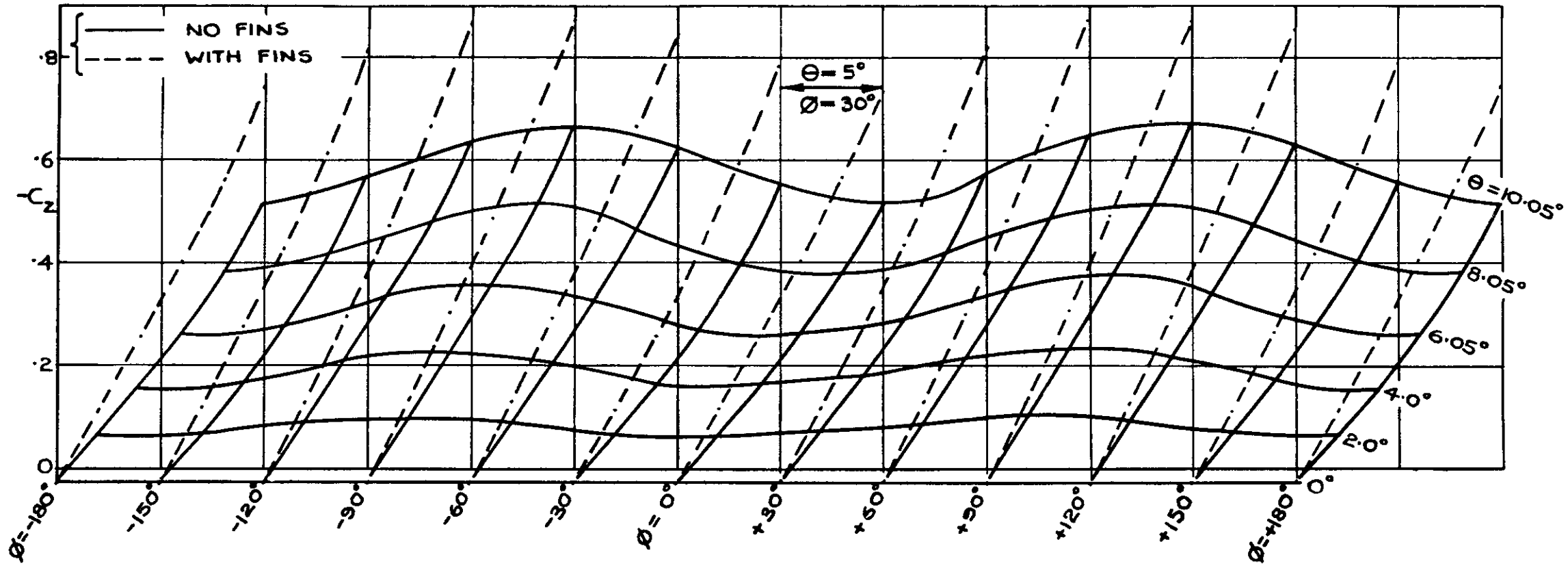

FIG. 11: $-C_Z$ v Θ : WITH HEAD 'B' AT M = 1·19

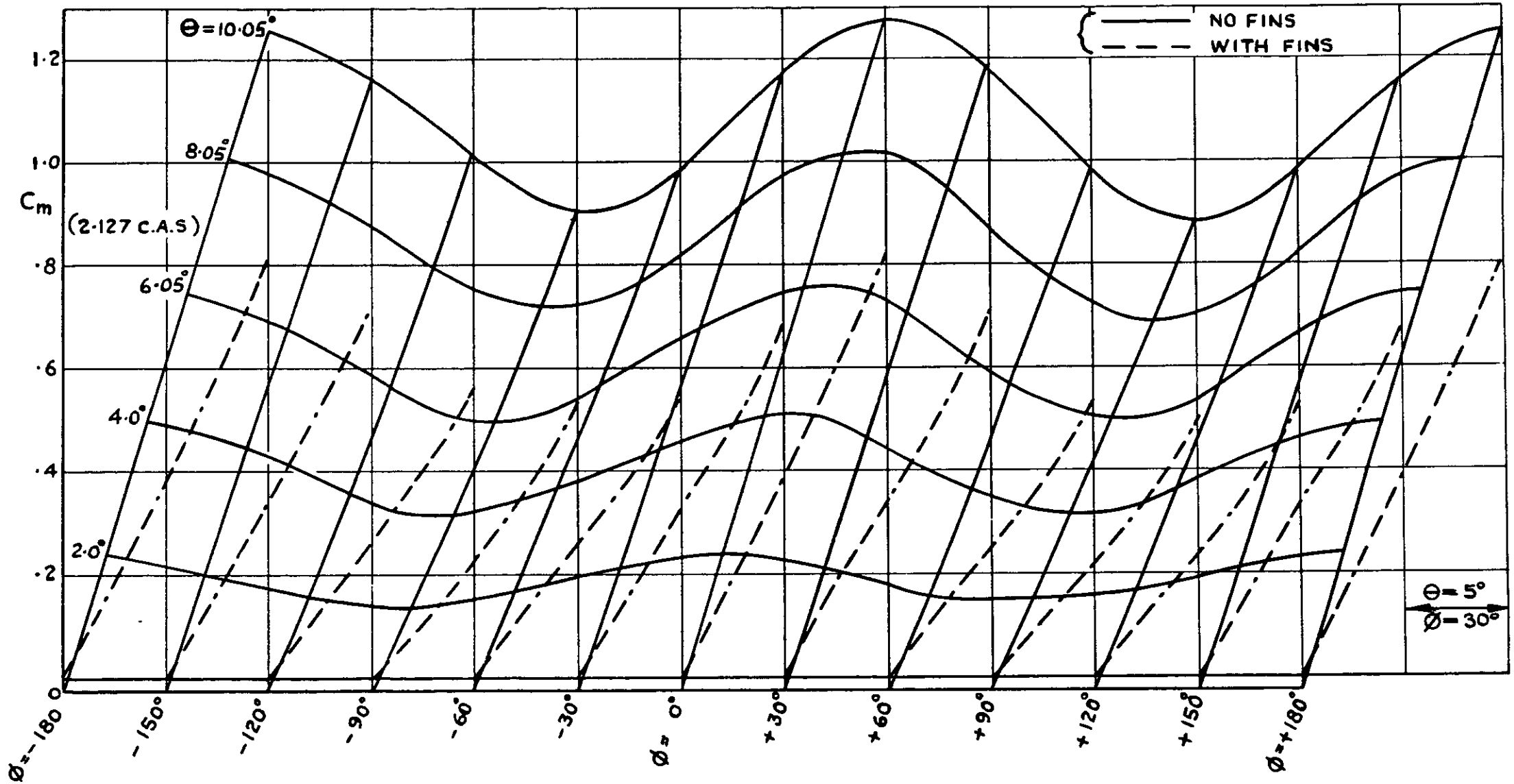

FIG.12: Cm v Θ: WITH HEAD 'B' AT M = 1·19

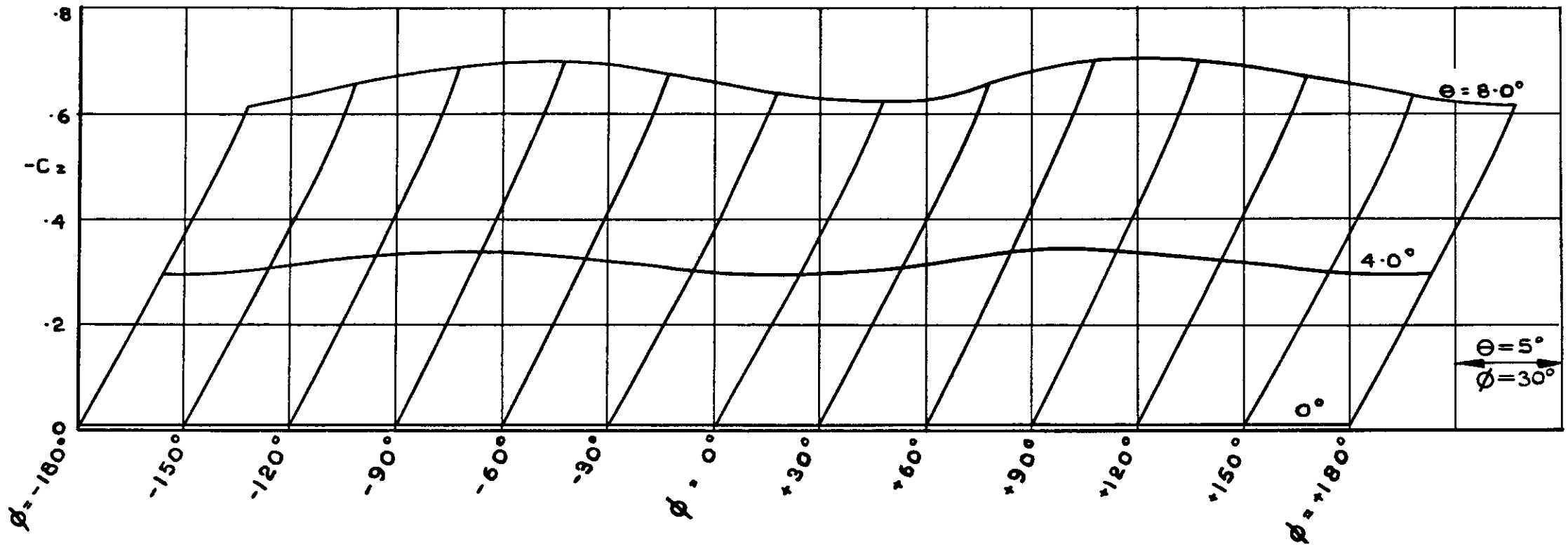

FIG. 13 $-C_z$ v Θ : WITH HEAD 'B' AT M = 1·40 : WITH FINS.

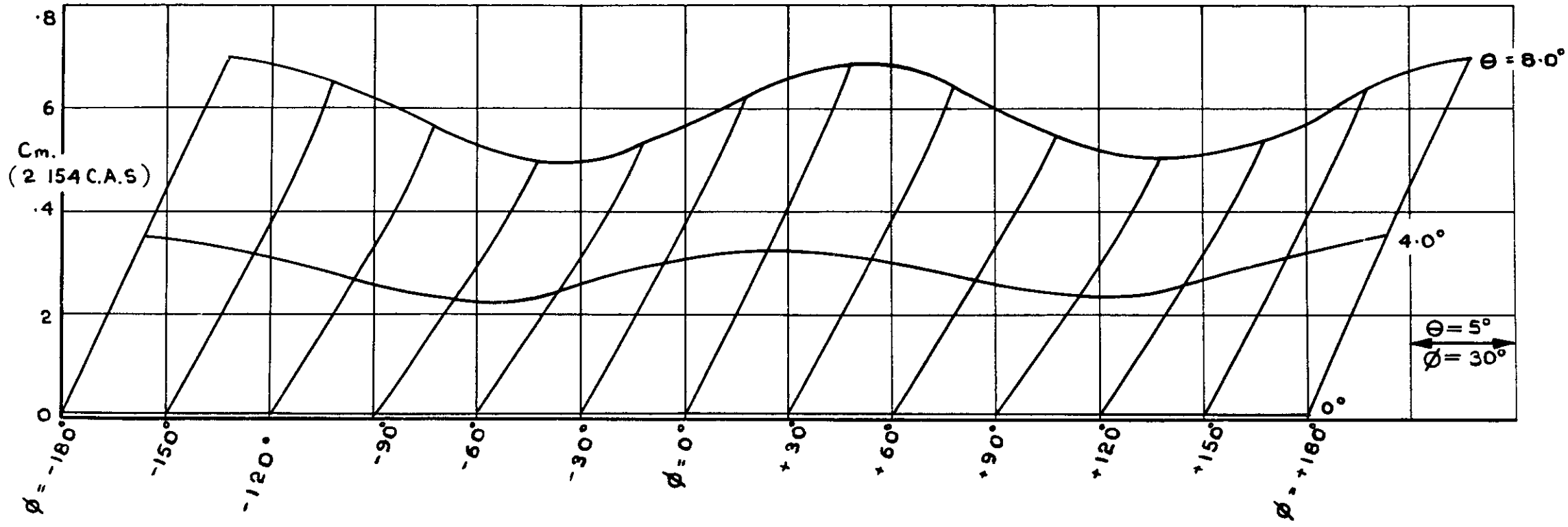

FIG 14: Cm v Θ : WITH HEAD 'B' AT M=1·40 : WITH FINS.

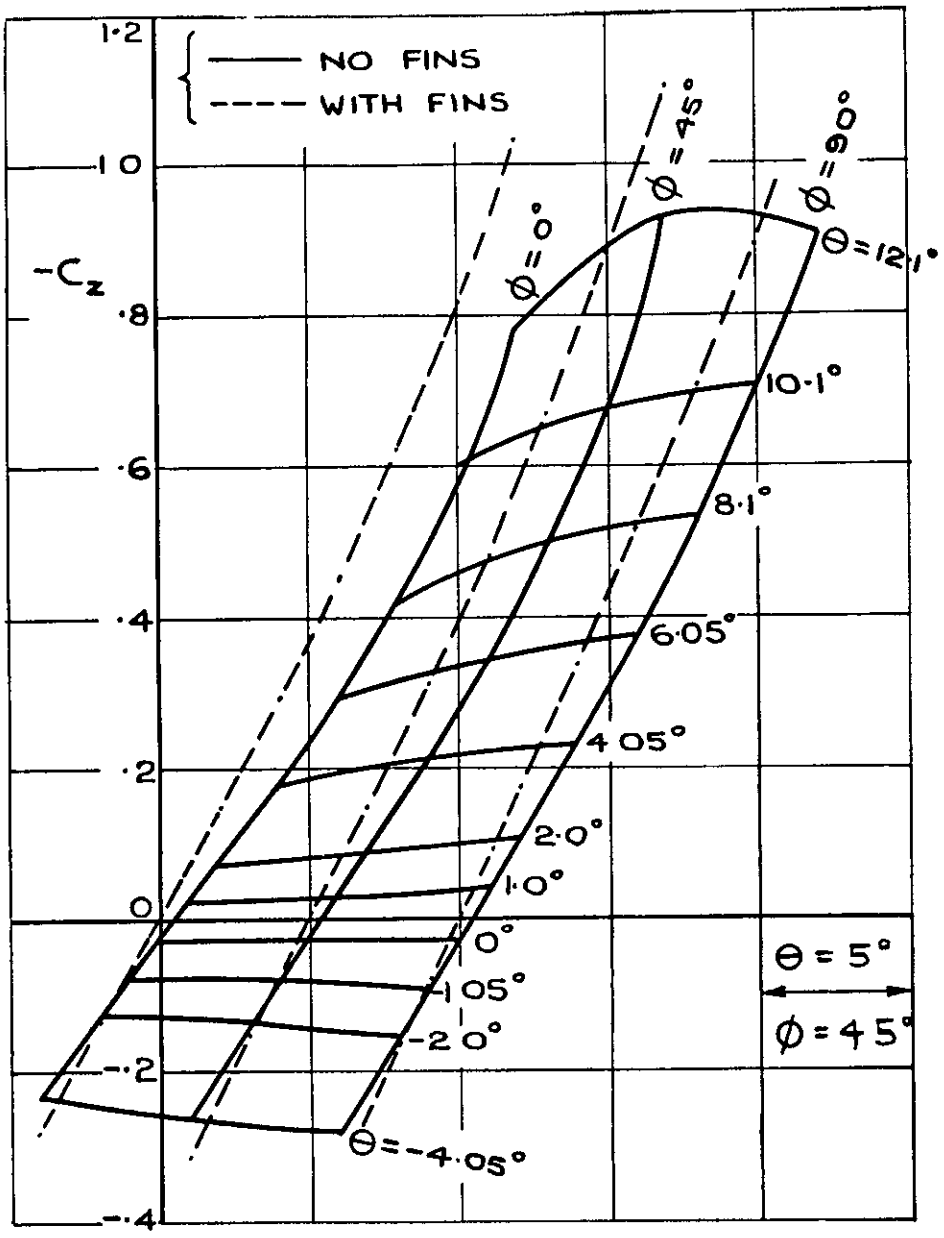

FIG. 15 : $-C_z$ v θ

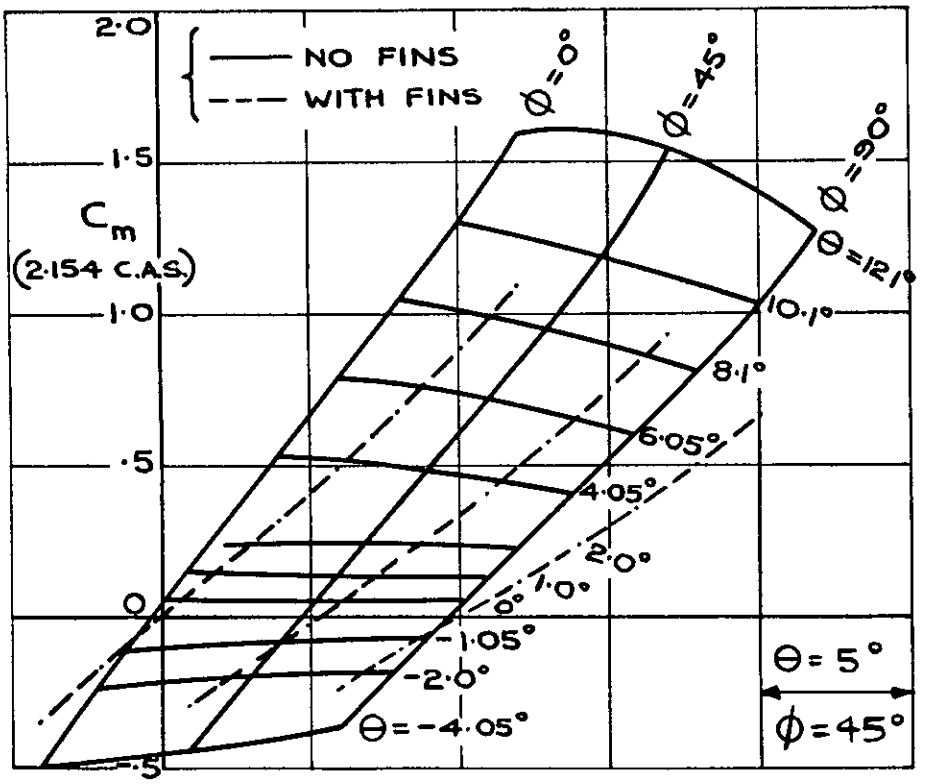

FIG. 16 : C_m v θ

FIG. 15 & 16: $-C_z$ v θ & C_m v θ: WITH HEAD 'B' AT M=1·40

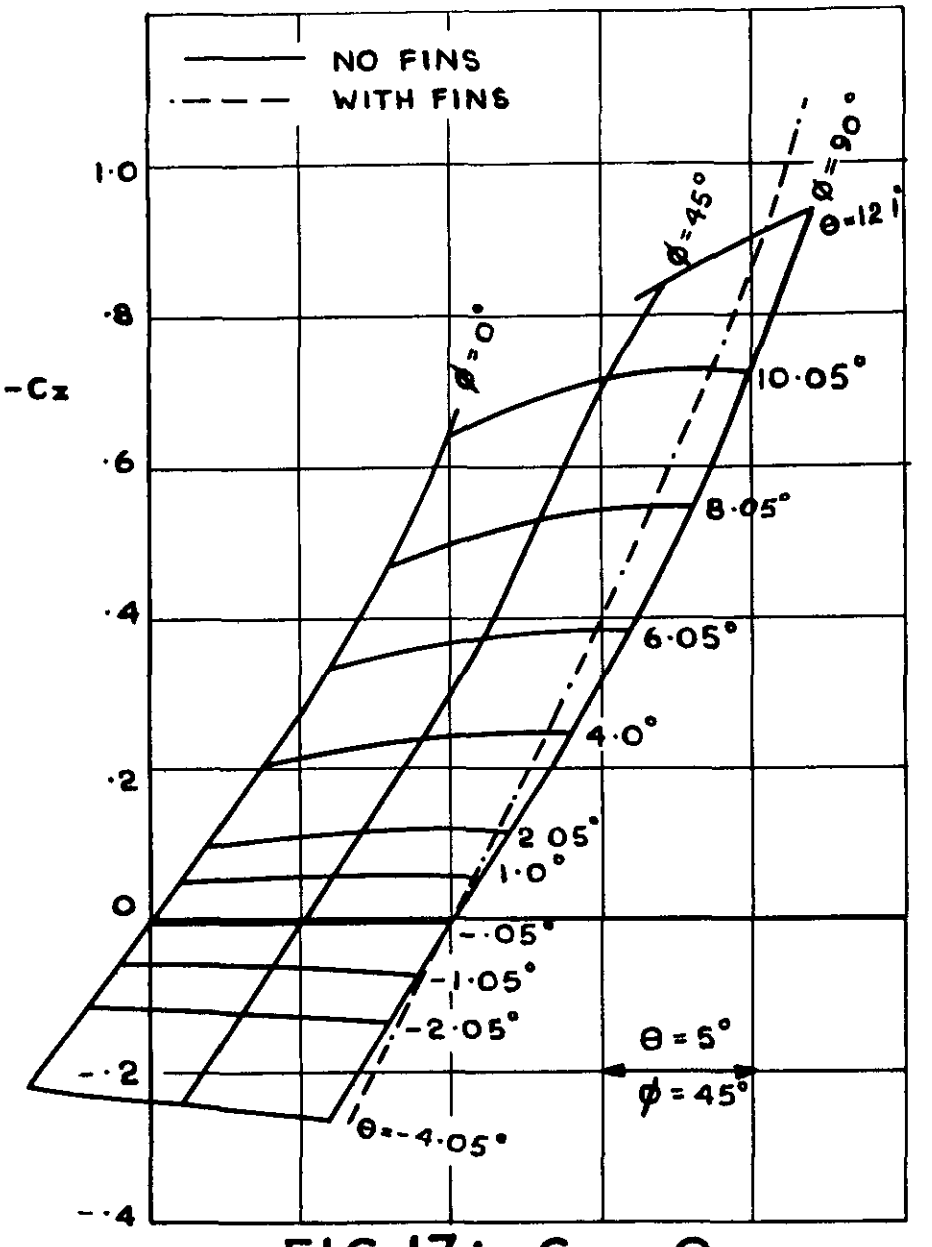

FIG 17 : $-C_z$ v θ

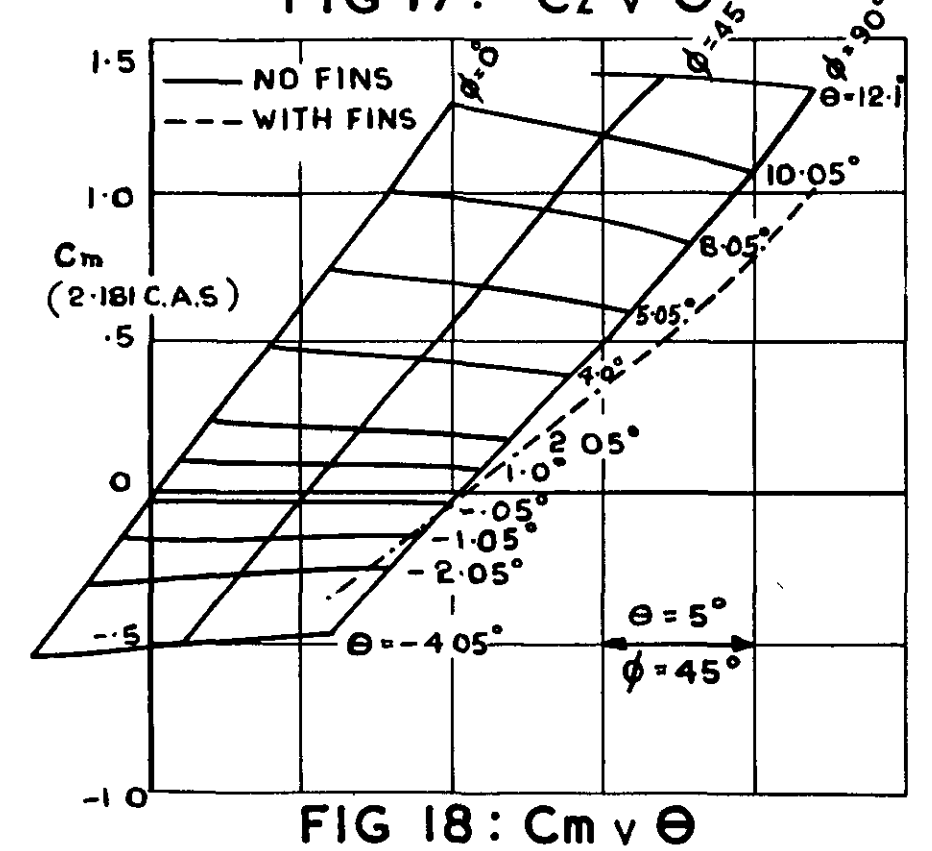

FIG 18 : Cm v θ

FIG 17 & 18 : $-C_z$ v θ AND Cm v θ :
WITH HEAD 'B' AT M = 1·60

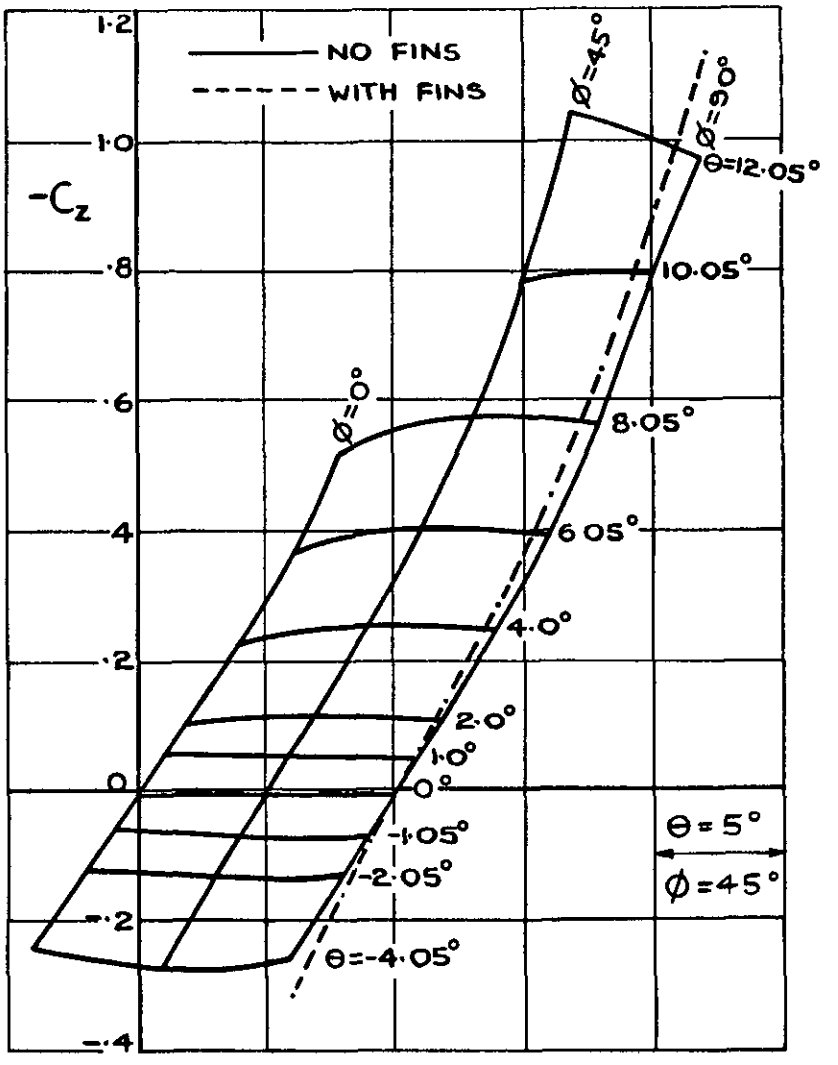

FIG. 19 : $-C_z$ v θ

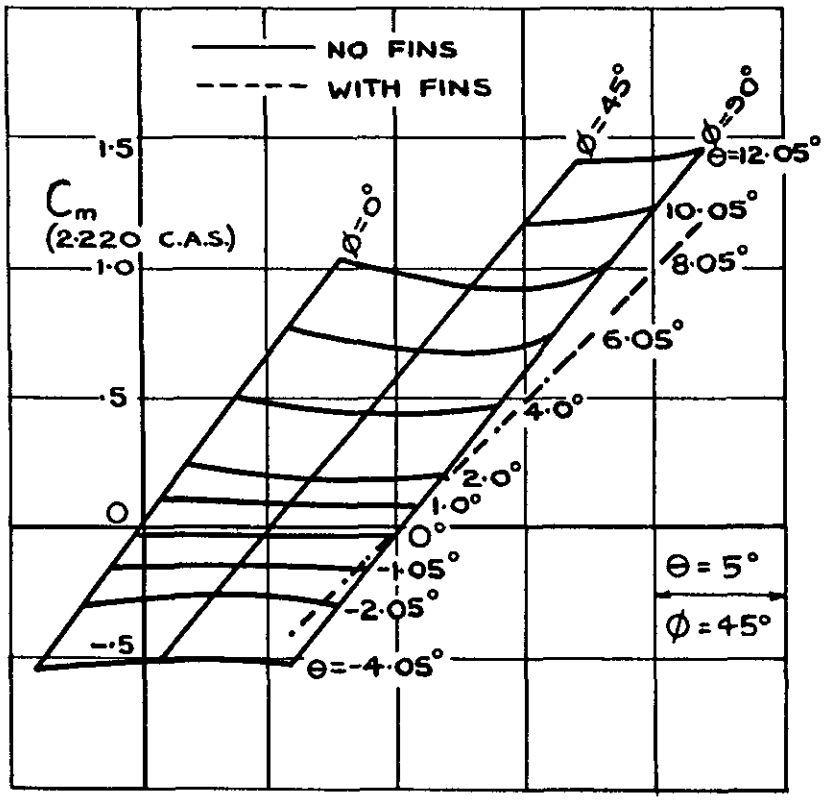

FIG. 20 : C_m v θ

FIG. 19.& 20: $-C_z$ v θ AND C_m v θ: WITH HEAD 'B' AT M=2·00

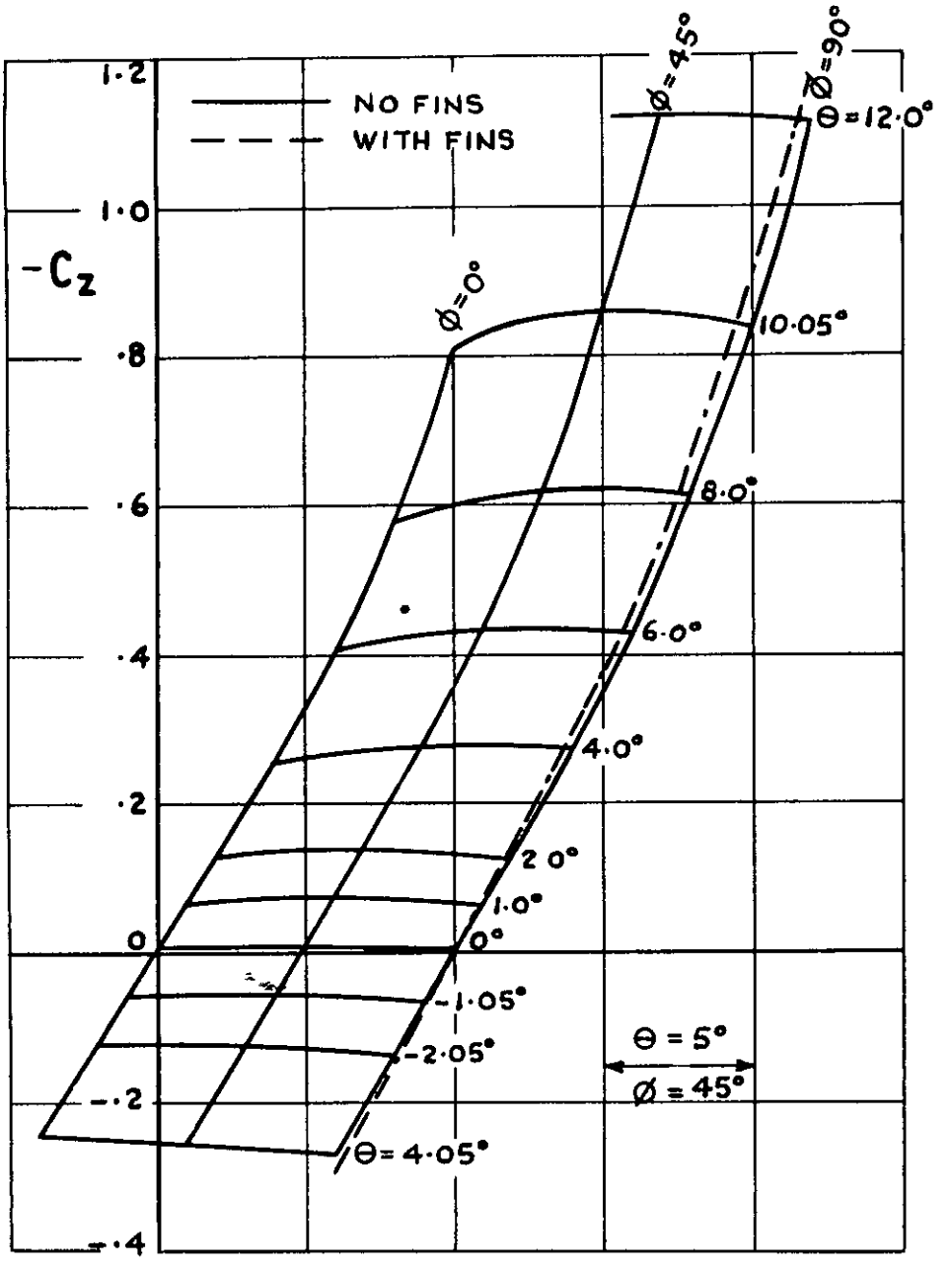

FIG. 21: $-C_z$ v Θ

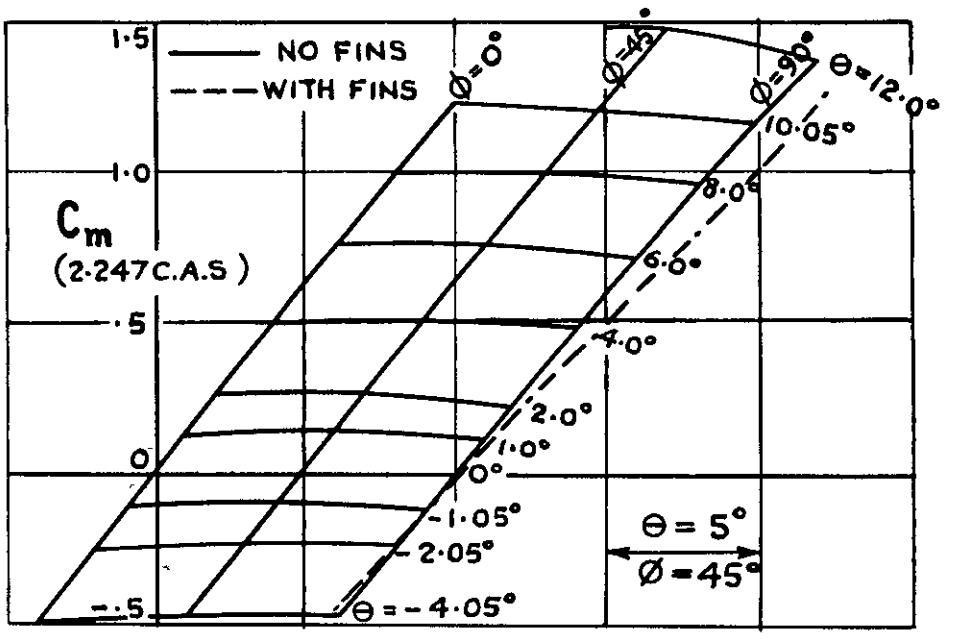

FIG. 22: C_m v Θ

FIG. 21 & 22: $-C_z$ v Θ AND C_m v Θ: WITH HEAD 'B' AT M = 2·40

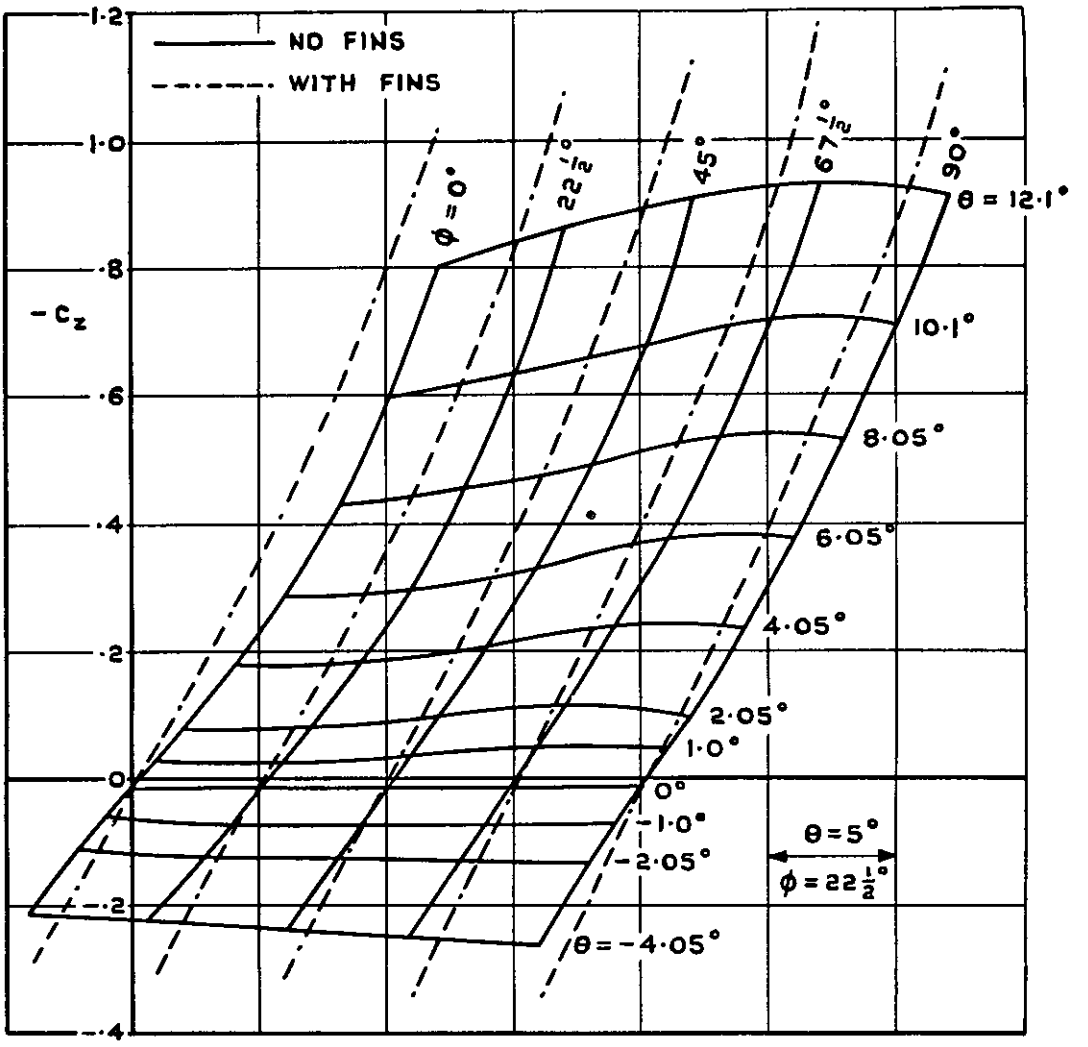

FIG. 23: $-C_z$ v Θ.

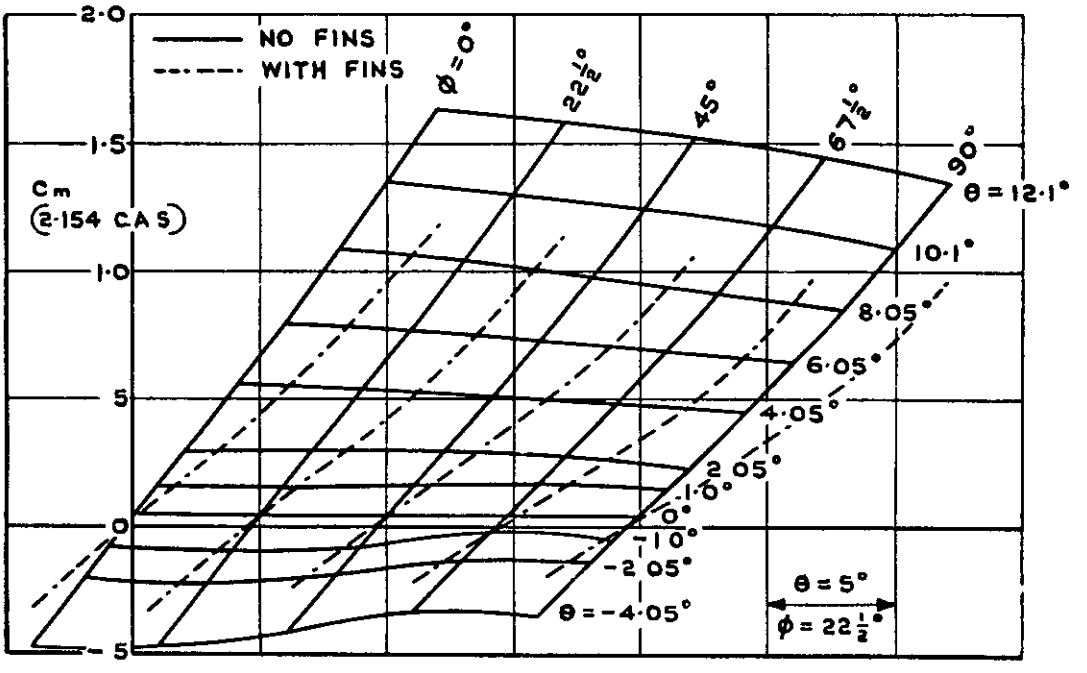

FIG. 24: Cm v Θ.

FIG. 23 & 24: $-C_z$ v Θ AND Cm v Θ: WITH HEAD 'D' AT M = 1·40.

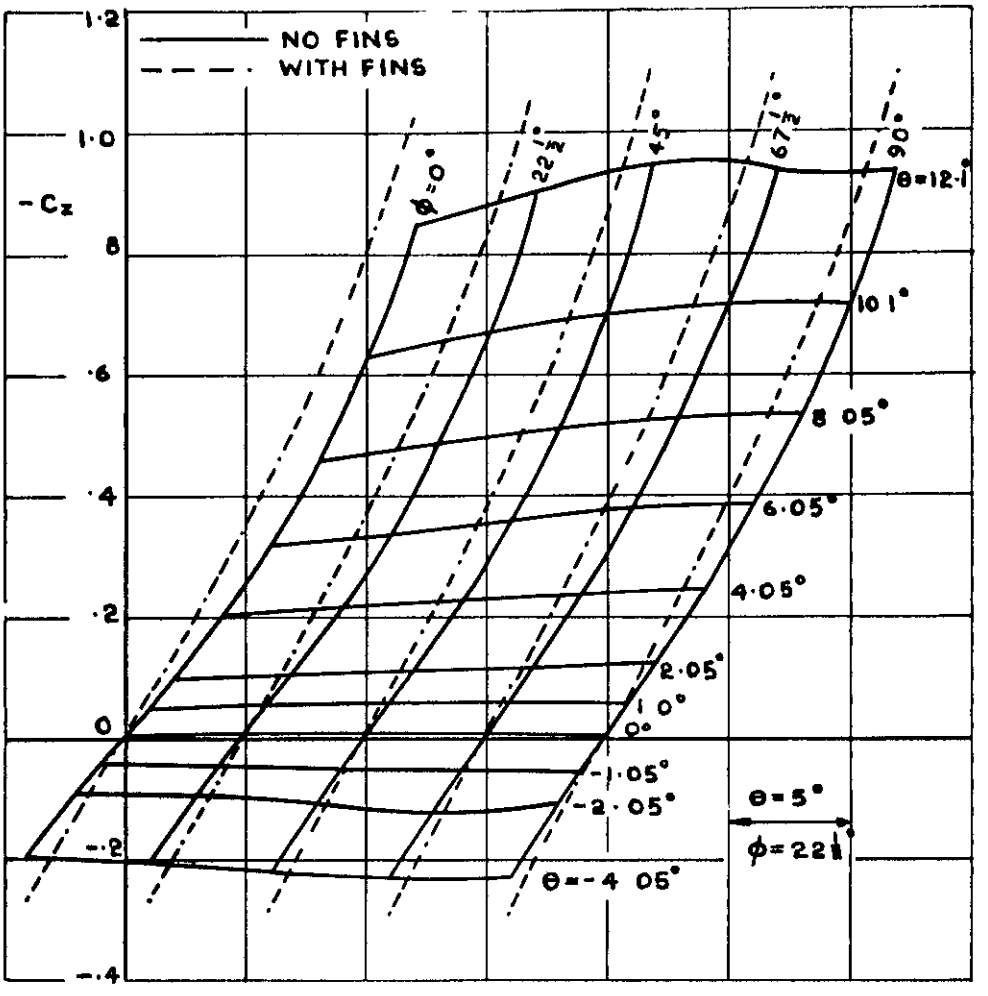

FIG. 25 : -Cz v θ

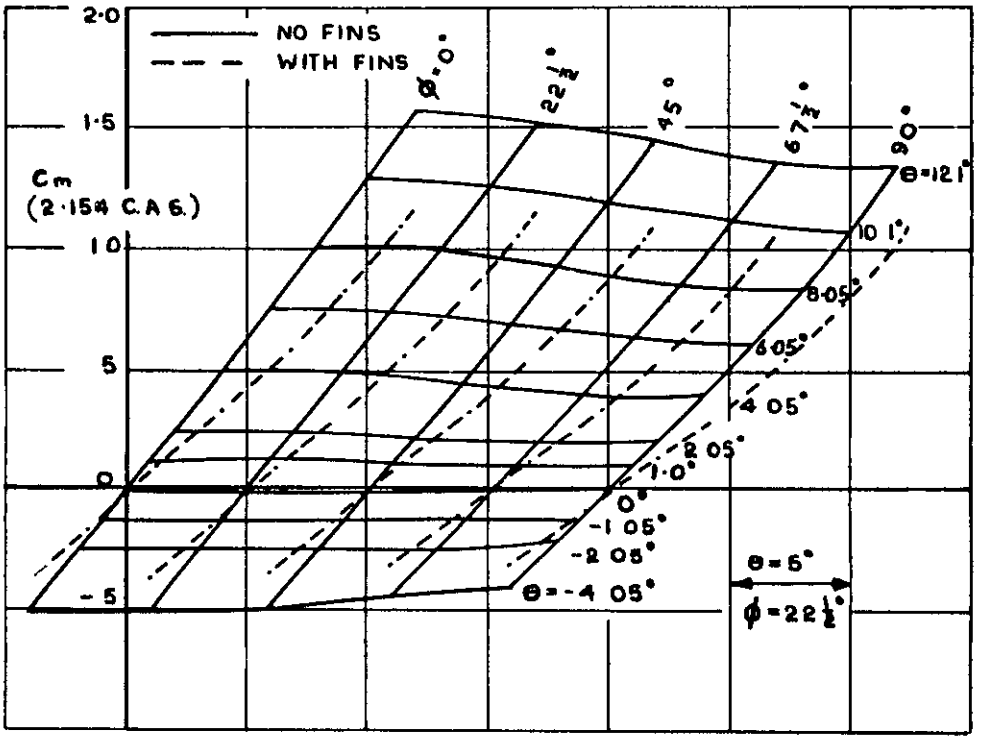

FIG. 26 : Cm v θ

FIG. 25 & 26: -Cz v θ AND Cm v θ :
WITH HEAD 'D' AT M = 1·60.

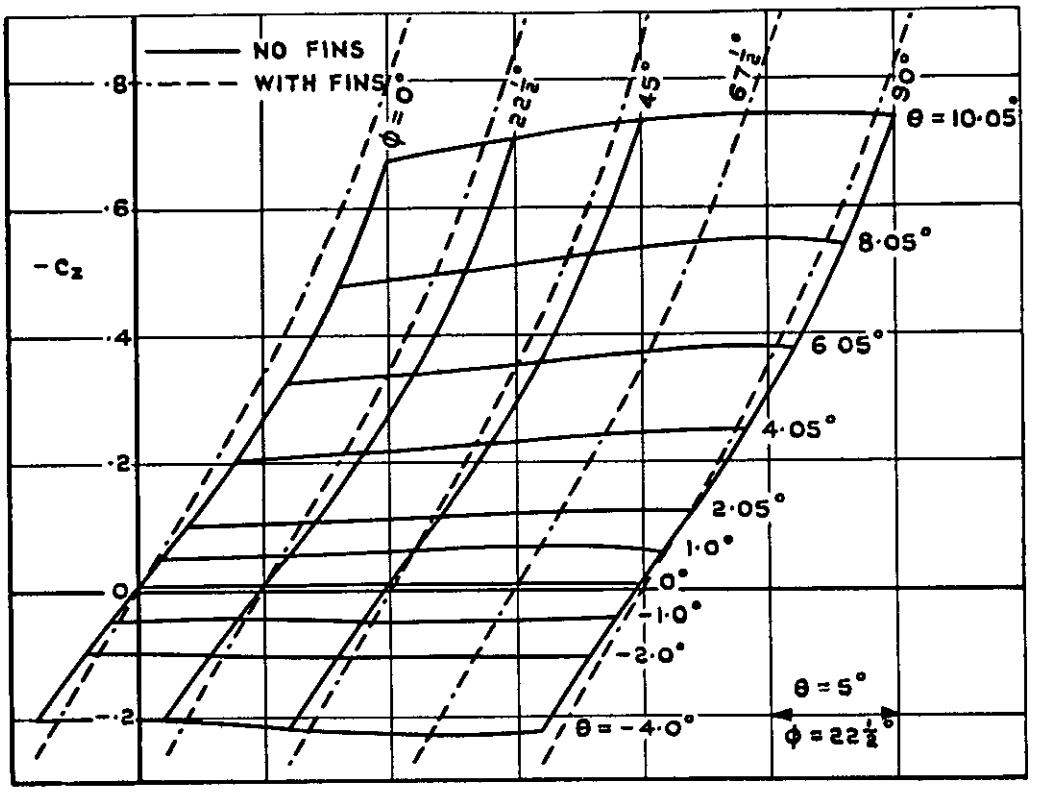

FIG. 27: $-C_z$ v Θ.

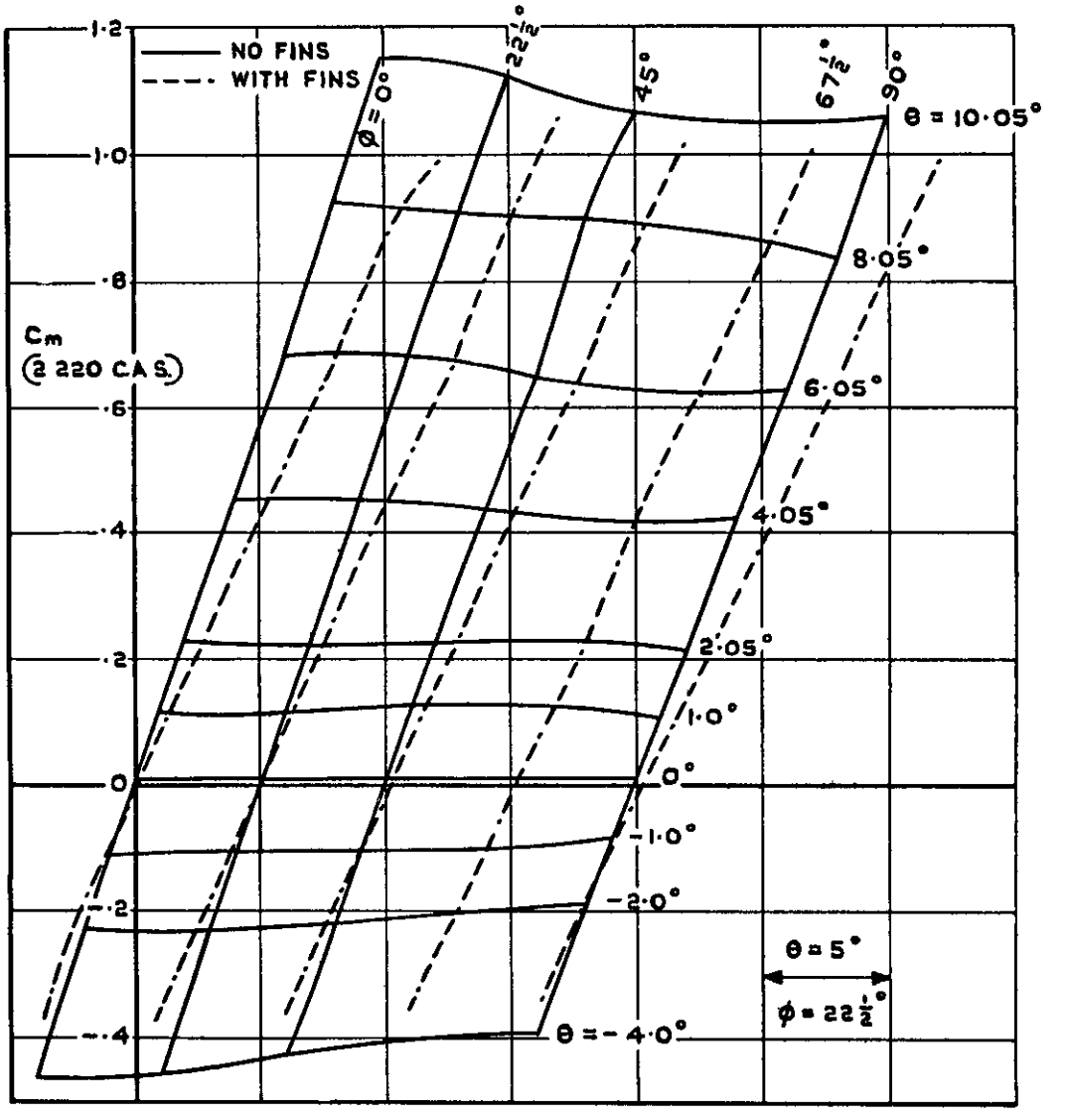

FIG. 28: Cm v Θ.

FIG. 27 & 28: $-C_z$ v Θ AND Cm v Θ: WITH HEAD 'D' AT M = 2·00.

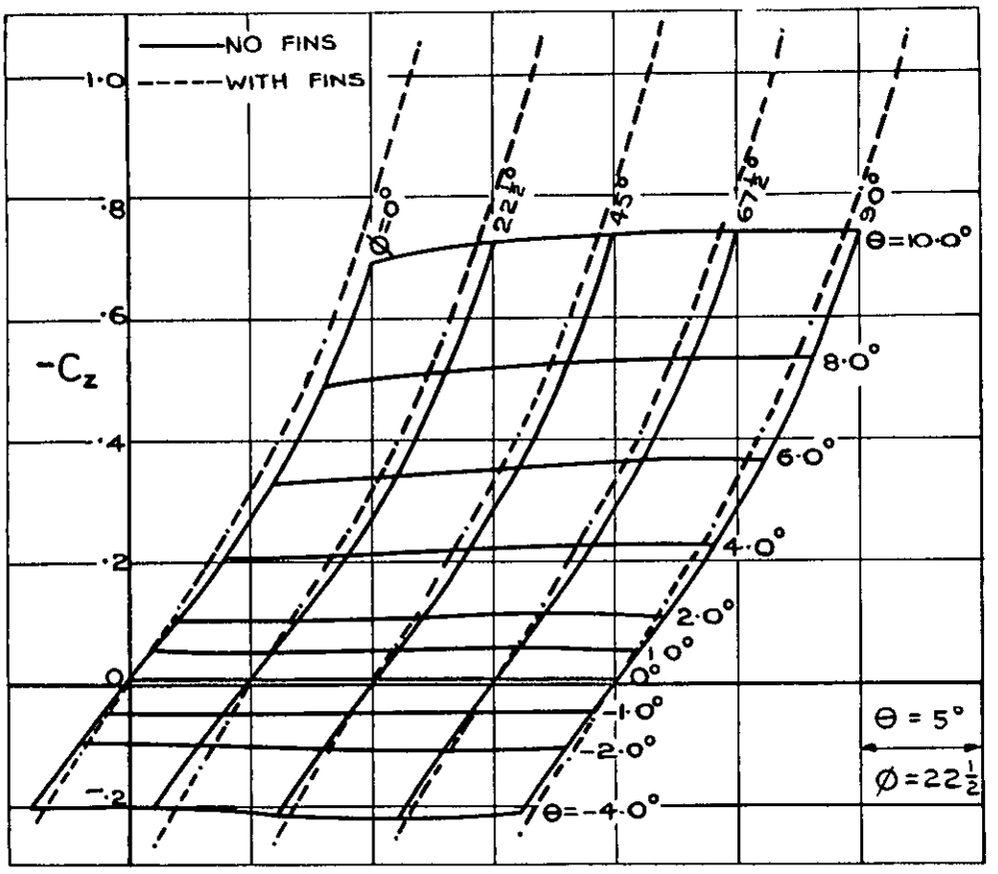

FIG. 29 : $-C_z$ v Θ

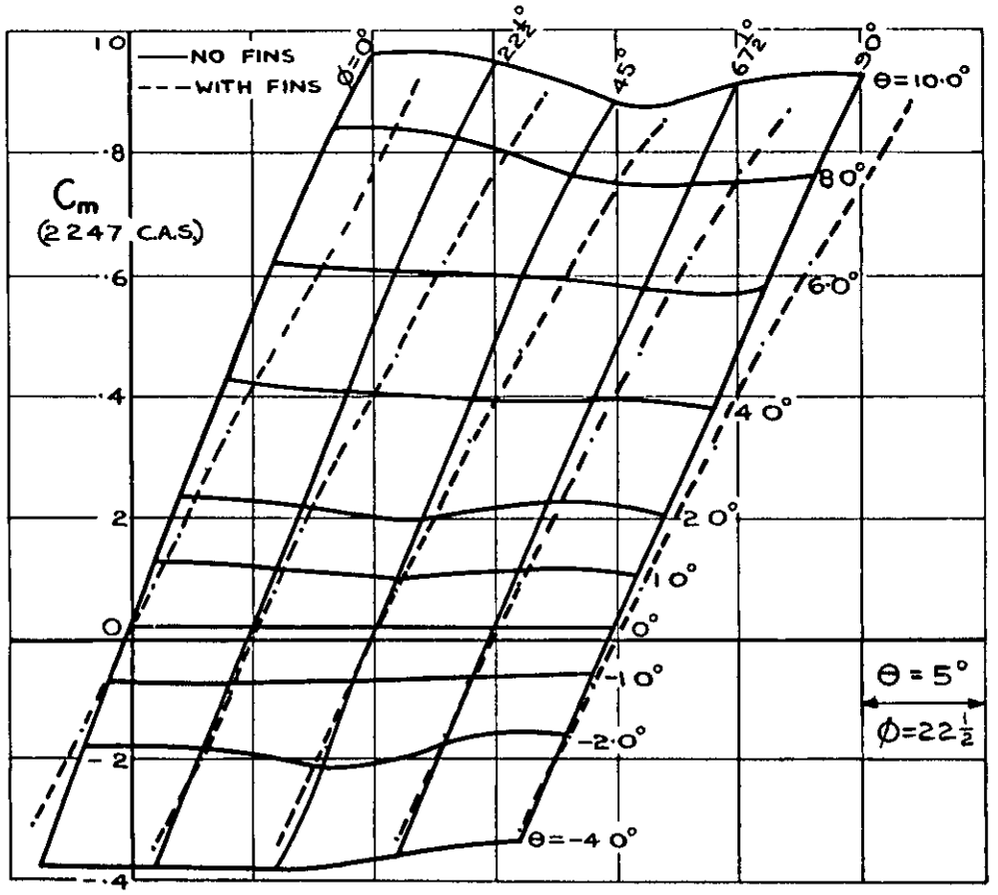

FIG. 30 : C_m v Θ

FIG. 29&30: $-C_z$ v Θ AND C_m v Θ: WITH HEAD 'D' AT M=2·40

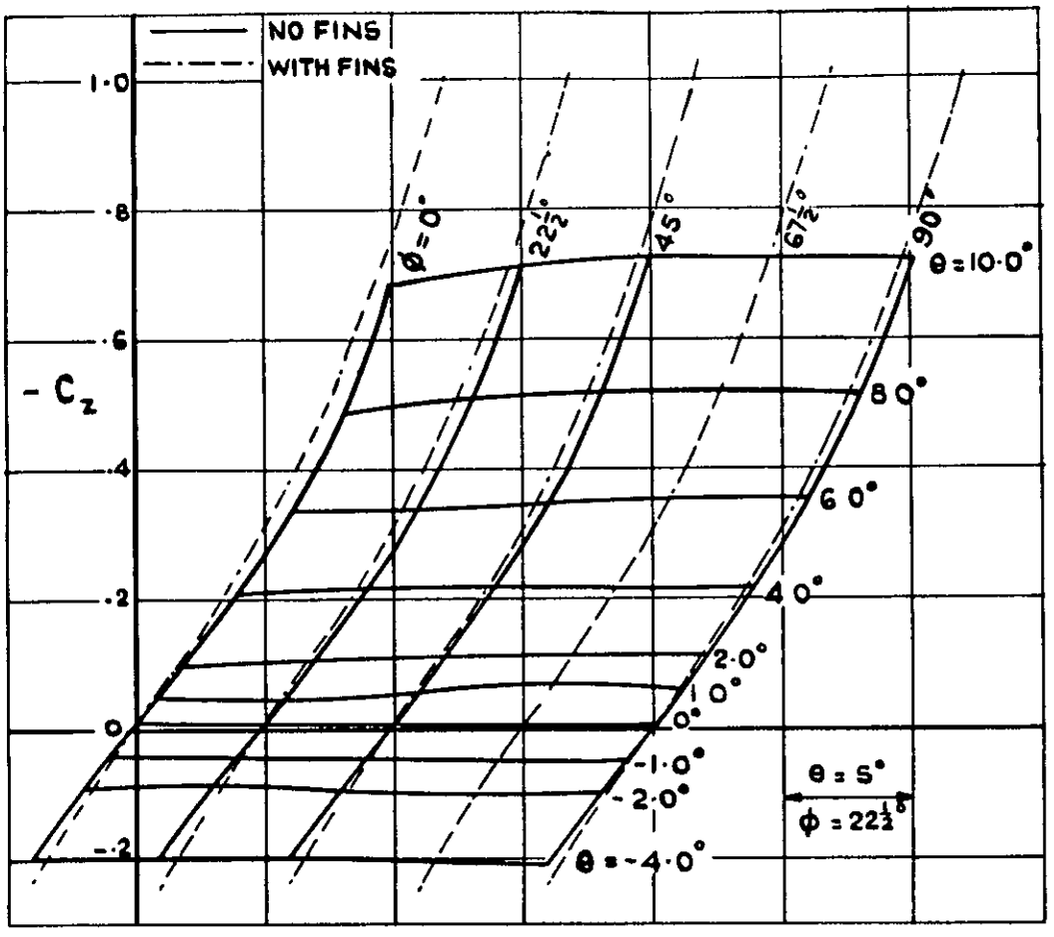

FIG 31 :- C_z v θ

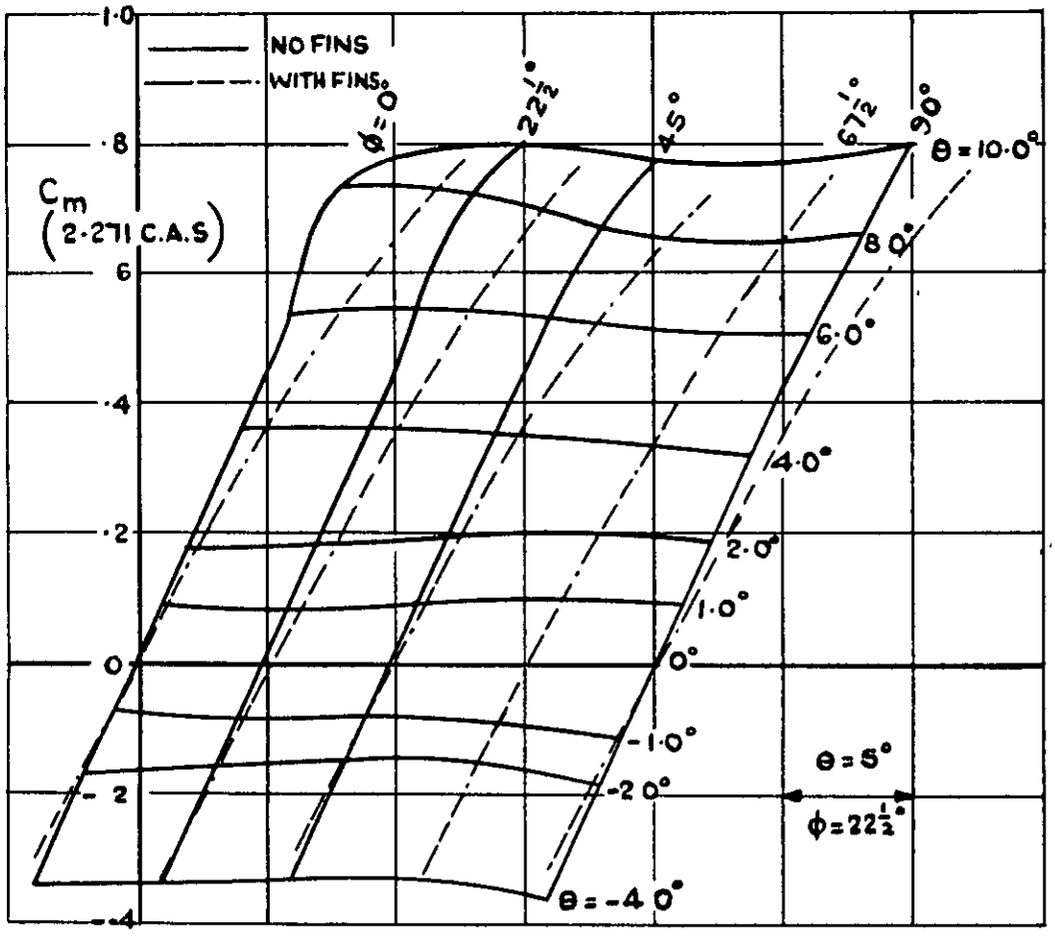

FIG 32 : C_m v θ

FIG 31 & 32 : - C_z v θ AND C_m v θ: WITH HEAD 'D' AT M = 2·80

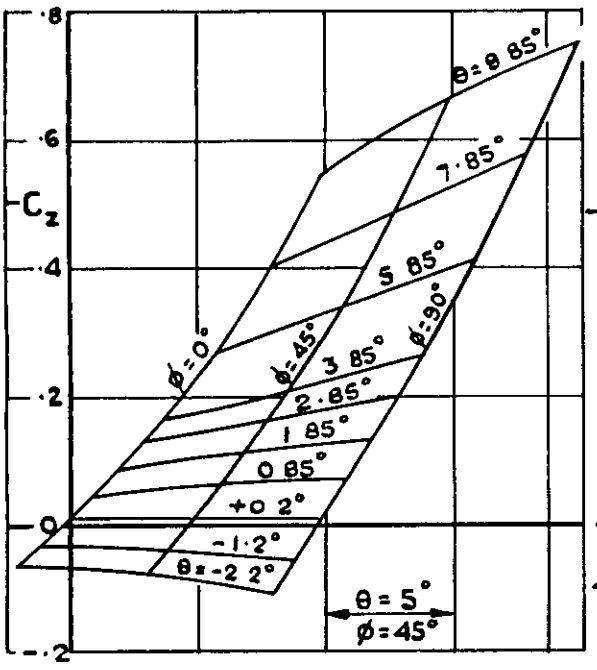

FIG33 :- C_z v Θ AT M=0·95

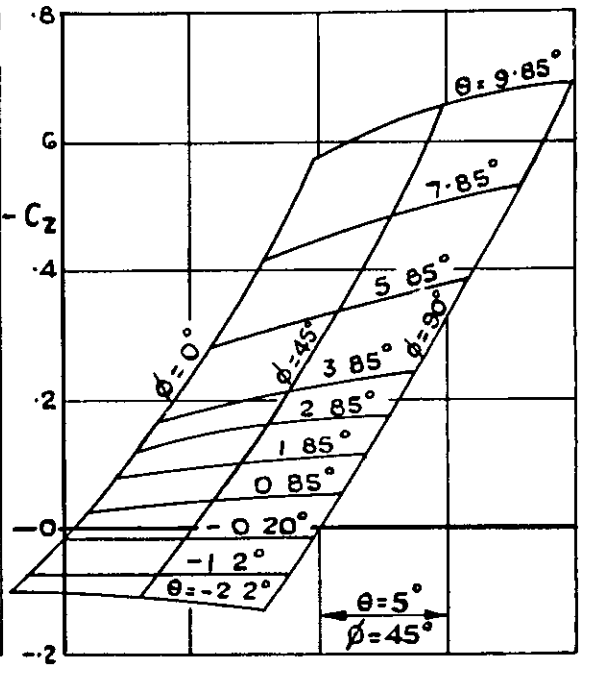

FIG 35:- C_z v Θ AT M=1·19

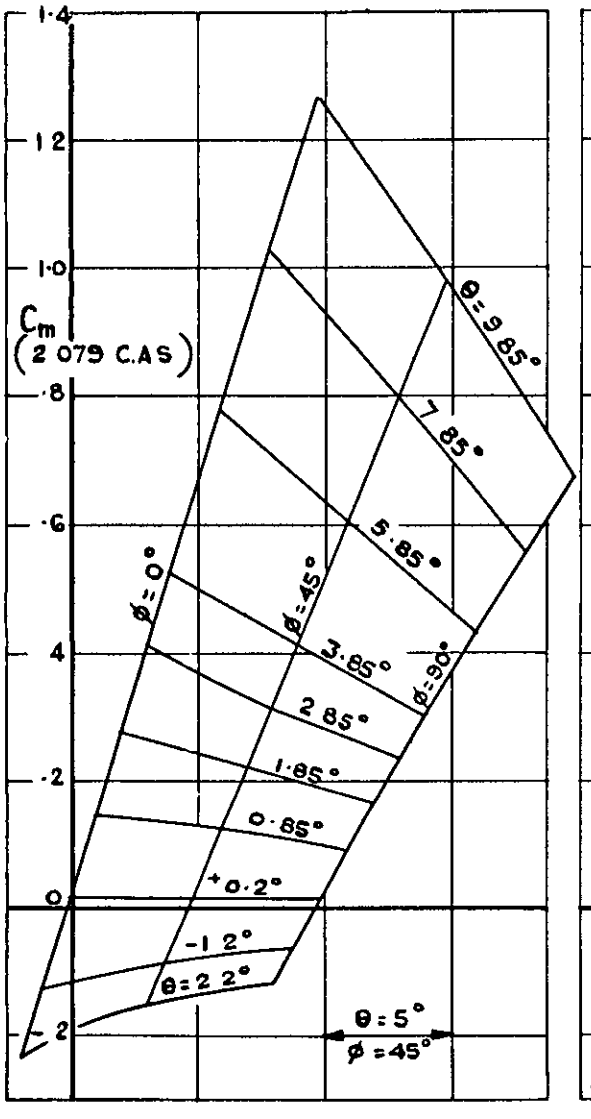

FIG 34 : C_m v Θ AT M=0·95

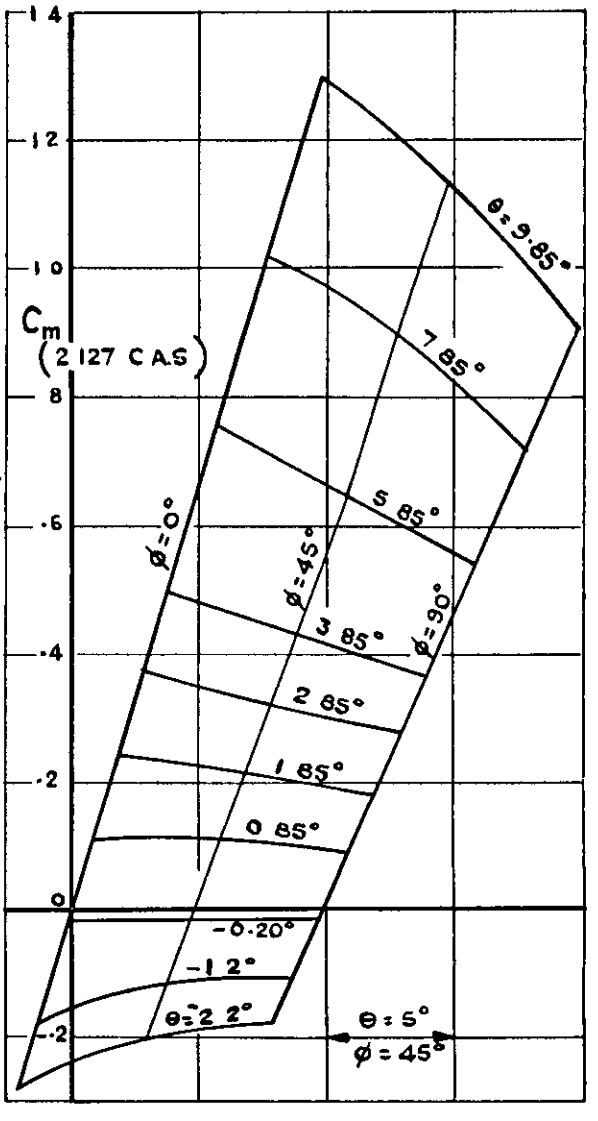

FIG 36 : C_m v Θ AT M= 1·19

FIG 33-36 : - C_z v Θ AND C_m v Θ : WITH HEAD 'E' AT M= 0·95 AND 1·19

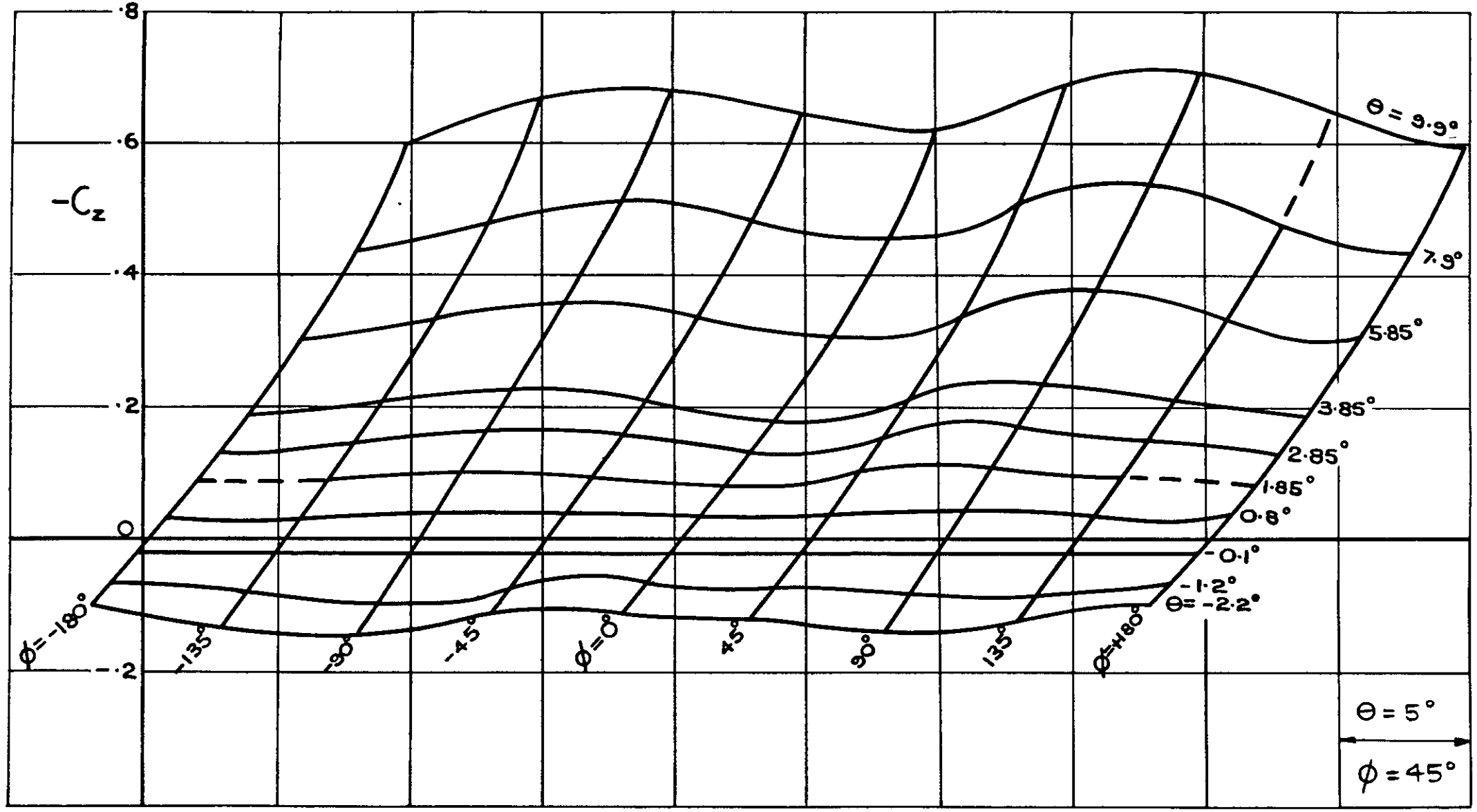

FIG. 37.: $-C_z$ v Θ : WITH HEAD 'E' AT M 1·40

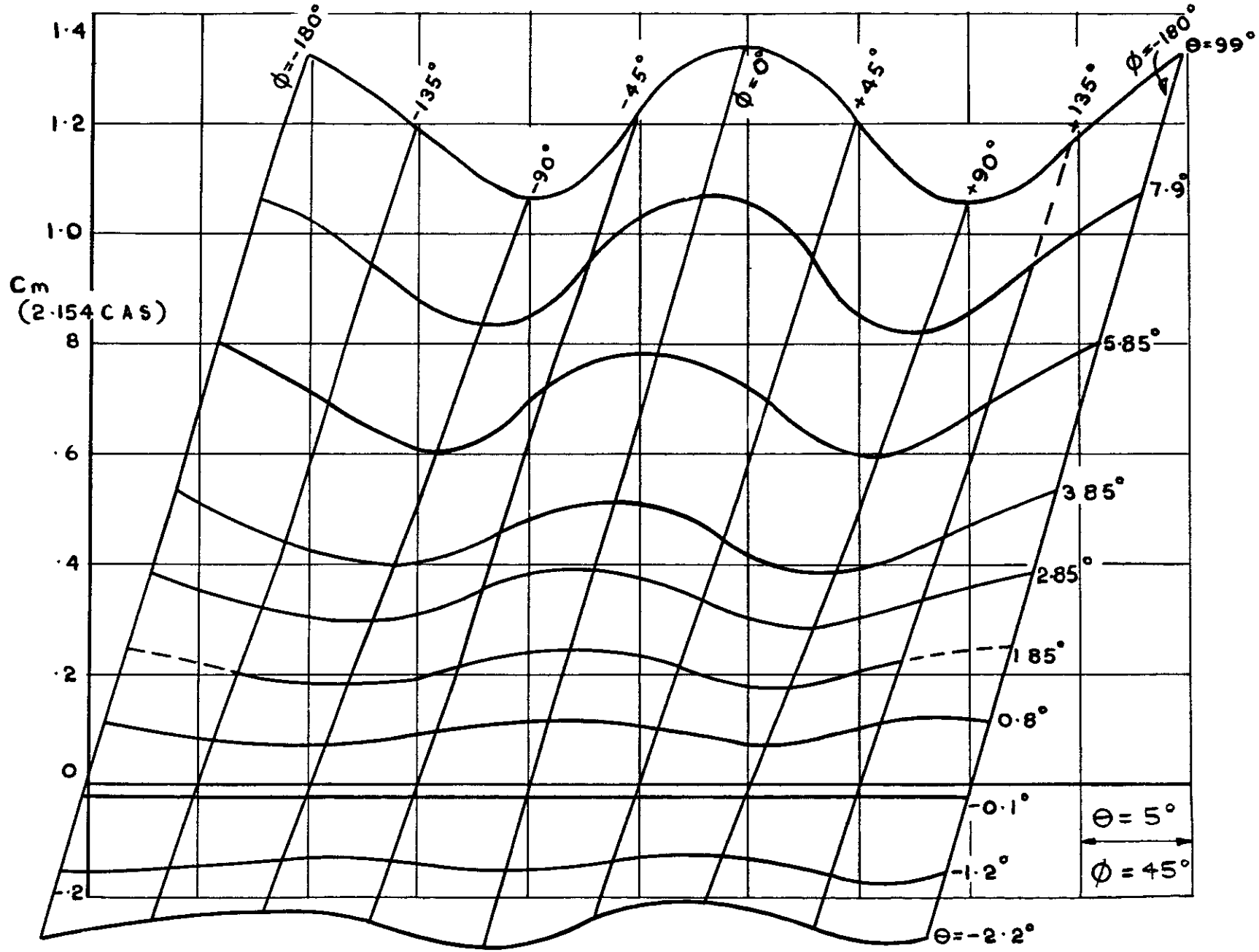

FIG. 38 : Cm v Θ : WITH HEAD 'E' AT M = 1·40

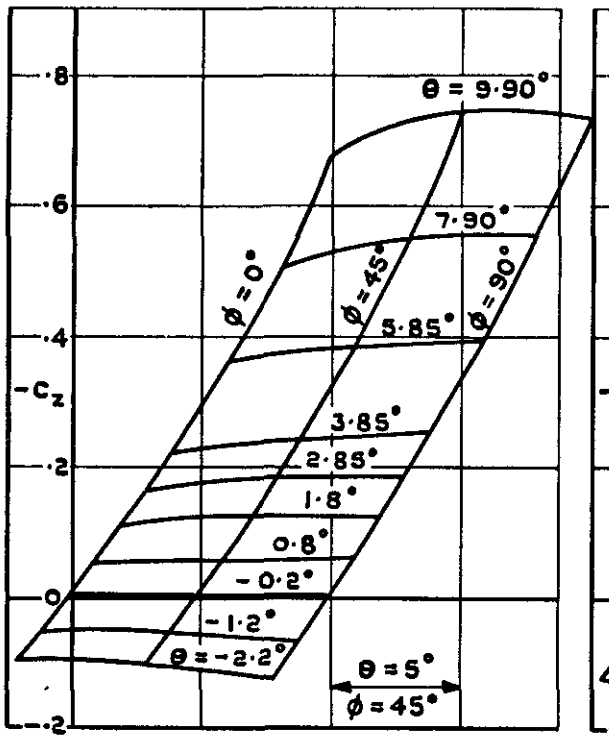

FIG. 39: $-C_z$ v Θ AT M=1·60.

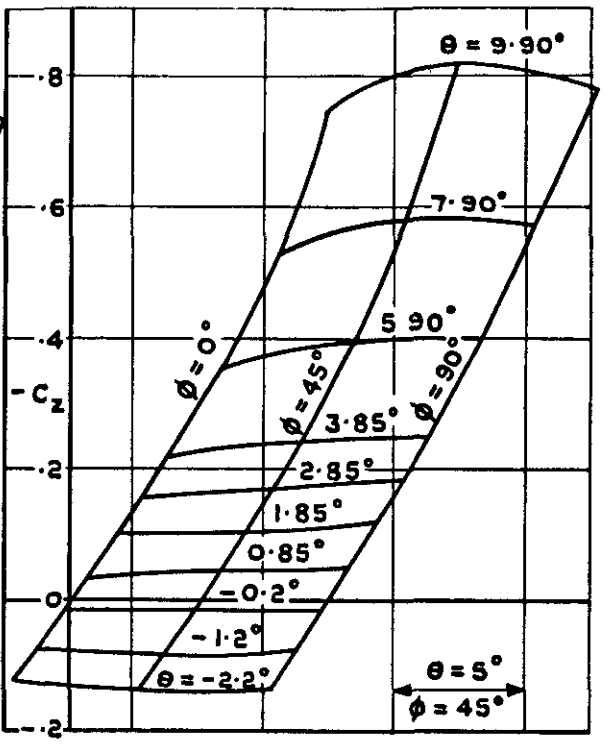

FIG. 41: $-C_z$ v Θ AT M=2·00.

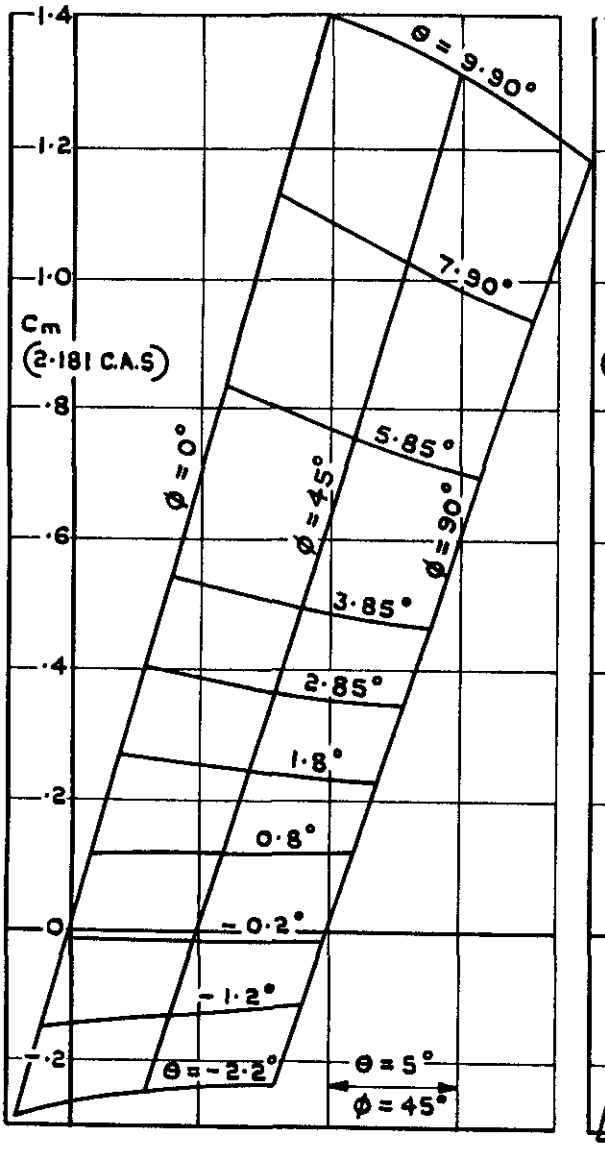

FIG. 40: Cm v Θ AT M=1·60.

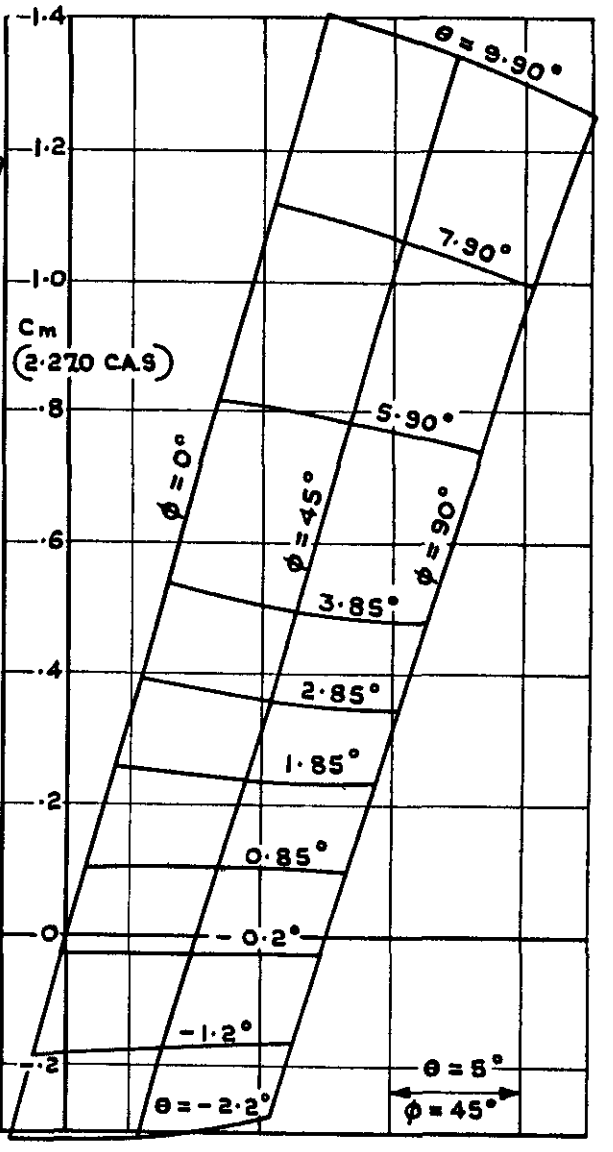

FIG. 42: Cm v Θ AT M=2·0.

FIG. 39–42: $-C_z$ v Θ AND Cm v Θ : WITH HEAD 'E' AT M = 1·60 AND 2·00.

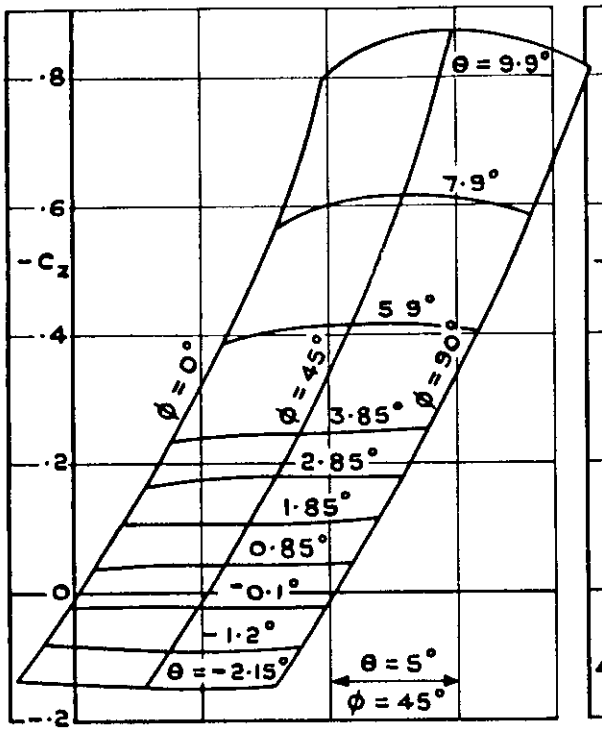

FIG. 43: $-C_z$ v Θ AT M=2·40.

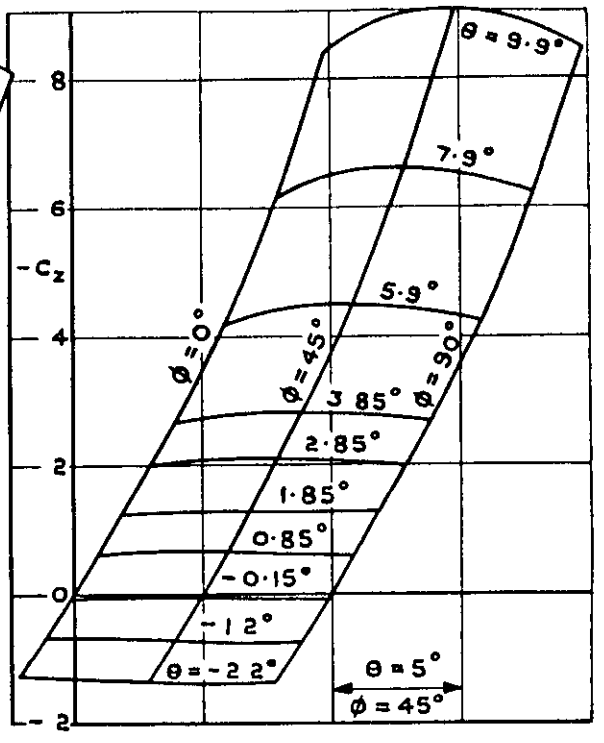

FIG. 45: $-C_z$ v Θ AT M=2·80.

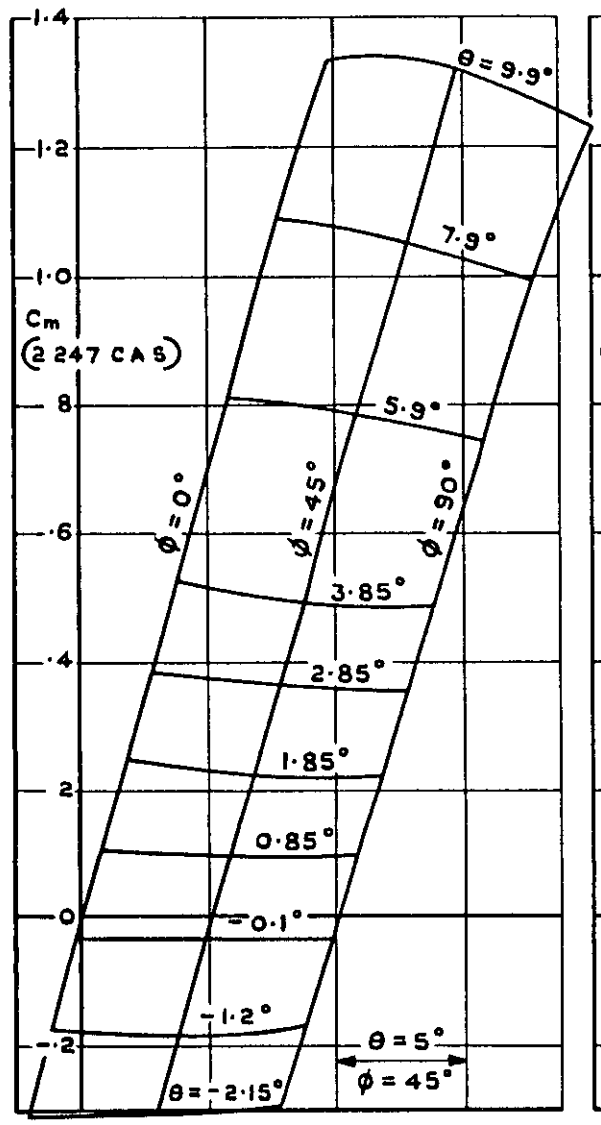

FIG. 44: Cm v Θ AT M=2·40.

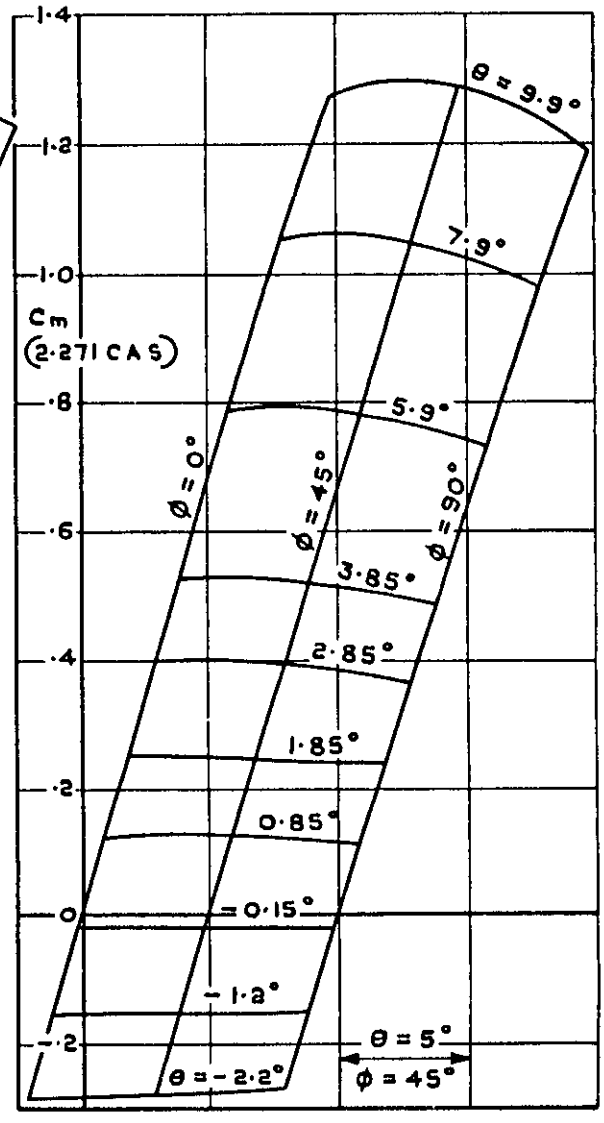

FIG. 46: Cm v Θ AT M=2·80.

FIG. 43–46: $-C_z$ v Θ AND Cm v Θ: WITH HEAD E AT M = 2·40 AND 2·80.

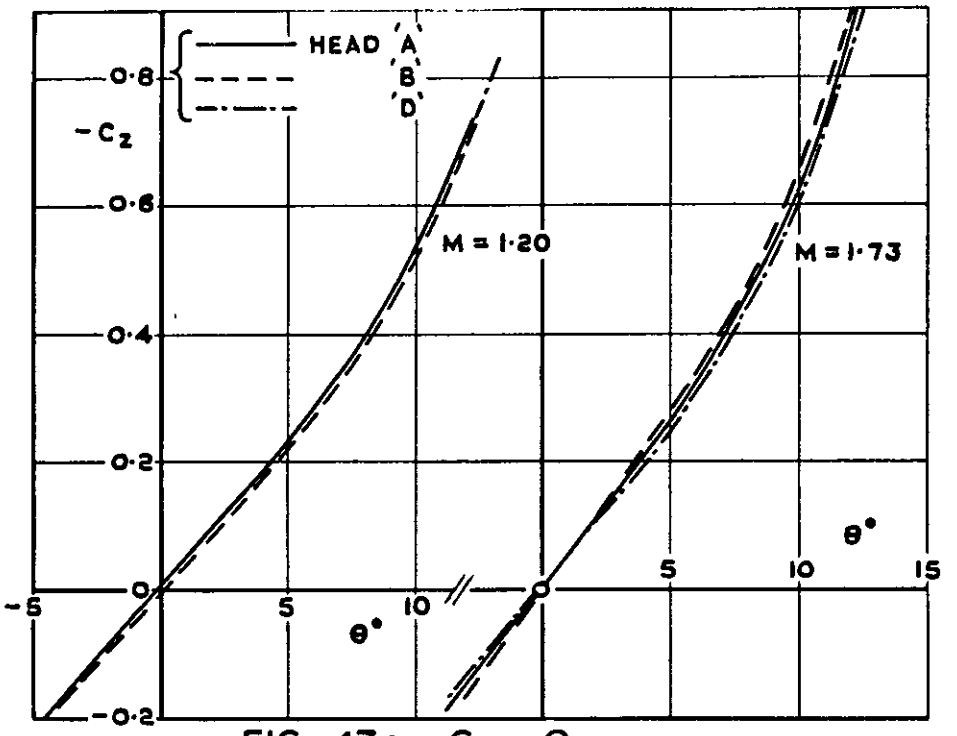

FIG. 47: $-C_z$ v Θ.

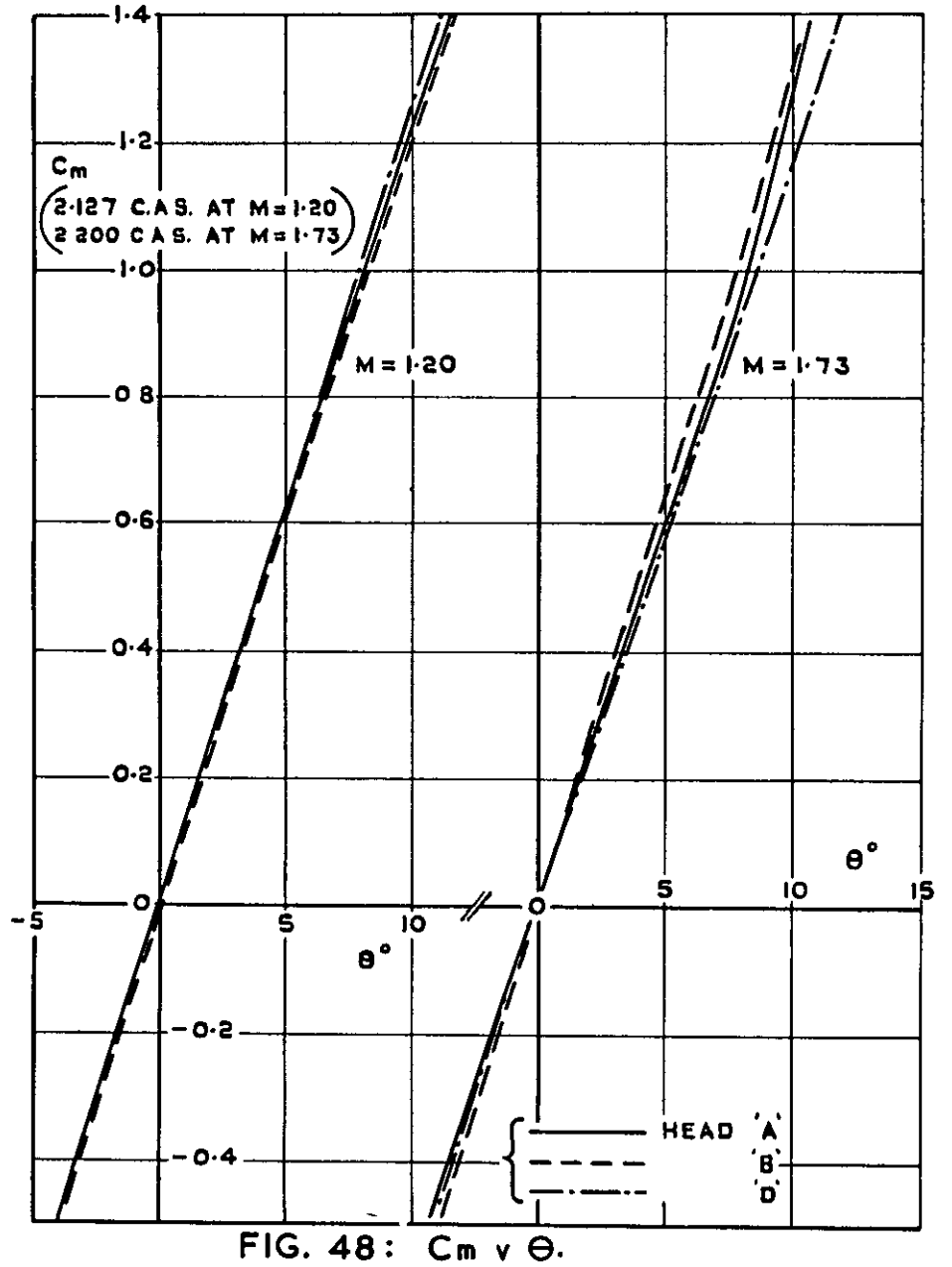

FIG. 48: Cm v Θ.

FIG. 47 & 48: EFFECT OF HEAD SHAPE ON C_z AND Cm AT $\phi = 0^\circ$, $R = 1{\cdot}21 \times 10^6$: NO FINS: REAR STEP FILLED: NOSE SPLINES FAIRED: PODS EXTENDED.

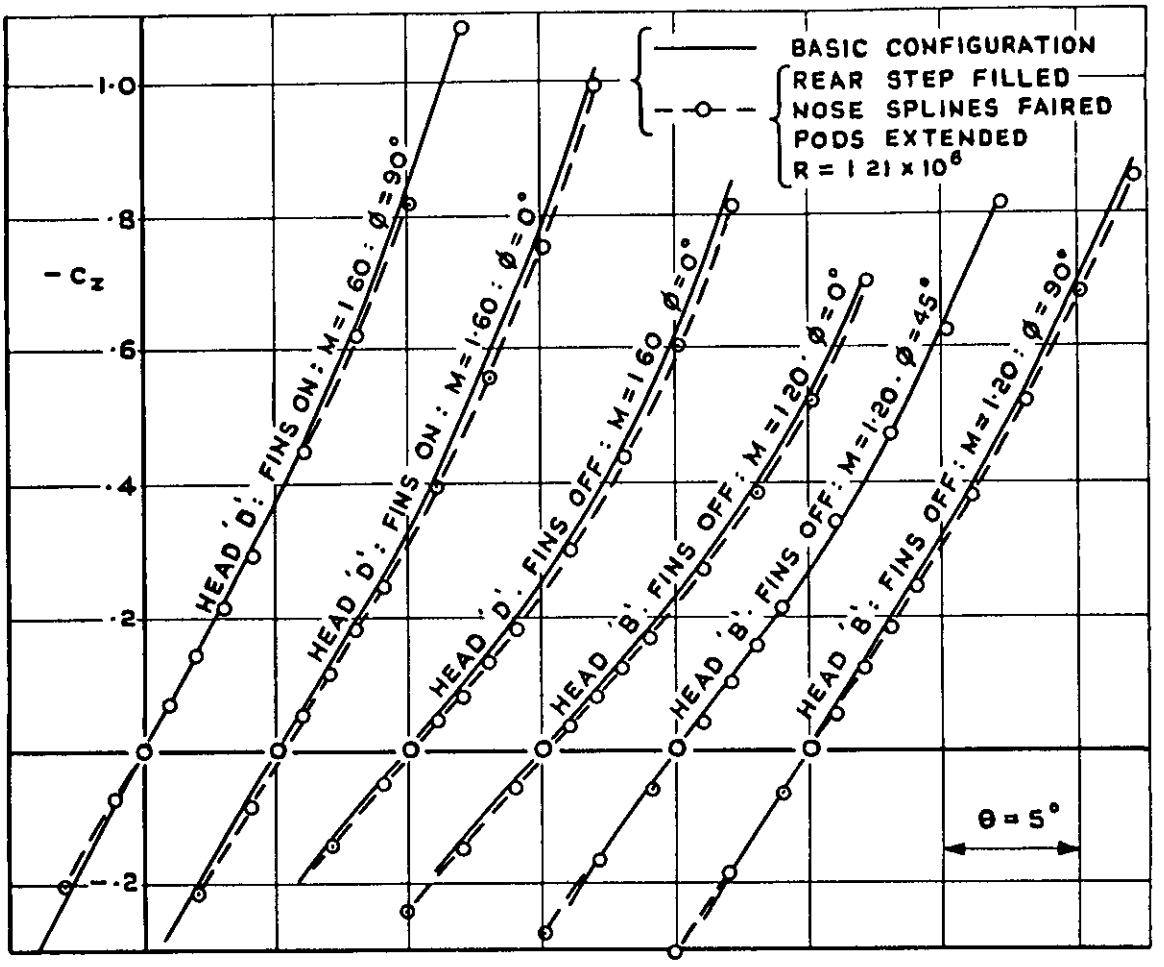

FIG. 49: $-C_z$ v Θ.

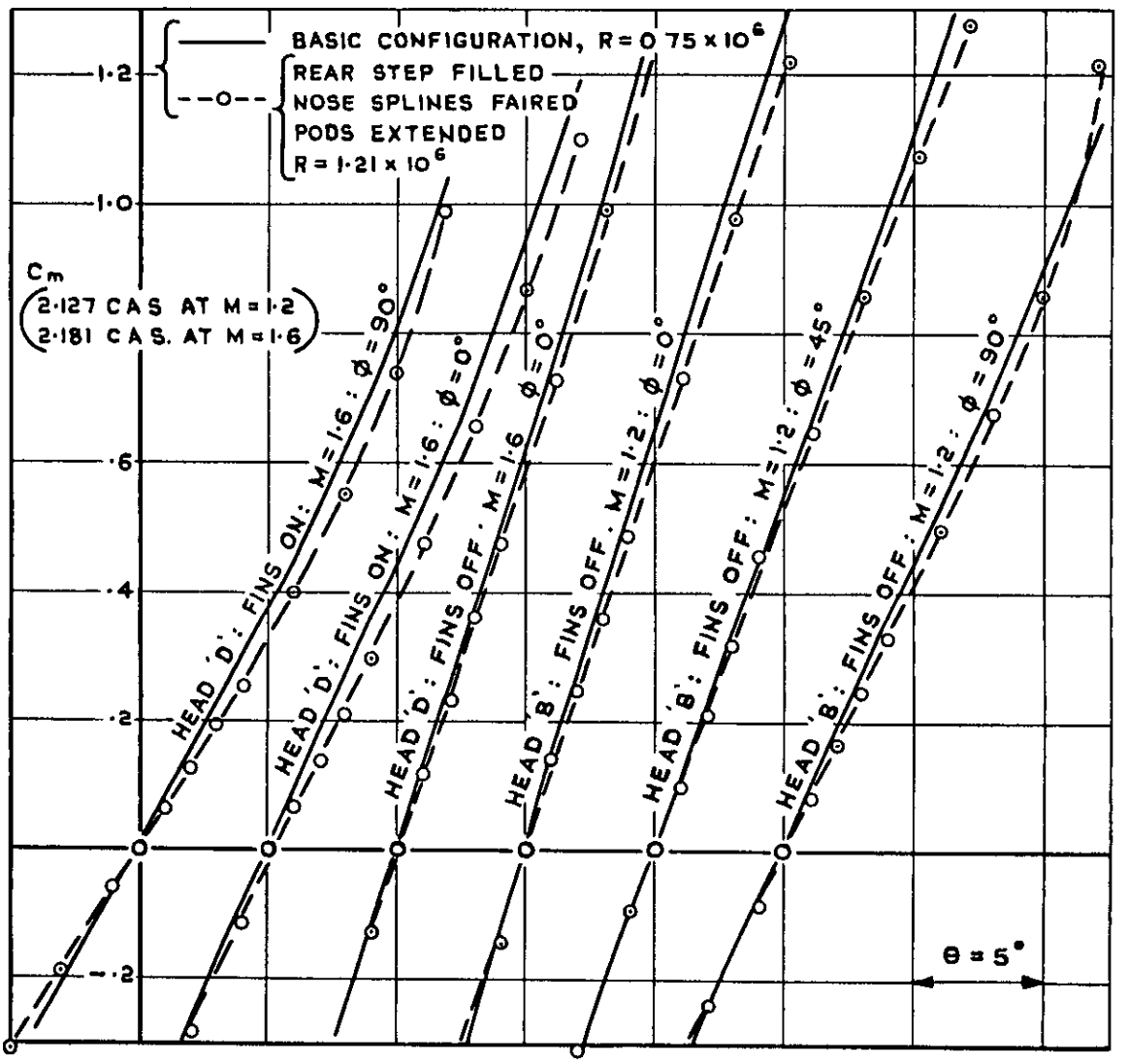

FIG. 50: Cm v Θ.

FIG. 49 & 50: EFFECT OF THE REAR STEP ON C_z AND Cm.

FIG. 51.

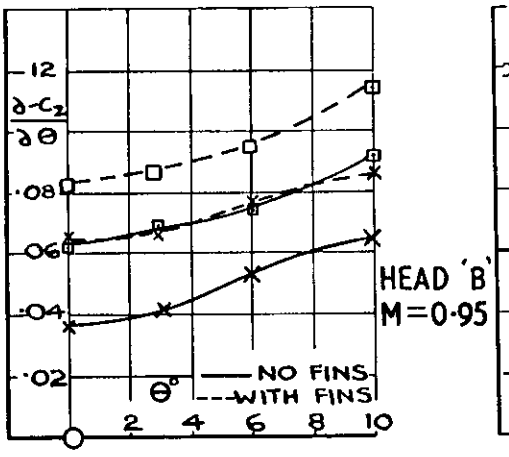

FIG. 52.

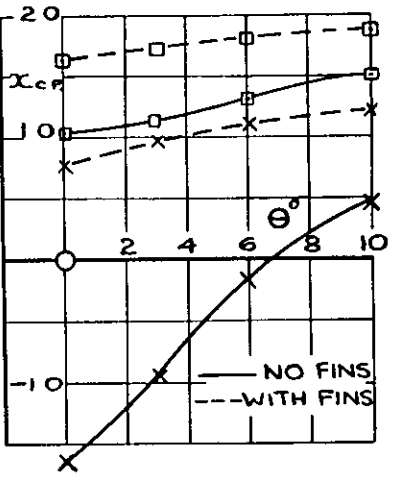

FIG. 53.

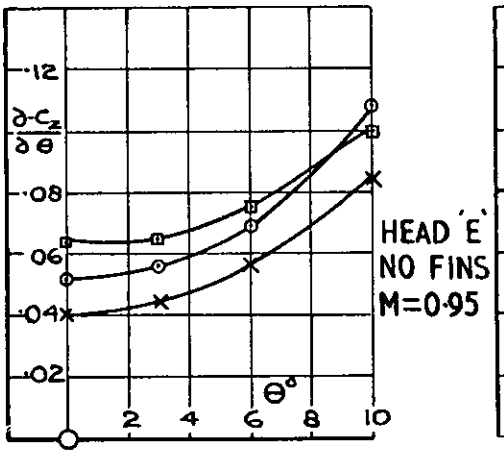

FIG. 54.

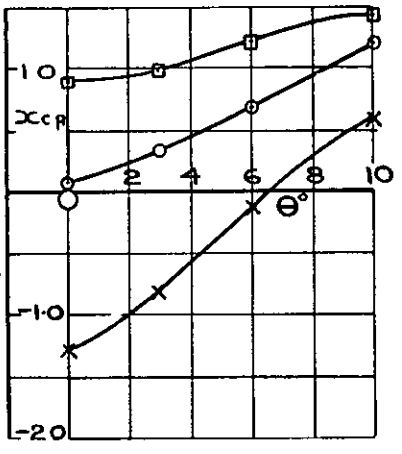

FIG. 55.

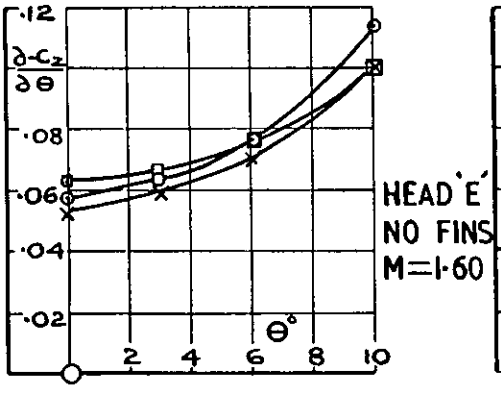

FIG. 56.

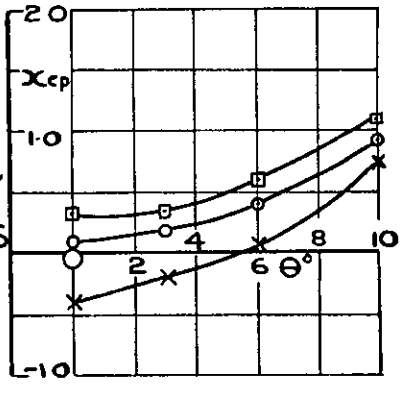

FIG. 57.

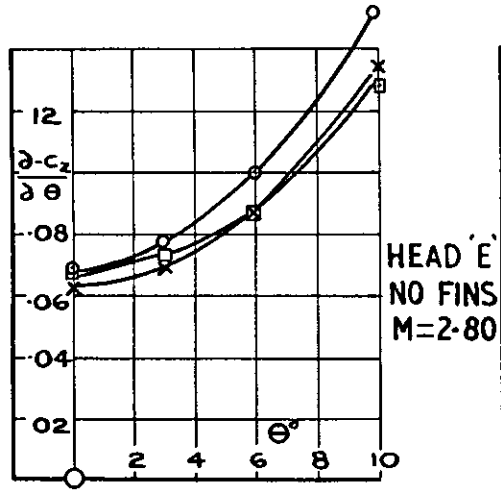

FIG. 58.

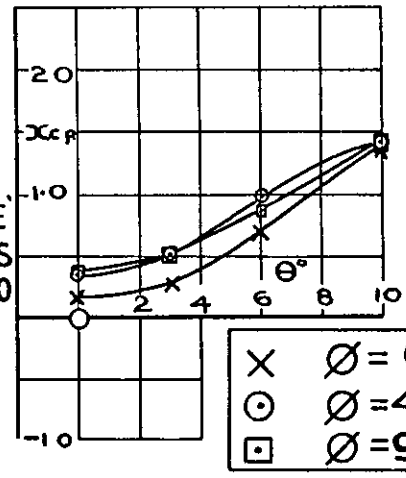

(N.B. $X_{c.p.}$ IS C.P. DISTANCE AFT SHOULDER IN CALIBRES)

FIG. 51-58: EFFECT OF Θ ON LIFT SLOPE AND C.P. POSITION.

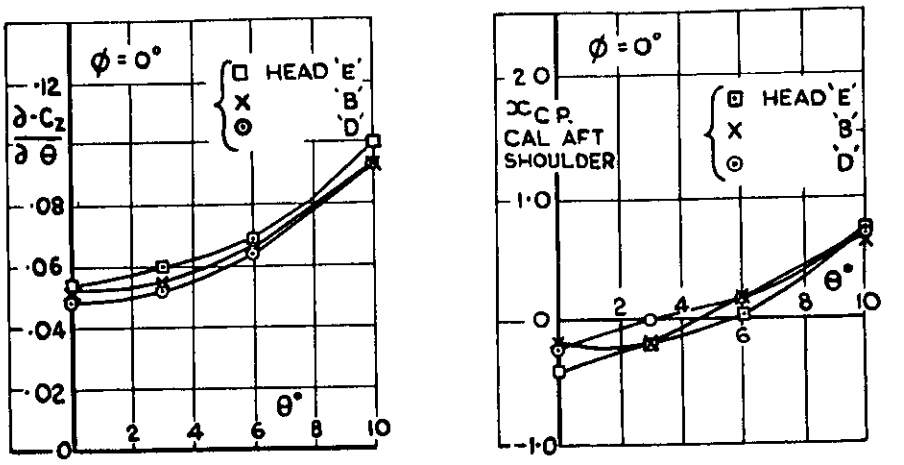

FIG. 59-60: EFFECT OF HEAD SHAPE ON LIFT SLOPE AND C.P. POSITION AT M = 1·6 (NO FINS)

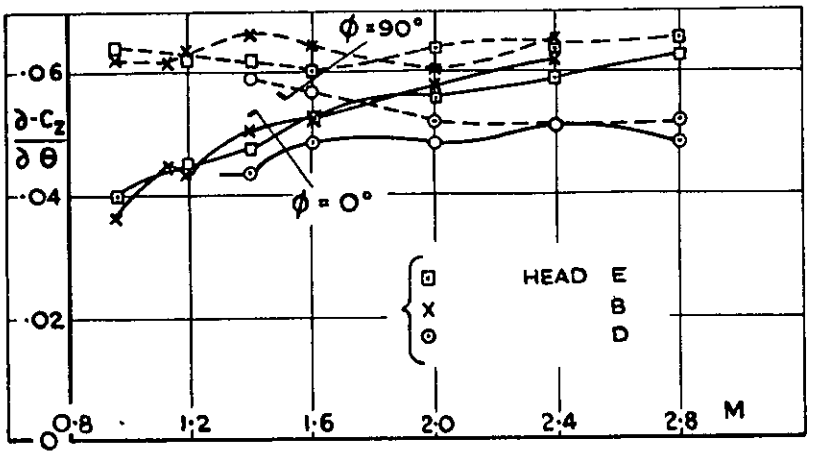

FIG.61: EFFECT OF HEAD SHAPE ON LIFT SLOPE AT θ = 0 (NO FINS)

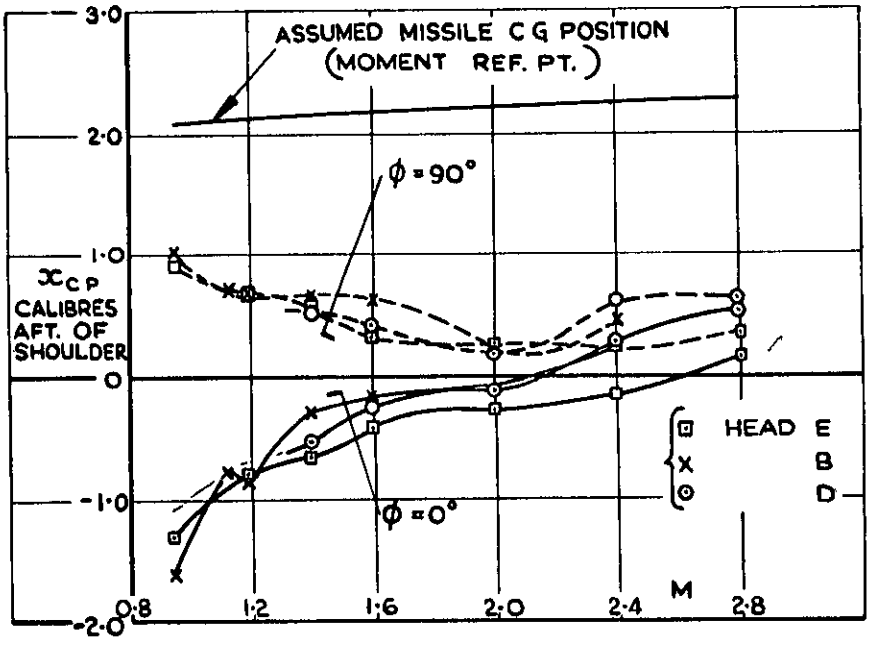

FIG.62: EFFECT OF HEAD SHAPE ON C.P. POSITION AT θ = 0 (NO FINS)

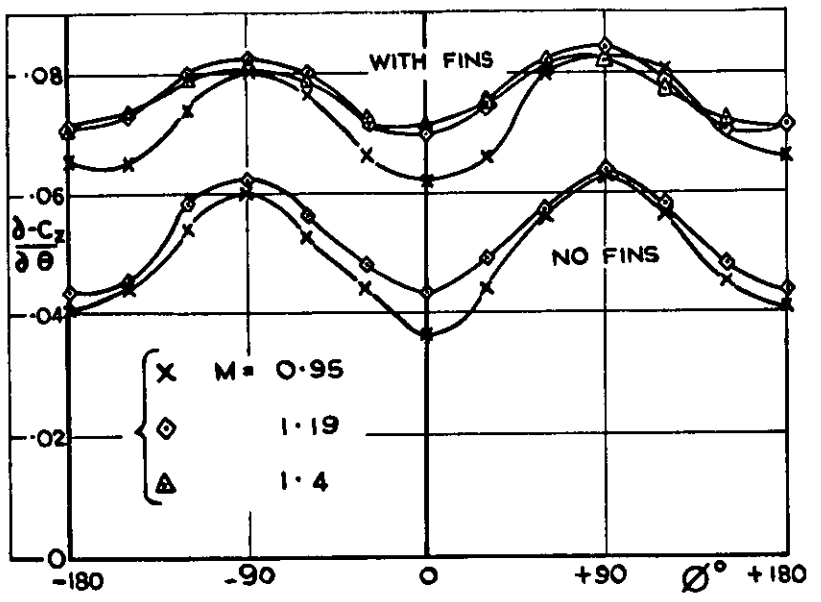

FIG. 63: HEAD 'B'.

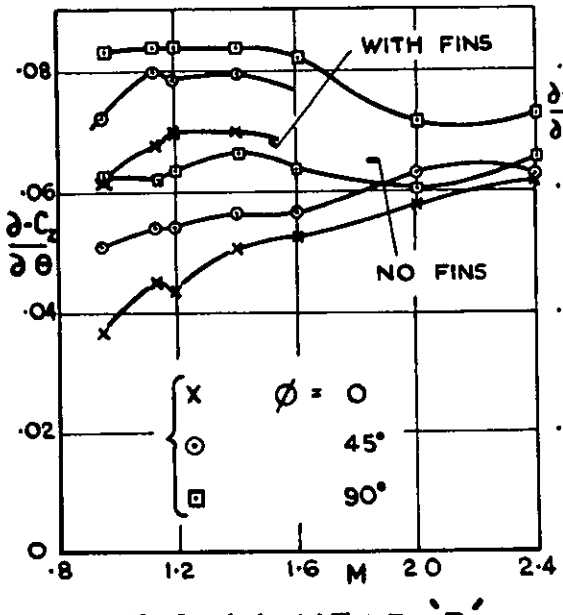

FIG. 64: HEAD 'B'.

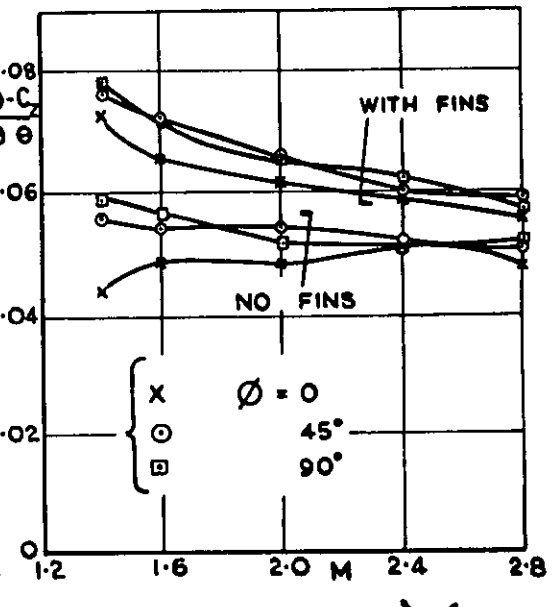

FIG. 65: HEAD 'D'.

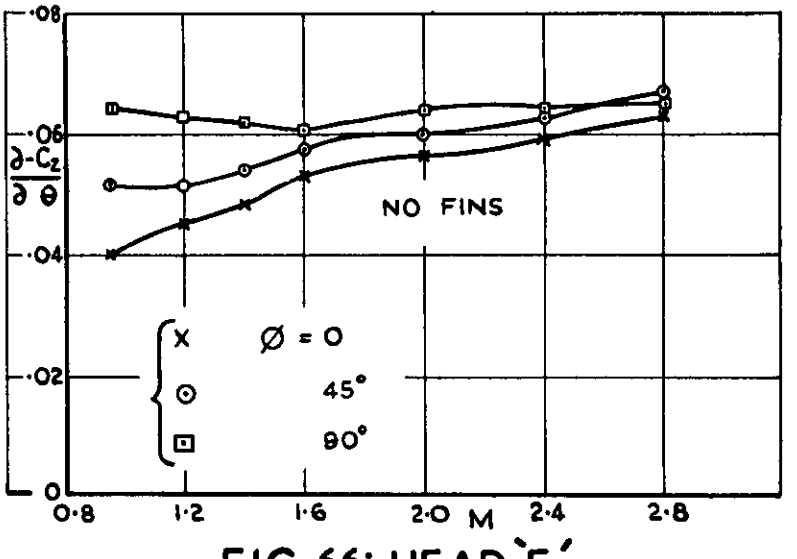

FIG. 66: HEAD 'E'.

FIG. 63-66: EFFECT OF MACH NUMBER AND ϕ ON LIFT SLOPE AT $\theta = 0^{\circ}$.

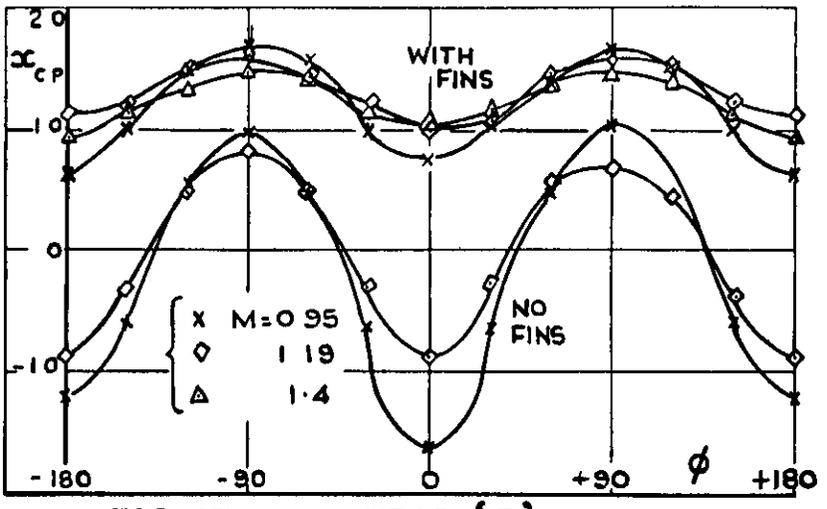

FIG. 67. HEAD 'B'

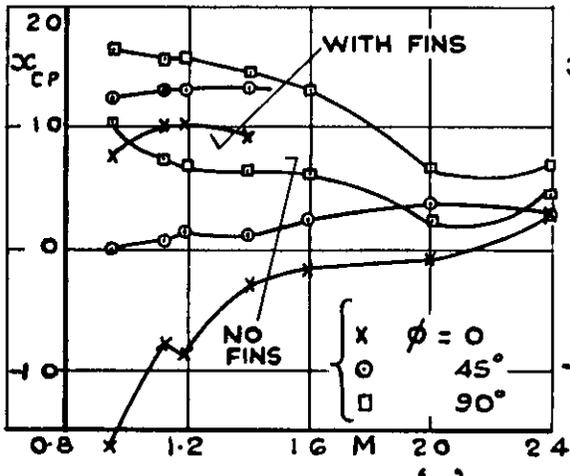

FIG 68 : HEAD 'B'

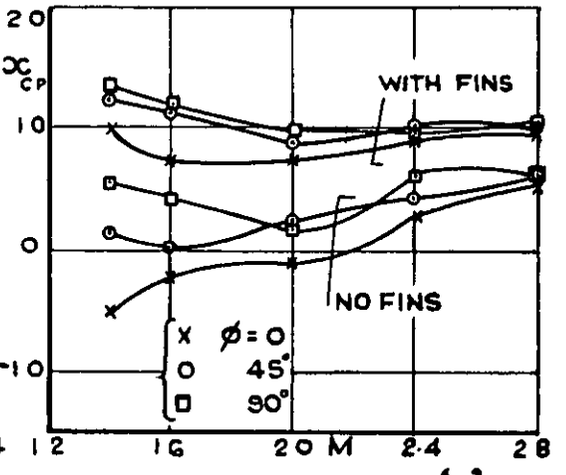

FIG 69 : HEAD 'D'

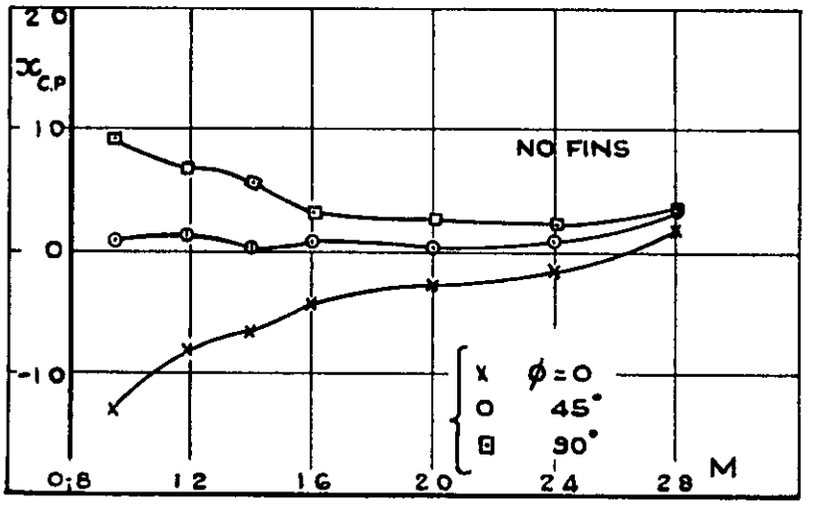

FIG 70 : HEAD 'E'

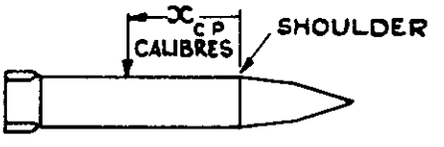

FIG 67-70 : EFFECT OF MACH NUMBER AND Ø ON C.P. POSITION AT Θ = 0

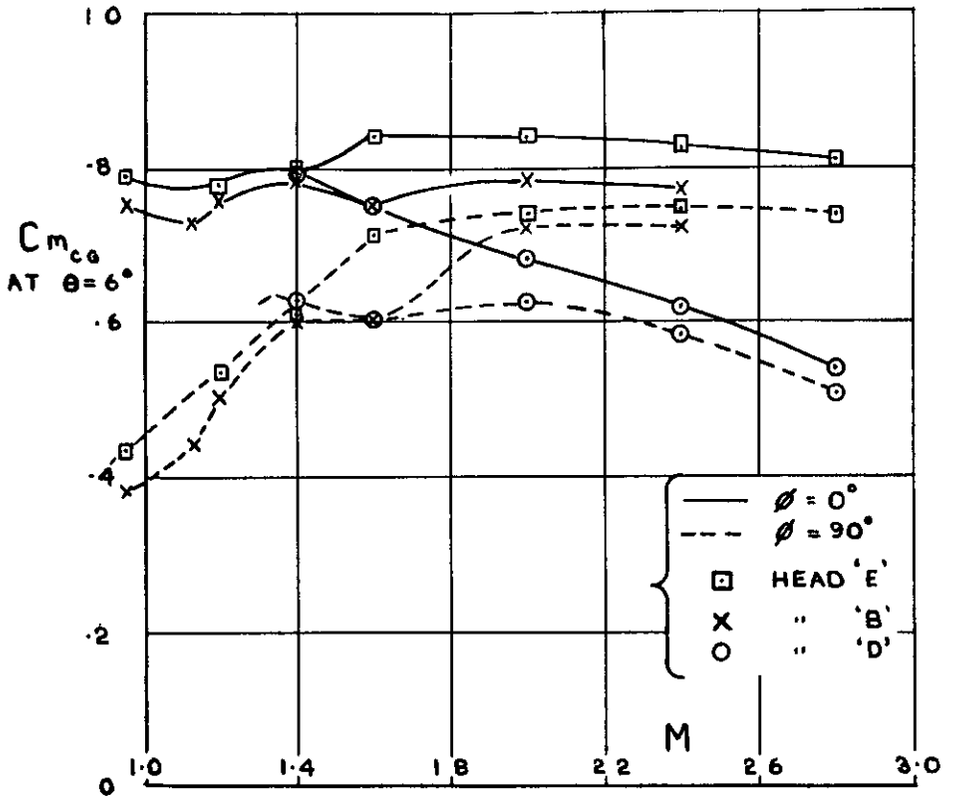

FIG. 71. PITCHING MOMENT COEFFICIENTS AT Θ = 6°

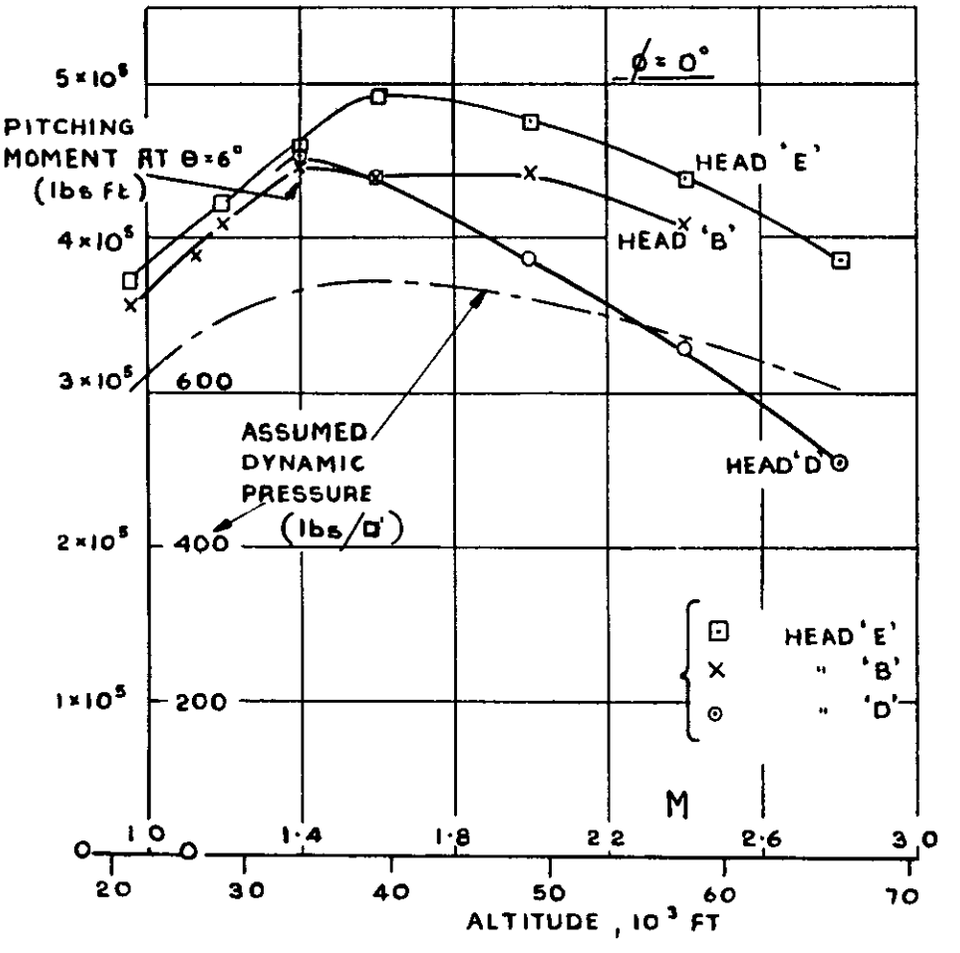

FIG. 72. AERODYNAMIC DE-STABILISING MOMENT AT Θ = 6°, ø = 0°

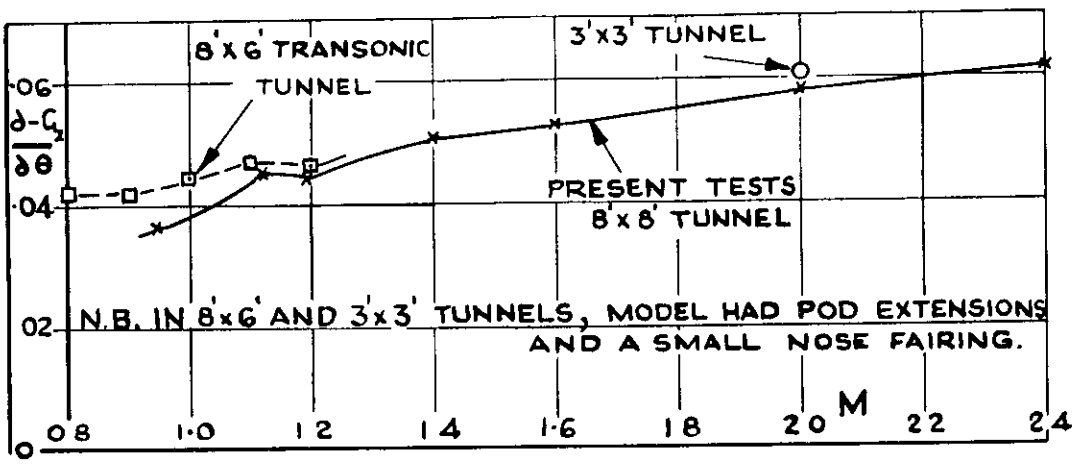

FIG 73: LIFT SLOPE COMPARISON : HEAD 'B', NO FINS, $\phi=\theta=0$

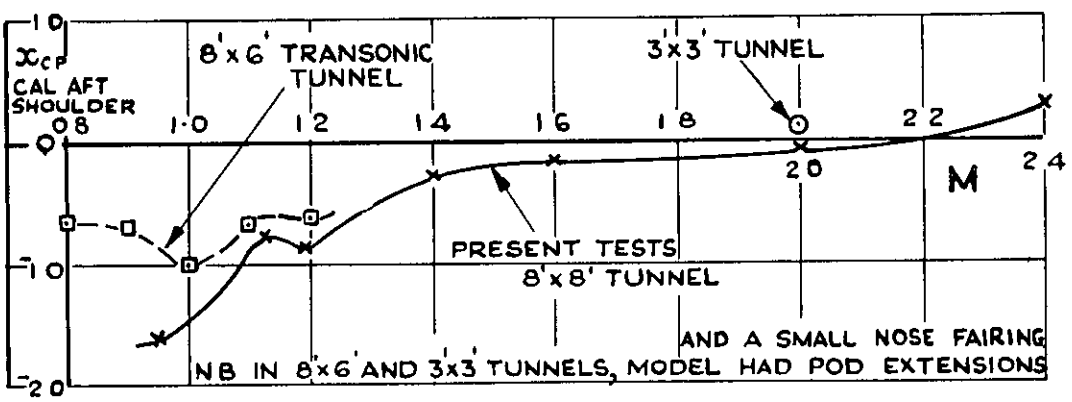

FIG 74 · C.P. POSITION COMPARISON : HEAD 'B', NO FINS, $\phi=\theta=0$

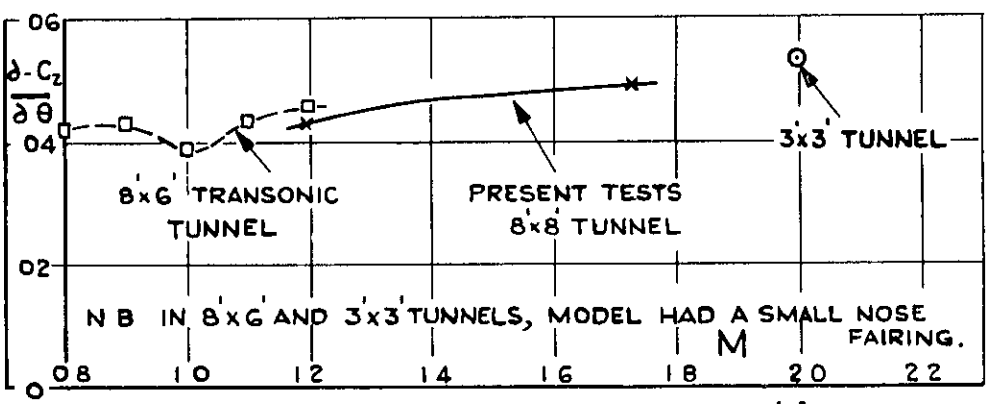

FIG 75: LIFT SLOPE COMPARISON: HEAD 'A', NO FINS, REAR STEP FILLED, NOSE SPLINES FAIRED, PODS EXTENDED $\phi=\theta=0$

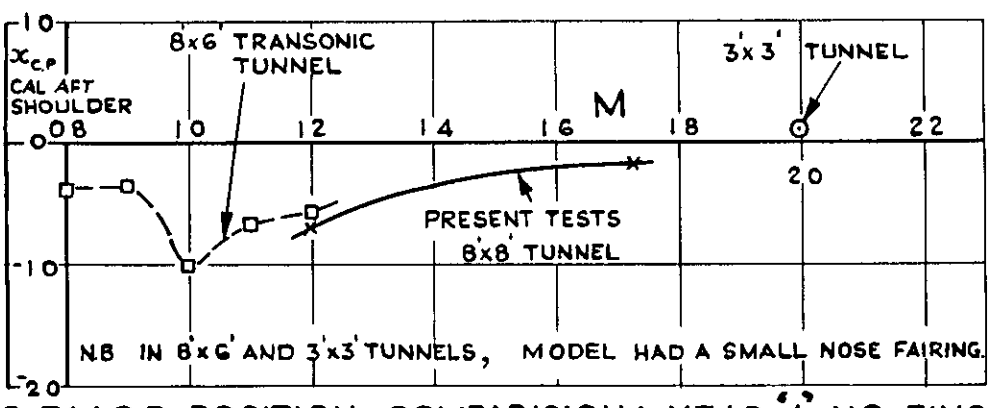

FIG 76 : C.P. POSITION COMPARISION: HEAD 'A', NO FINS, REAR STEP FILLED, NOSE SPLINES FAIRED, PODS EXTENDED $\phi=\theta=0$

FIG 73-76 : COMPARISON OF RESULTS OBTAINED FROM 8'x8', 8'x6' AND 3'x3' TUNNELS

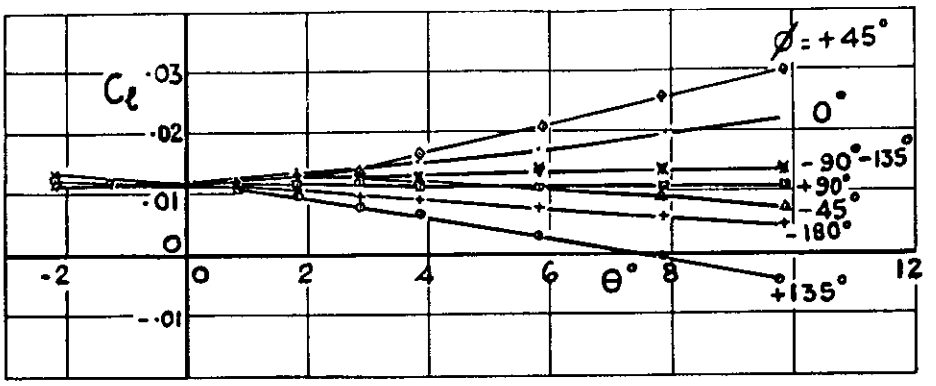

M = 1·40

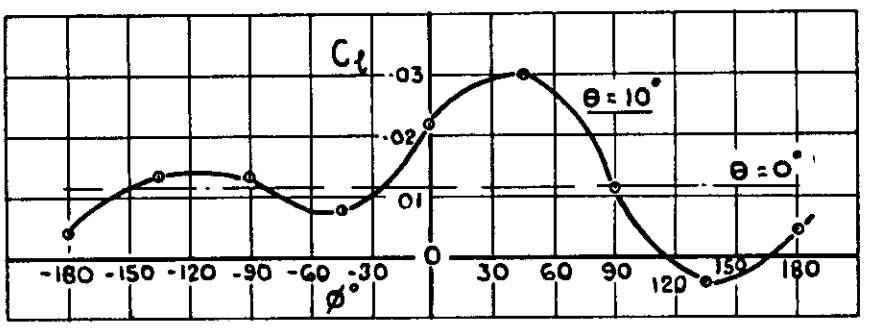

M = 1·40

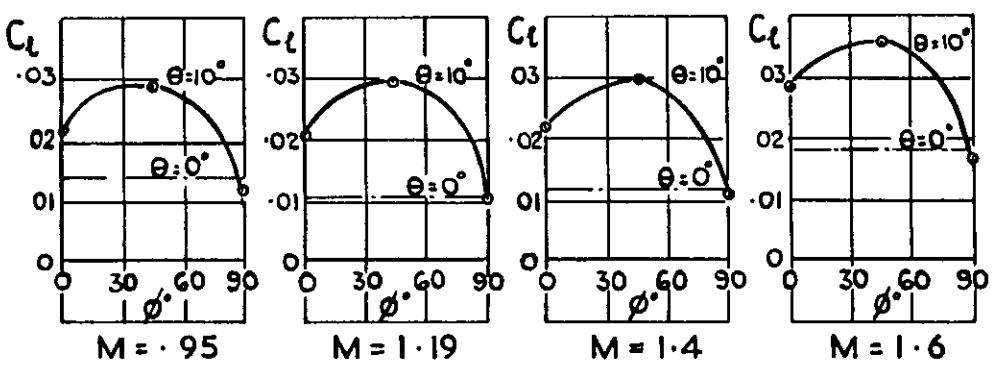

M = · 95 M = 1·19 M = 1·4 M = 1·6

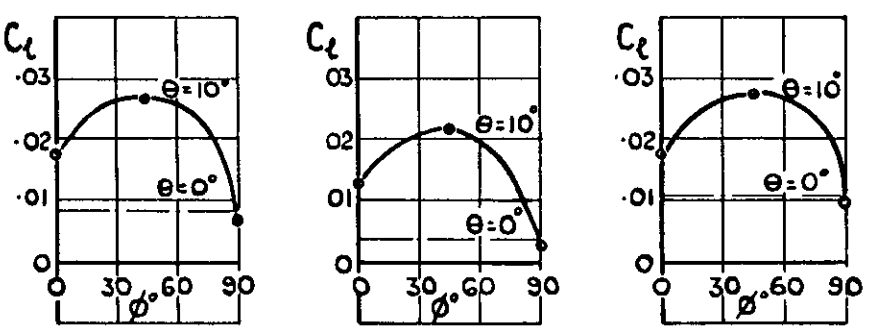

M = 2·0 M = 2·4 M = 2·8

FIG. 77 : ROLLING MOMENTS, HEAD 'E', NO FINS

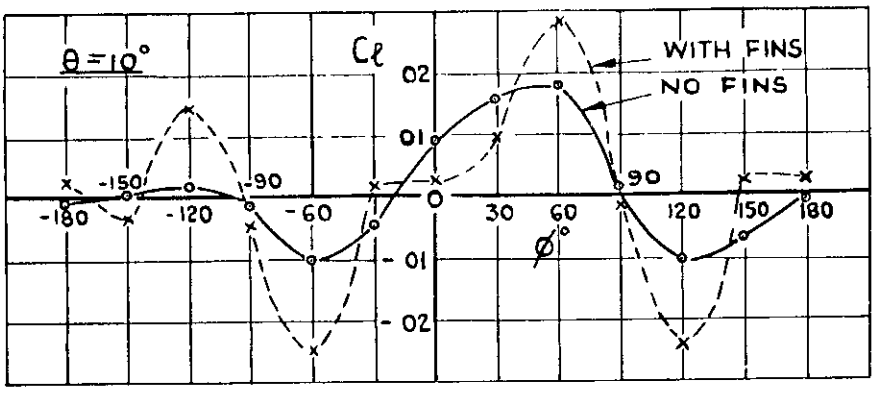

HEAD 'B' : M = 0·95

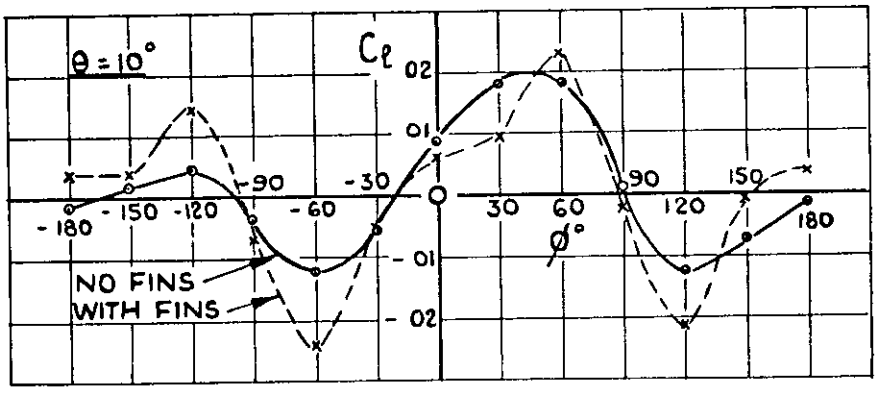

HEAD 'B' : M = 1·19

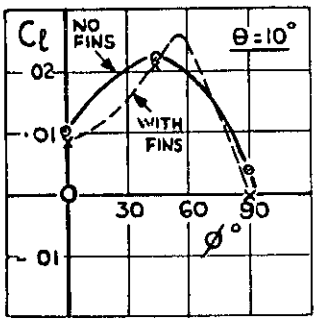

HEAD 'B': M = 1·40

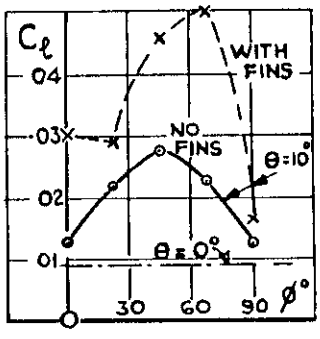

HEAD 'D': M = 1·40

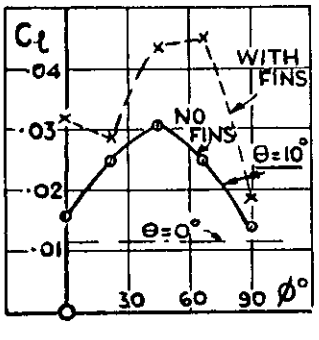

HEAD 'D' M=1·60

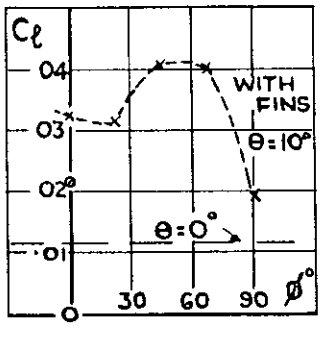

HEAD 'D' M=2·00

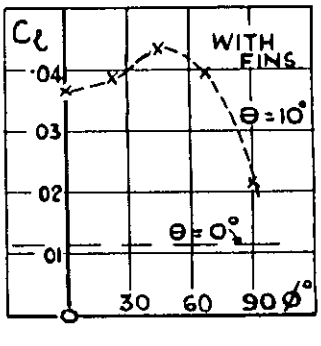

HEAD 'D' M= 2·80

NB. WITH HEAD 'B' C_ℓ WAS ZERO AT $\Theta = 0°$

FIG 78 : ROLLING MOMENTS, EFFECT OF FINS.

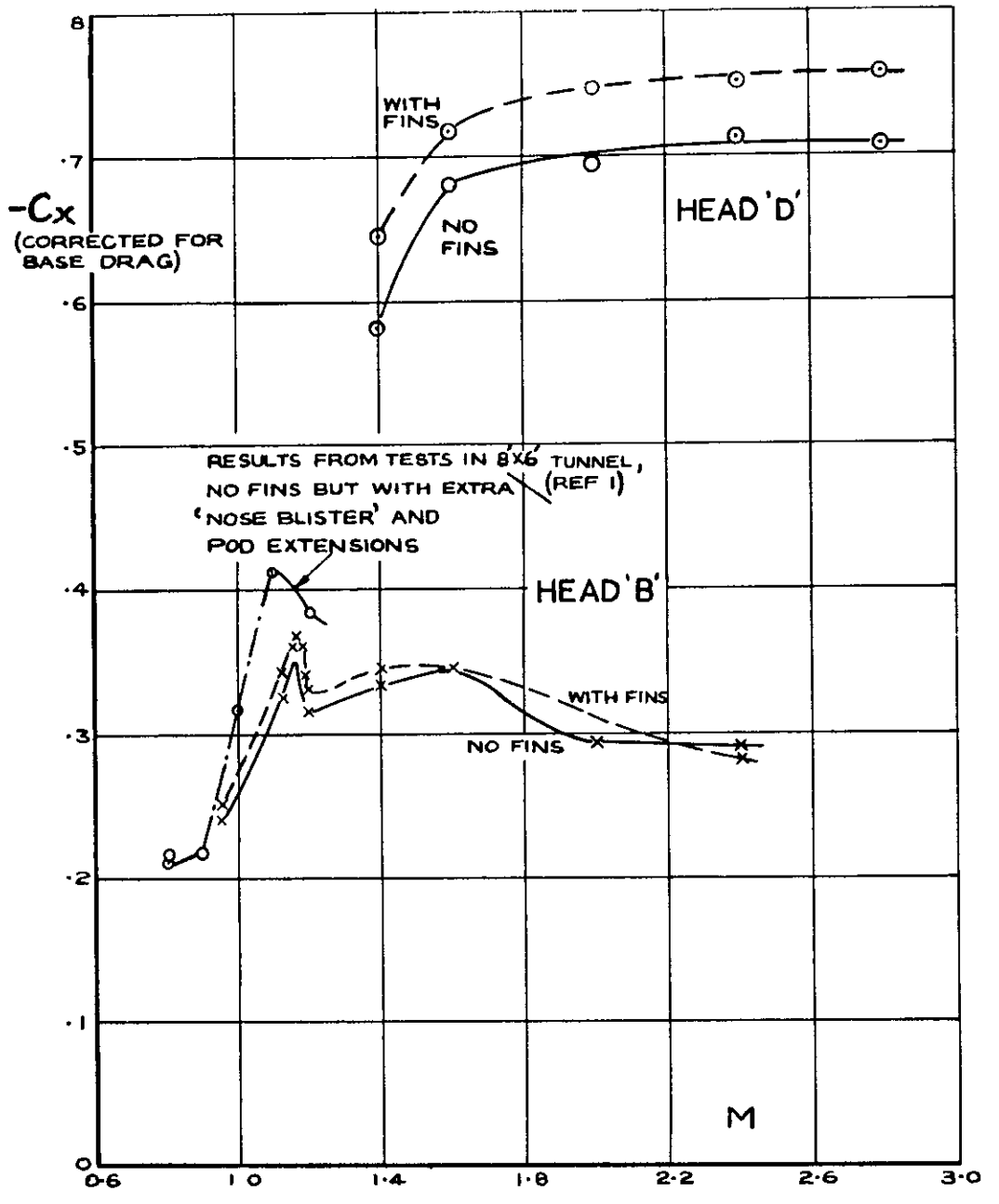

FIG.79 : AXIAL FORCE COEFFICIENTS AT $\Theta = 0^{\circ}$

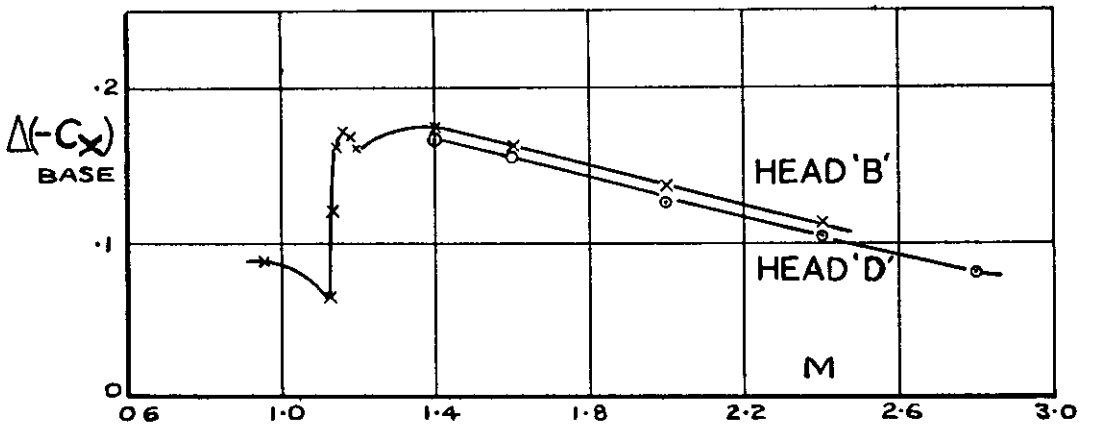

FIG.80 : BASE DRAG CORRECTION SUBTRACTED FROM MEASURED $-C_x$ VALUES.

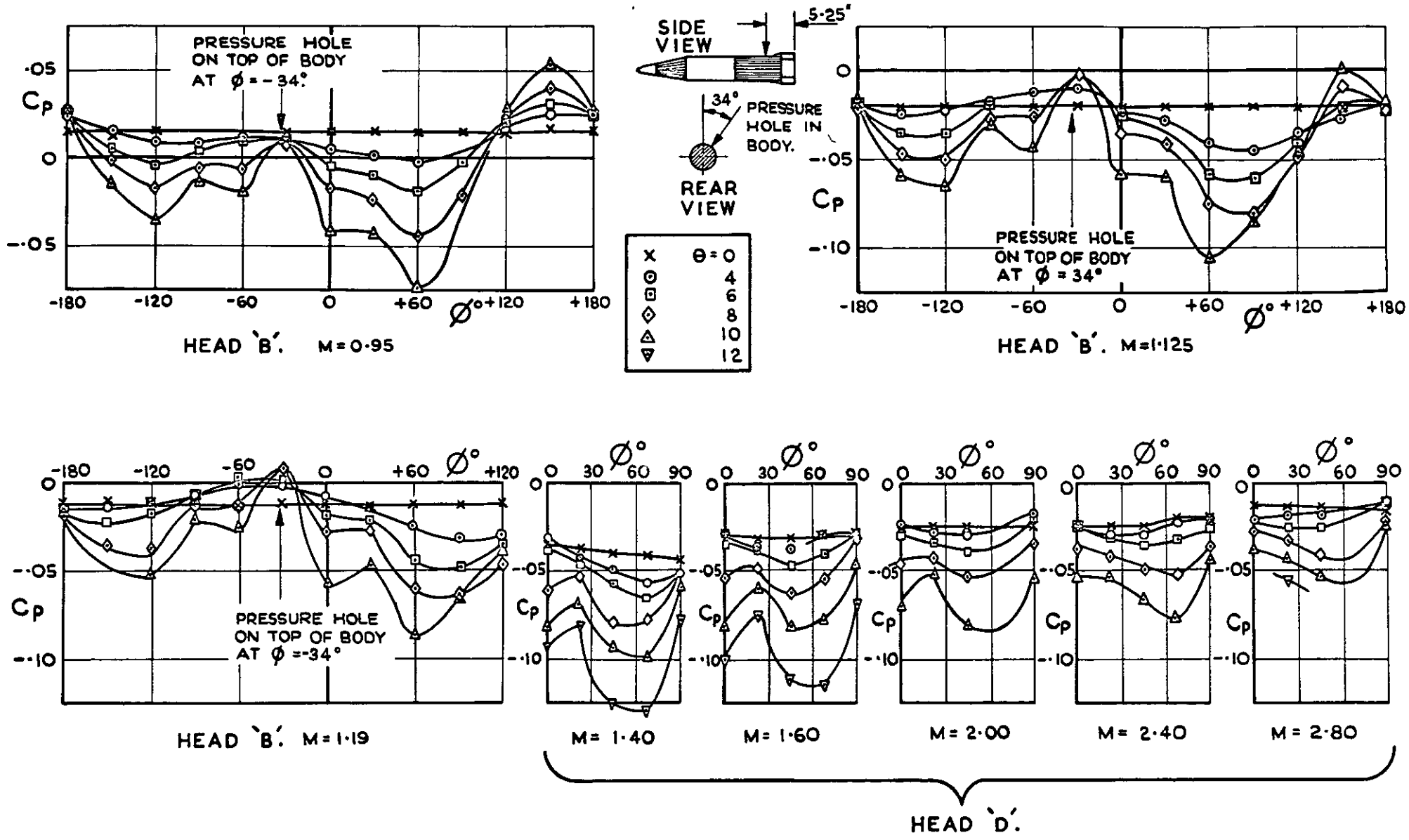

FIG. 81: BODY STATIC PRESSURE DISTRIBUTION (FROM ONE STATIC HOLE IN THE BODY SIDE) HEADS 'B' AND 'D'. NO FINS.

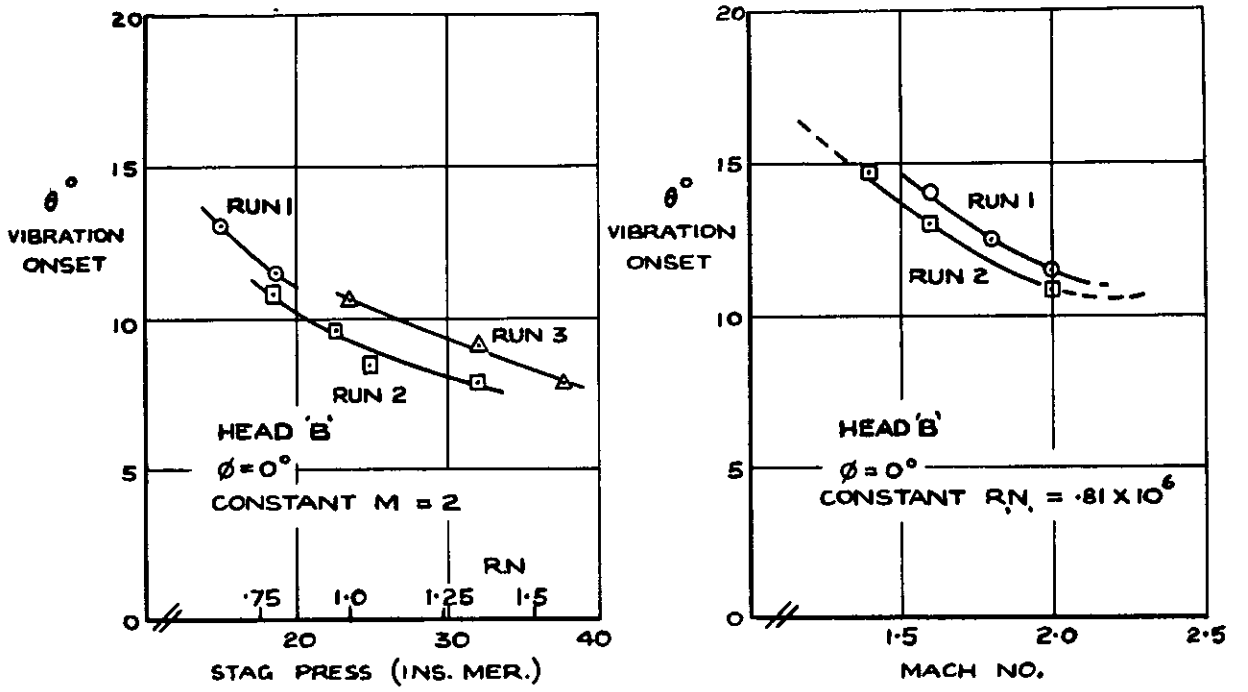

FIG. 82 : EFFECT OF STAGNATION PRESSURE AND MACH. NO. ON θ FOR VIBRATION ONSET.

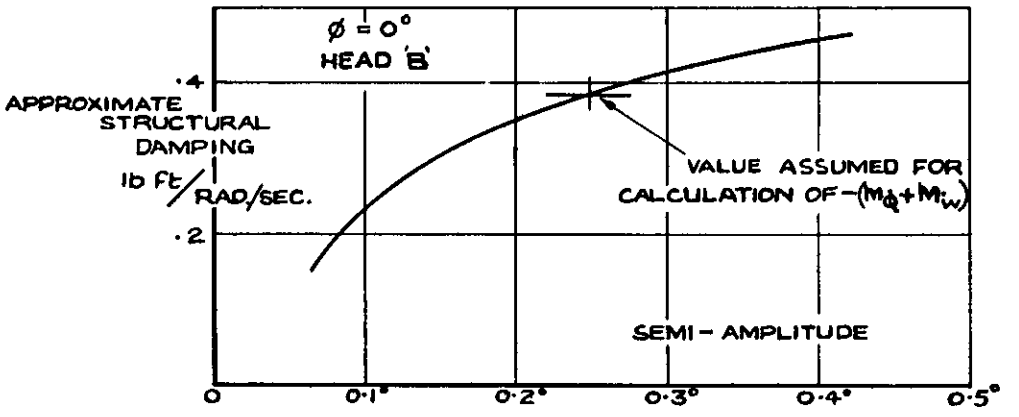

FIG. 83 : STRUCTURAL DAMPING FOR PITCHING VIBRATIONS

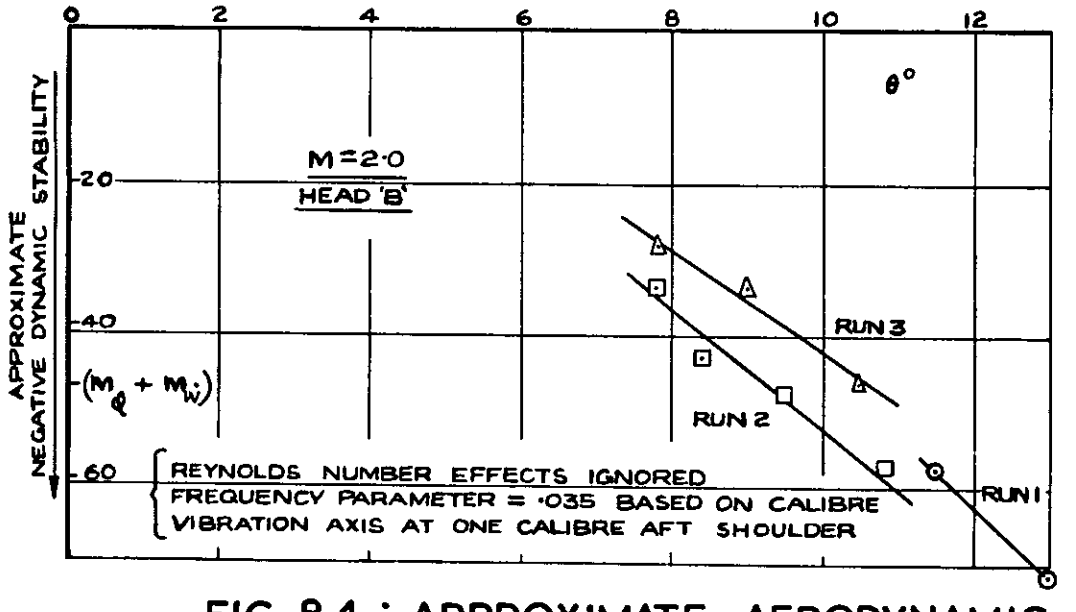

FIG. 84 : APPROXIMATE AERODYNAMIC DAMPING COEFFICIENT.

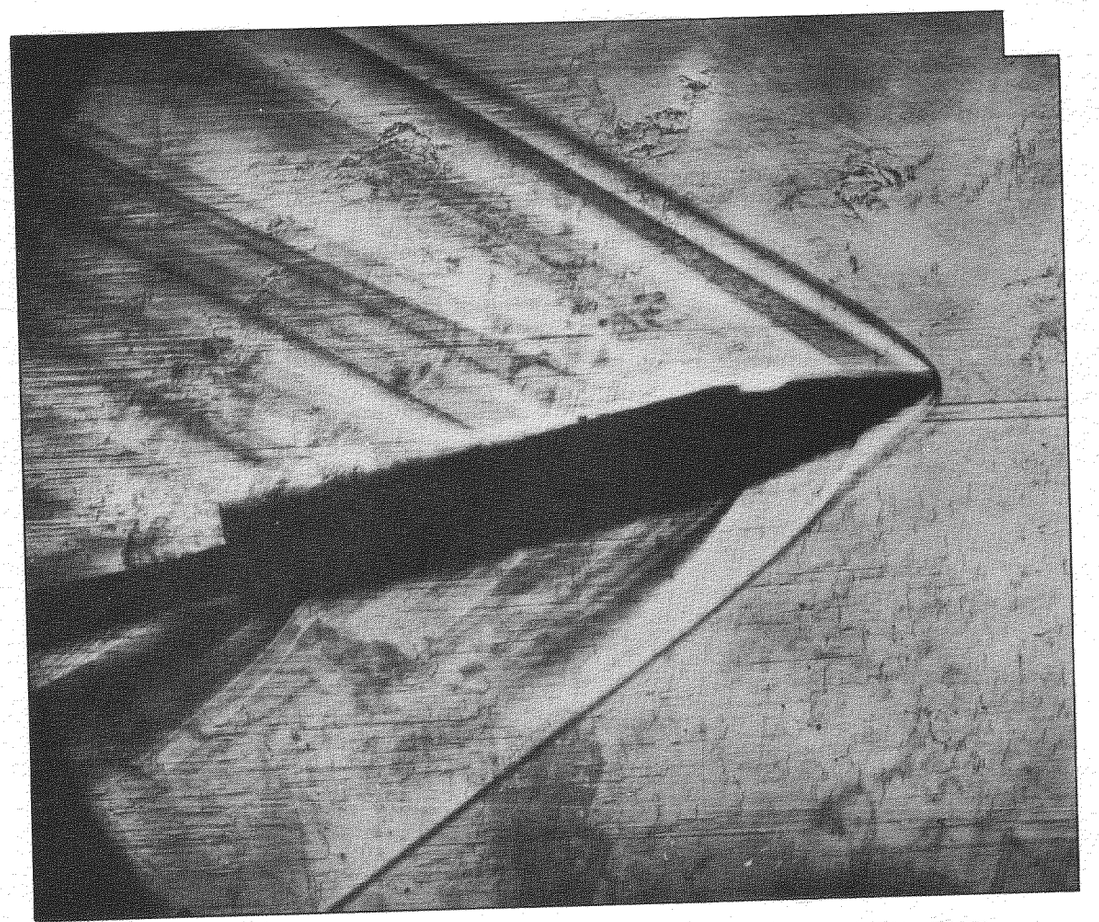

$\phi = 35^0$: $\theta = 12^0$: STAG. PRESS. = 18.5 INS. MER.: MODEL FREE

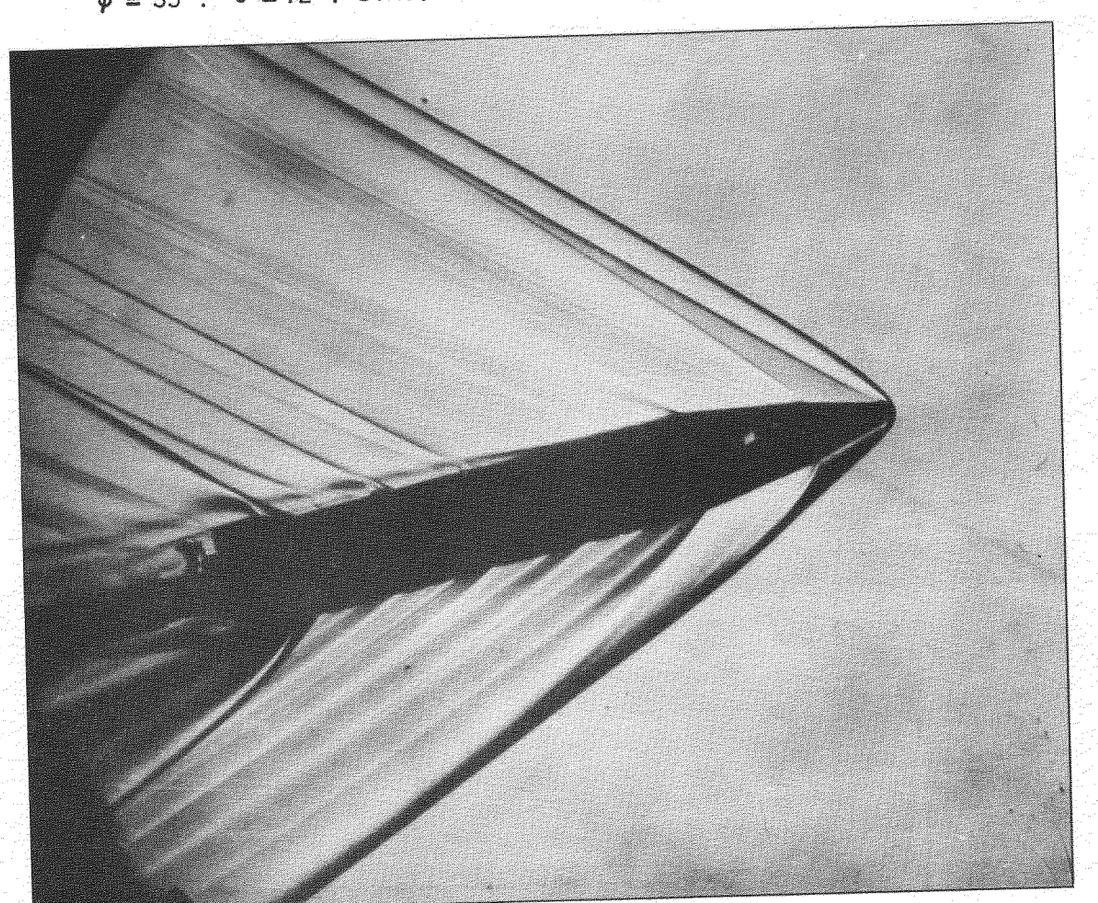

$\phi = 0^0$: $\theta = 13^0$: STAG. PRESS. = 25 INS. MER.: MODEL CLAMPED

FIG.85. SCHLIEREN PHOTOGRAPHS: HEAD 'B': M = 2·00

A.R.C. C.P. No. 734

533.665 :
533.6.013.15 :
533.6.013.412 :
533.6.048.2 :
533.6.011.35/5
[GW] Blue Streak (42)

8 FT x 8 FT TUNNEL TESTS ON A MODEL OF THE DE HAVILLAND 'BLUE STREAK'. Moss, G. F. and Isaacs, D. July, 1961.

Six component balance tests have been made on a 1/30th scale model at Mach numbers from 0.95 to 2.80. Some measurements of static pressure over the engine pods were made, and an investigation of the dynamic stability in pitch carried out.

The results show that there are significant effects due to head shape and fins on the size of the de-stabilizing pitching moments in a typical trajectory. The effect of body vortices on the measured static pressure is shown and the derived negative aerodynamic damping coefficients given. The reason for the latter is shown to be the presence of a step in the body profile, but the total damping is likely to be adequate for the rigid mode on the full scale missile.

A.R.C. C.P. No. 734

533.665 :
533.6.013.15 :
533.6.013.412 :
533.6.048.2 :
533.6.011.35/5
[GW] Blue Streak (42)

8 FT x 8 FT TUNNEL TESTS ON A MODEL OF THE DE HAVILLAND 'BLUE STREAK'. Moss, G. F. and Isaacs, D. July, 1961.

Six component balance tests have been made on a 1/30th scale model at Mach numbers from 0.95 to 2.80. Some measurements of static pressure over the engine pods were made, and an investigation of the dynamic stability in pitch carried out.

The results show that there are significant effects due to head shape and fins on the size of the de-stabilizing pitching moments in a typical trajectory. The effect of body vortices on the measured static pressure is shown and the derived negative aerodynamic damping coefficients given. The reason for the latter is shown to be the presence of a step in the body profile, but the total damping is likely to be adequate for the rigid mode on the full scale missile.

A.R.C. C.P. No. 734

533.665 :
533.6.013.15 :
533.6.013.412 :
533.6.048.2 :
533.6.011.35/5
[GW] Blue Streak (42)

8 FT x 8 FT TUNNEL TESTS ON A MODEL OF THE DE HAVILLAND 'BLUE STREAK'. Moss, G. F. and Isaacs, D. July, 1961.

Six component balance tests have been made on a 1/30th scale model at Mach numbers from 0.95 to 2.80. Some measurements of static pressure over the engine pods were made, and an investigation of the dynamic stability in pitch carried out.

The results show that there are significant effects due to head shape and fins on the size of the de-stabilizing pitching moments in a typical trajectory. The effect of body vortices on the measured static pressure is shown and the derived negative aerodynamic damping coefficients given. The reason for the latter is shown to be the presence of a step in the body profile, but the total damping is likely to be adequate for the rigid mode on the full scale missile.

Published by
HER MAJESTY'S STATIONERY OFFICE

To be purchased from
York House, Kingsway, London W.C.2
423 Oxford Street, London W.1
13A Castle Street, Edinburgh 2
109 St. Mary Street, Cardiff
39 King Street, Manchester 2
50 Fairfax Street, Bristol 1
35 Smallbrook, Ringway, Birmingham 5
80 Chichester Street, Belfast 1
or through any bookseller

S.O. CODE No. 23-9015-34